# The deubiquitylase TRABID coordinates sex-specific neurodegeneration in *Drosophila melanogaster*




A thesis submitted for the degree of Doctor of Philosophy

in the University of Oxford Trinity Term 2022

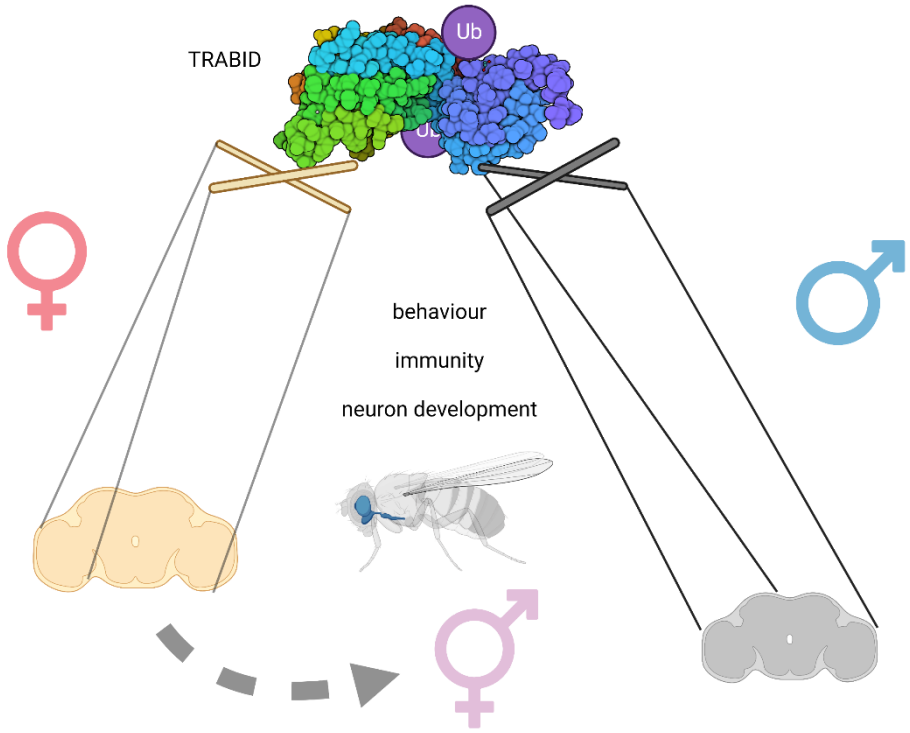
Jingnu Xia

Hertford College

Department of Biochemistry

# Abstract

Ubiquitin-related post translation modification (PTM) plays an important role in cellular signalling. TRABID is a deubiquitylase that preferentially hydrolyses Lys29 and 33 ubiquitin chains and is known to affect inflammation and consequently, neurodegeneration as the latter is considered functionally linked to the former. However, sex differences are widely observed in both inflammation as well as neurodegeneration phenotypes. In this study, I investigated sex dimorphism, in ubiquitination at the intersection of inflammation and neurodegeneration. I demonstrated *Drosophila* TRABID has similar enzymatic activity as human TRABID and generated an enzymatically inactive TRABID (*trbdC518A*) in *Drosophila* flies. I discovered that *trbdC518A* has a sexually dimorphic impact in the insect's locomotor activity, sleep pattern, lifespan, cerebral cells count, brain volume and NF-κB signalling. When blocking female development in astrocytes or immunocompetent cells, sex dimorphisms in locomotor activity and NF-κB signalling are partially eliminated. Further evidence ubiquitinomics and proteomics of fly heads, provided insight into the sex-specific impact of *trbdC518A.*




**Graphic abstract**: The deubiquitylase TRABID regulates neurodegeneration, head immunity and neurological phenotypes in a sex dimorphism pattern. Creating tissue specific intersex flies partially reduces the sex-specific difference in an inactive TRABID background.

# Acknowledgements

I would like to use this page to pay my sincere appreciation to my supervisors: Prof. Petros Ligoxygakis and Dr. Paul Elliott, for their patience, guidance, and encouragement. I enjoyed discussing science questions with them with inspiring insights and critical thinking.

I would like to thank Dr. Jeff Lee for helping me in histology research and other members in the Davis lab. I also would like to thank Dr. Andan Pinto Fernandez and Dr. Andreas Damianou for their help with ubiquitinomics and proteomics experiments and other members in the Kessler lab.

I am extremely fortunate to have had fantastic friends during my study in Oxford. I enjoyed the time with friends in Biochemistry department, including Larissa Dietz, Maribel Schonewolff, Srishti Arora, Maria Kiourlappou, Honglin Chen Yuntao Wang, Dr. Gege Yang, Xinyi Feng and Zhihan Bo, for sharing the successes and failures. I also would like to thank Dr. Dingxi Zhou, Zhu Liang, Fei Gao, Wenbo Wang and Jinyi Zhao for their help in my presentations and writings, exchange of ideas in our studies and the joy in life.

Finally, I would like to thank my parents, Prof. Yuxian Xia and Deyu Zeng, for their endless support, financially and spiritually that carried me through the storms and high waves.

This study could not have been done without the help of my mentors, colleagues, friends, and family members.

# Abbreviations

| abbrevation | full name |
|---|---|
| AD | Alzheimer's disease |
| AMP | antimicrobial peptide |
| Ank | ankyrine repeat |
| AnkUBD | ankyrin repeat UBD |
| APP | amyloid precursor protein |
| *AttA* | *attacin A* |
| *AttB* | *attacin B* |
| Aβ | amyloid β |
| BACE1 | β-site APP cleaving enzyme-1 |
| C443 | Cystine443 |
| C518A/C2A | Cystine518 to Alanine518 |
| CBX | chromobox |
| CD | Crohn's disease |
| *CecC* | *cecropin C* |
| CHIP | carboxyl terminus of heat-shock cognate (Hsc)70-interacting protein |
| cIAP2 | inhibitor of apoptosis protein2 |
| CL | STRING cluster |
| DAM | *Drosophila* activity monitoring |
| DBH | dopamine monooxygenase |
| DME | reactome |
| DP | dark period |
| *DptA* | *diptericin A* |
| *Dro* | *drosocin* |
| dTrabid | *Drosophila* Trabid |
| DUB | deubiquitylase |
| ERG | E-twenty-six related gene |
| FADD | Fas-associated death domain |
| GO | gene ontology |
| HA20 | A20 haploinsufficiency |
| HCC | hepatocellular carcinoma |
| Hsc | heat-shock cognate |
| hTrabid | human Trabid |
| IAP | immunoaffinity purification |
| IBD | inflammatory bowel disease |

| | |
|---|---|
| IKK | IκB kinase complex |
| IL | interleukin |
| Ile | isoleucine |
| Imd | immune deficiency |
| IPTG | Isopropyl β-D-1-thiogalactopyranoside |
| ISG15 | interferon-stimulated gene 15 |
| LP | light period |
| LUBAC | linear ubiquitin chain assembly complex |
| LUBEL | linear ubiquitin E3 ligase |
| Lys | lysine |
| Met | Methionine |
| MINDY | MIU containing novel DUB family |
| MIU | motif interacting with ubiquitin |
| MST | mean sleep time in each episode |
| NEDD8 | neuronal precursor cell expreesd developmentally downregulated protein 8 |
| NEMO | NF-κB essential modulator |
| NF-κB | nuclear factor κB |
| NZFs | Npl4 zinc fingers |
| ORAS | OTULIN-related autoinflammatory syndrome |
| OTU | ovarian tumor |
| PCA | principal component analysis |
| PD | Parkinson’s disease |
| PINK1 | PTEN induced putative kinase 1 |
| Prkn | Parkin |
| PTM | post-translation modification |
| RID | raw integrated density |
| RIP1 | receptor-interacting protein 1 |
| SUMO | small ubiquitin-like modifier |
| TAB2 | TAK1-binding protein2 |
| TAK1 | transforming growth factor-β (TGF-β)-activated kinase 1 |
| TNFR1 | Tumor necrosis factor receptor 1 |
| TLRs | Toll-like receptors |
| tra | transformer |

| | |
|---|---|
| TRADD | TNF receptor-associated death domain |
| TRAF2 | TNFR-associated factor 2 |
| trbdKO | trbd knockout |
| TSE | total sleep episode |
| TST | total sleep time |
| Twist1 | Twist Family BHLH Transcription Factor 1 |
| UBA | ubiquitin associated domain |
| UbcH5B | Ubiquitin-conjugating Enzyme H5b |
| UBD | ubiquitin binding domain |
| UBD | ubiquitin-binding domain |
| UC | ulcerative colitis |
| UCH | ubiquitin carboxy-terminal hydrolase |
| UIM | ubiquitin ineracting motif |
| UPS | ubiquitin-proteosome system |
| USP | ubiquitn specific protease |
| USP16 | ubiquitin-specific peptidase 16 |
| USP26 | ubiquitin-specific peptidase 26 |
| USP9X | ubiquitin-specific peptidase 9, X chromosome-linked |
| ZnF-A20 | A20 zinc-fingers |

# Table of Content

Abstract ..... ii

Acknowledgements ..... iv

Abbreviations ..... vi

Table of Content ..... ix

Figures and Tables ..... xv

Chapter 1: Introduction ..... 1

1.1 Ubiquitin ..... 1

1.2 Ubiquitylation ..... 5

1.3 Deubiquitylation ..... 7

1.4 Cysteine protease family DUBs ..... 13

1.5 A20 sub-family DUBs ..... 19

1.6 TNFR1/IMD-induced NF-**κB** signalling ..... 22

1.7 neurodegeneration, ubiquitylation and NF-κB signalling ..... 28

1.7.1 Neurodegeneration ..... 28

1.7.2 Ubiquitylation and neurodegeneration ..... 28

1.7.3 NF-**κB** signalling and neurodegeneration ..... 29

1.7.4 Sex dimorphism ..... 30

1.8 Why TRABID? ..... 31

1.8.1 Current known function of TRABID beside NF-κB signalling ..... 31

1.8.2 Current limitation in TRABID research ..... 32

1.9 Thesis aim and findings ..... 33

Chapter 2: Assessing dTRABID biochemistry, *in vitro* ..... 35

2.1 Introduction ..... 35

2.2 Sequence alignment ..... 35

2.3 dTRABID has similar enzyme specificity as hTRABID ..... 38

2.4 Discussion ..... 40

Chapter 3: Inactivating dTRABID *in vivo* has a different impact on males and females' locomotor activity, sleep patterns, and lifespan ..... 41

3.1 Introduction ..... 41

3.2 Locomotor activity assay ..... 41

3.3 *Drosophila* sleep monitoring ..... 44

3.4 Lifespan assay ..... 48

3.5 Immunofluorescence quantification of neuron and glia ..... 51

3.5.1 Projected brain area and total cerebral cell quantification.....51

3.5.2 Glia quantification .....52

3.5.3 Neuron quantification .....52

3.6 Discussion .....57

Chapter 4: Reversing sex in *trbd* female flies reduces sex bias in locomotor activity.....60

4.1 Introduction .....60

4.2 Reducing female development in astrocyte or immunocompetent tissues closes sex bias gap in locomotor under *trbdC518A* background .....62

4.3 Discussion .....64

Chapter 5: Brain AMP expression differences.....65

5.1 Introduction .....65

5.2 Difference in antimicrobial peptides and neurodegeneration maker expression in *trbdC518A* and $w^{1118}$ brains .....66

5.3 Tissue specific blocking female development reduced sex bias in certain AMPs .....69

5.4 Discussion .....75

Chapter 6: TRABID has sex-specific impacts in ubiquitination accumulation

and protein ubiquitination *in vivo.* ..... 78

6.1 Introduction ..... 78

6.2 Genes and pathways enriched in STRING database search ..... 81

6.2.1 Hsc70-4 is sex-specifically regulated ..... 81

6.2.2 Female specific Yp family proteins and related pathways ..... 84

6.2.3 Sex bias in pathways related to locomotor activity ..... 84

6.3.4 Female specific ubiquitylation in circadian rhythm ..... 85

6.3.5 Sex dimorphism in neuron development and neurotransmitter ..... 85

6.3.6 Divergence in immunity between males and females ..... 86

6.3.7 Sex dimorphism in ubiquitin linkages and ubiquitin-proteasome system (UPS) ..... 88

6.3.8 *In silicon* analysis of dTRABID directly regulated pathways ..... 91

6.4 Discussion ..... 93

Chapter 7 Conclusion and discussion ..... 95

7.1 Conclusion ..... 95

7.2 Discussion ..... 95

7.2.1 Biochemistry ..... 95

7.2.2 Cellular biology ..... 98

7.2.3 Neurobiology ..... 100

7.2.4 Omics studies ..... 102

7.3 Limitation of the study ..... 103

7.4 Significance of the study ..... 104

Chapter 8: Materials and methods ..... 105

8.1 dTRABID-AnkOTU and dTRABID-AnkOTU cloning and protein purification ..... 105

8.1.1 Cloning dTRABID-AnkOTU and dTRABID-AnkOTUC518A into pOPIN vectors. ..... 105

8.1.2 Protein expression and purification ..... 108

8.1.3 Deubiquitylase assays ..... 113

8.2 Behaviour and brain histology assays ..... 113

8.2.1 Fly husbandry and crossing ..... 113

8.2.2 Locomotor activity assay ..... 114

8.2.3 *Drosophila* activity monitoring (DAM) ..... 116

8.2.4 Lifespan assay ..... 116

8.2.5 *Drosophila* brain immunofluorescence assay ..... 117

8.3 Method of reducing female development in *trbdC518A* background .. 119

8.4 Sample preparation for *Drosophila* brain AMPs expression..... 122

8.5 Sample preparation for GlyGly enrichment and LC-MS..... 124

Chapter 9: Appendices..... 131

9.1 Supplement figures and tables for LC-MS ..... 131

9.1.1 Volcano plots and table..... 131

9.1.2 Tables for Venn diagram analysis and STRING database search ... 140

9.1.3 Reagent and material table..... 150

9.2 COVID-19 statement..... 152

9.3 Bibliography..... 152

## Figures and Tables

Graphic abstract..... iii

Figure 1.1 Ubiquitin structure, linkages, and modification.....3

Figure 1.2 The process ubiquitylation .....6

Figure 1.3 The function and mechanism of DUBs.....12

Figure 1.4.1 The process of cysteine protease hydrolysis. .....14

Figure 1.4.2 Representative structure of different cysteine protease domains .....18

Figure 1.5 Cartoon drawing of the A20 family members .....21

Figure 6.1 Cartoon drawing of TNFR1 and IMD pathway activation .....26

Figure 2.2 Amino acid sequence and structure alignment of hTRABID and dTRABID.....37

Figure 2.3 dTRABID-AnkOTU and dTRABIDAnkOTUC518A enzymatic activities toward diubiquitins.....39

Figure 3.2 Climbing assay showed that trbdC518A was more deleterious in male flies.....43

Figure 3.3 DAM result for total sleep time (TST), total sleep episode (TSE) and mean sleep time (MST) at light period (LP) and dark period (DP) .....46

Figure 3.4 Survival plot of trbdC518A and w1118 on females and males .....50

Figure 3.5 Immunofluorescence quantification indicated neuron and glia lost in *trbdC518A* males ..... 55

Figure 4.2 Climbing assay of *trbdC518A*, *UAS-traRNAi/alrm-Gal4;trbdC518A* and *UAS-traRNAi/J6-Gal4;trbdC518A* with their controls ..... 63

Figure 5.2 AMPs expression in day 3 and 18 *trbdC518A* and $w^{1118}$ flies' brains. ..... 68

Figure 5.3.1 AMPs expression in day 3 and 18 *alrm-Gal4/UAS-*$tra^{RNAi}$*;trbdC518A* and *alrm-Gal4;trbdC518A* flies' brains..... 71

Figure 5.4.2 AMPs expression in day 18 *J6-Gal4/UAS-*$tra^{RNAi}$*;trbdC518A* and *J6-Gal4;trbdC518A* flies' abdomen and thorax or brains..... 74

Figure 6.3.1 Ubiquitinomics and proteomics analysis reveals sex bias in gene ontology and interactome enrichment in the heads of *trbdC518A* and $w^{1118}$ .. 83

Figure 6.3.8 Venn diagram of cross referencing GOs generated by Harris et al., and GOs from our GlyGly enrichment. ..... 92

Figure 7.2 Phosphorylation and ubiquitylation site of TRABID..... 97

Figure 8.1.1 Molecular data for cloning dTRABID-AnkOTU and dTRABID-AnkOTUC518A. ..... 107

Figure 8.1.2.1 Chromatography result for dTRABID-AnkOTU ..... 110

Figure 8.1.2.2 Chromatography result for dTRABID-AnkOTUC518A ..... 111

Figure 8.2 Generating homozygous trbdC518A fly and climbing assay. ..... 115

Figure 8.3 Strategy of integrating tissue specific *tra*$^{RNAi}$ into trbdC518A background. ..... 120

Table 8.4 Primers for qPCR assay. ..... 123

Figure 8.5.1 Quality control of ubiquitinomics and proteomics data. ..... 127

Figure 8.5.2 Distributions of total protein exclusive protein reads after log transformation and width adjustment normalisation. ..... 130

Figure 9.1.1 Volcano plots and tables for t-tests ..... 132

Table 9.1.2.1 Result table for Venn diagram analysis ..... 140

Table 9.1.2.1 STRING database search pathway results ..... 143

# Chapter 1: Introduction

## 1.1 Ubiquitin

Ubiquitin is a 76 amino acid protein widely conserved from invertebrates to vertebrates. It was first discovered by Avram Hershko, Aaron Ciechanover and Irwin Rose, who were awarded the 2004 Nobel Prize in Chemistry. They were using rabbit immature red blood cell lysates, which lack lysosomes and are rich in proteases, to test proteolysis and discovered that the observed degradation was driven by ATP and was dependent on a small heat stable proteinaceous substance. They published their result about an unusual small ATP-dependent and heat stable protein that “aggregates” during protein degradation (Ciechanover et al., 1980). However, subsequent analysis by Wilkinson et al., (1980) found that this “universally presented” protein, ubiquitin, had already been identified twice in the mid-70s in other studies (Wilkinson et al., 1980). Since the discovery, for many years, ubiquitin was closely linked to the ubiquitin-proteasome system (UPS). Only around the new millennium, researchers started to realise its non-proteolytic role (Callis, 2014).

This 8 kDa protein can be conjugated to each other ubiquitin molecules via seven internal lysine residues (Lys6, 11, 27, 29, 33, 48 and 63) and N terminus (Met1) (Figure 1.1A), forming eight different ubiquitin linkages (Figure 1.1B). Polyubiquitin chains can be homozygous or heterozygous (Figure 1.1C first row) (Amer-Sarsour et al., 2021). The topology of the ubiquitylated substrate will determine its future in

the context of cellular processing. Additional complexity of the ubiquitin code results from the observation that ubiquitin can be further modified by other post-translation modification, including NEDDylation, SUMOlyation, acetylation phosphorylation etc (Figure 1.1C second row). There can be multiple post-translation modification on ubiquitin chains (Figure 1.1C third row).

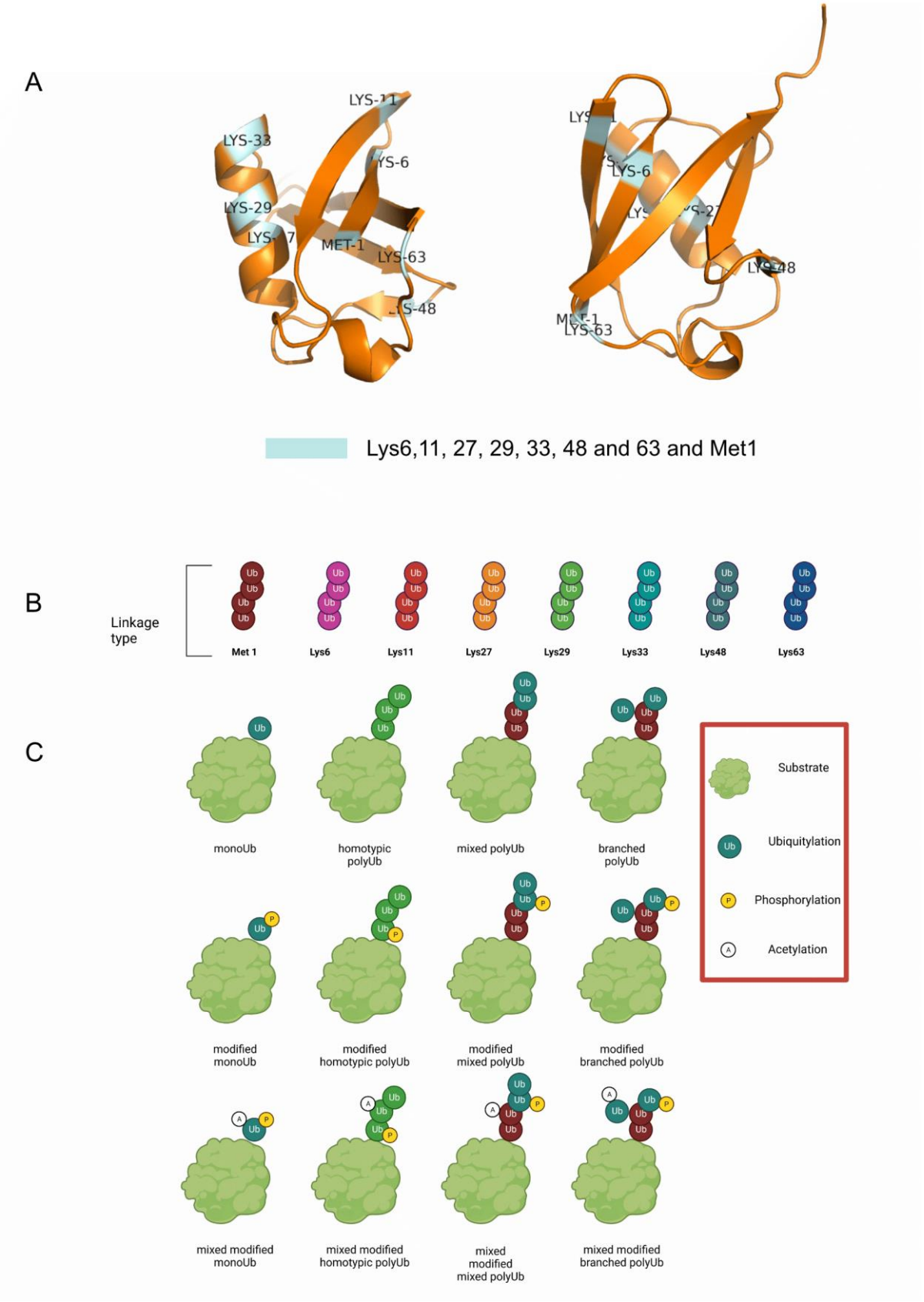



**Figure 1.1 Ubiquitin structure, linkages, and modification**. (A) Ubiquitin (PDB:1UBQ) structure showing seven Lys residues and N terminal Met (coloured in sky blue) that are able for polyubiquitylation. (B) Ubiquitin can link to each other from

seven Lys residues and N-terminal Met and form eight different type of linkages. (C) Substrate can be modified by ubiquitin (monoUb), homotypic polyubiquitin chain (homotypic polyUb), mixed polyubiquitin chain or branched polyubiquitin chain (branched polyUb) (first row). Ubiquitin modification can occur at multiple sites simultaneously. Ubiquitin signals can be further modified by other post-translation modification, including phosphorylation, acetylation, NEDD8 and SUMO (second row). These further modification signals can be combined together to provide a new degree of modification to the ubiquitylation signals (third row). Free-float ubiquitin chains, ubiquitin chains that are not attached to a substrate, serve as messengers in cells and can be modified by the same way as substrate-attached ubiquitin chains.

## 1.2 Ubiquitylation

Ubiquitylation involves in a cascade of ubiquitin ligases known as E1s, E2s and E3s. In humans, there are 2 E1s, 38 E2s and about 1000 E3s (Amer-Sarsour et al., 2021). Firstly ubiquitin-activating enzyme (E1) hydrolysis an ATP and adenylates ATP to the glycine residue at the C terminal of ubiquitin. The ubiquitin is further linked to the active cysteine site of E1 (Passmore and Barford, 2004). The activated ubiquitin is further passed on to an active cysteine residue on a E2 ubiquitin conjugating enzyme (E2) through transthiolation reaction. An E3 ubiquitin ligase (E3) works with an E2 to transfer ubiquitin onto a substrate, usually on to a lysine residue. E3 can bind to E2 and the substrate at the same time (Figure 1.2) (Stewart et al., 2016). E3s are categorized into four classes – HECT (homologous to the E6AP carboxyl terminus), RING (Really Interest New Gene), RBR (RING-Between-RINGS) and U-box (Passmore and Barford, 2004; Yang et al., 2021). HECT family is categorized by the E6-associate protein C-terminus domain, where the active E2 transfer the ubiquitin to the cysteine site. Unlike HECT ligases, which transfer ubiquitin from active E2 to HECT E3 and then transfer ubiquitin to substrate, RING family ligases only bind to active E2 ligase through RING domain and help ubiquitin transfer from E2 ligase to substrate. RBR is categorized by RING1, a central in-between-RING (IBR) and RING2 domain. The RING1 domain binds to active E2 conjunction enzyme and RING2 and IBR are able to receive ubiquitin at a cysteine site. U-box ligase family is characterized by a 70 amino acids U-box domain. E2 conjunction enzyme bind to U-box domain and transfer ubiquitin to substrate (Yang et al., 2021).

Besides processing ubiquitin, they also can process ubiquitin-like proteins (UBL) (Amer-Sarsour et al., 2021).

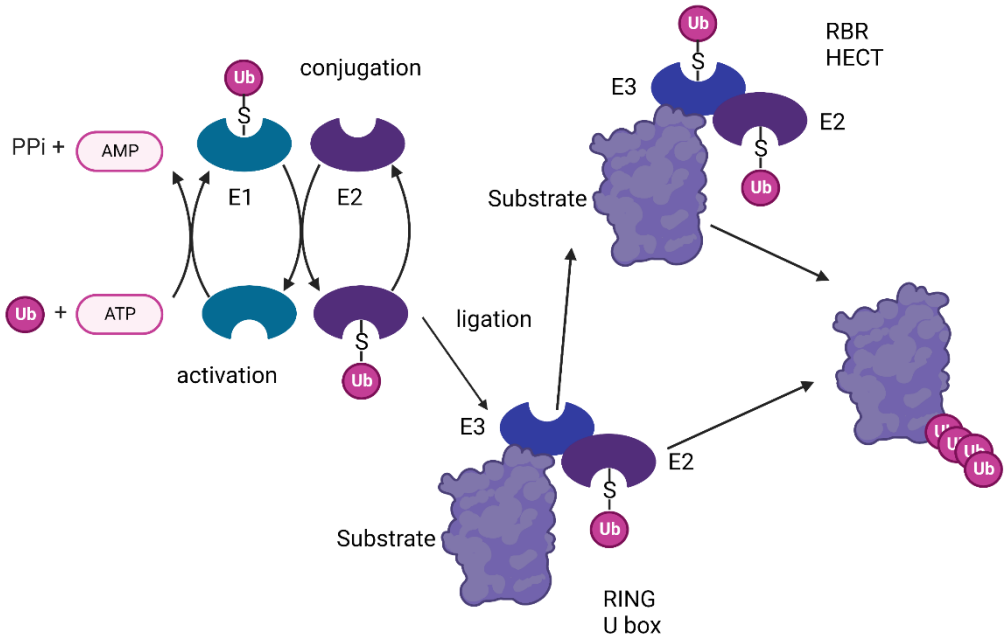



**Figure 1.2 The process of ubiquitylation**. E1 catalyses the adenylation of ubiquitin C-terminal carboxyl group and ubiquitin is transferred to a cystine residue on E1 forming a thioester bonded ubiquitin. This step is called activation. After ubiquitin is activated, the ubiquitin is further transferred to a cystine residue on the E2. This step is called conjugation. The last step is ligation. Depending on the E3 ligase, the ligation step can be direct or indirect. For example, RING and U box E3 ligases bind to the substrate and the E2-bonded ubiquitin is transferred to the substrate. On the other hand, RBR and HECT E3 ligases need to transfer the E2-bonded ubiquitin to a cysteine on the E3 and then transfer to the substrate. Ubiquitin can form thioester bond with lysine, serine or cystine residues on the substrate.

## 1.3 Deubiquitylation

The process of ubiquitylation is usually dynamic and rapid. After the signal is decoded and processed, ubiquitin signals need to be “erased” by ubiquitin hydrolysis enzymes, which are known as deubiquitylases (DUBs). DUBs have three major functions — process, recycle and edit. First, ubiquitin is transcribed from polygene or conjugated with ribosomal proteins. Deubiquitylase is needed to process polyubiquitins and ribosomal-conjugated ubiquitins into free monoubiquitins. (Komander et al., 2009; Pickart, 2001) (Figure 1.3.1A). After substrate ubiquitin signal is processed, deubiquitylase is recruited to hydrolyse ubiquitin chains into free monoubiquitin for recycle (Figure 1.3.1B). The recycle process can prevent substrate been processed, for example cleavage of Lys48 ubiquitin chains can rescue a substrate from degradation from proteasome (Komander et al., 2009). Deubiquitylase can also prune ubiquitin chains on substrate and edit cellular signal (Figure 1.3.1C) (Komander et al., 2009). Cleaved monoubiquitins are recycled into the free ubiquitin pool.

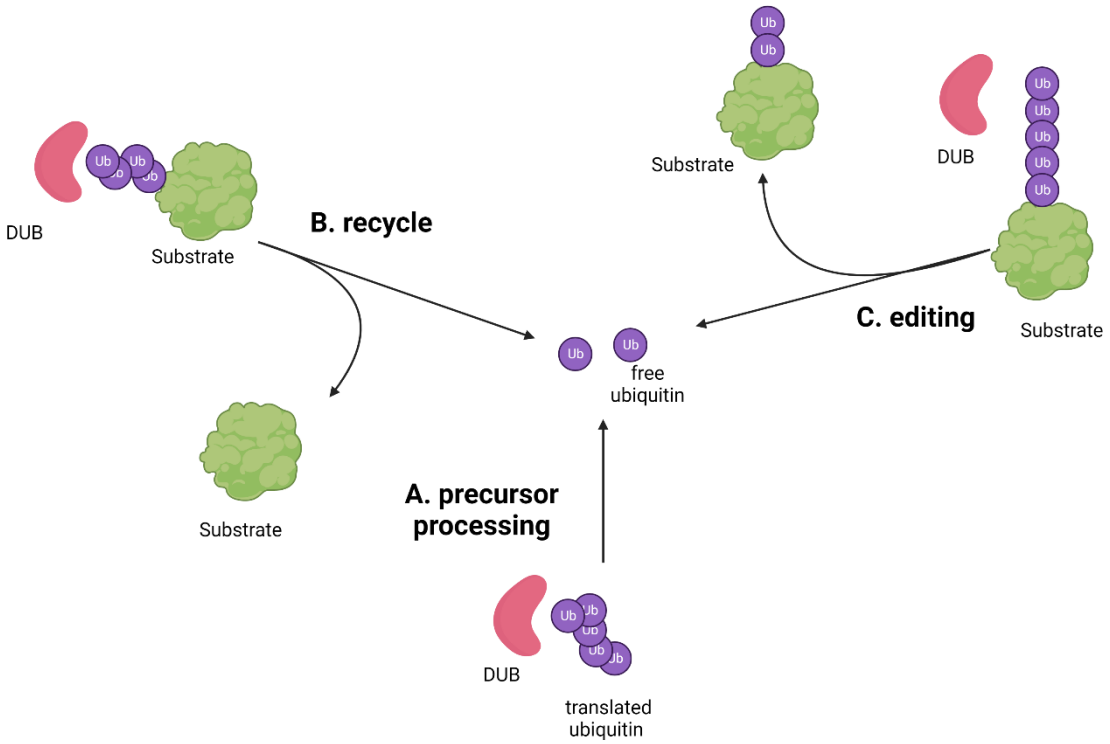



**Figure 1.3.1 Different roles of deubiquitylases (DUB).** (A) Some genes code polyubiquitin. DUBs are involved in the process of modifying these translated polyubiquitin to free ubiquitin. (B) DUBs can cleave ubiquitin chains off substrates preventing them from degradation and other cellular processing. The cleaved-off ubiquitin chains are further hydrolysed and recycled. (C) Ubiquitin chains on substrate are partially hydrolysed by DUB, a way of editing the topology of ubiquitin chain, and generating new ubiquitin signal for cellular processing. The hydrolysed ubiquitins are recycled.

There are two major recognition mechanisms depending on recognition target. Some DUBs recognize topology of ubiquitin chain (Figure 1.3.2A) and some recognize specificity of substrate (Figure 1.3.2B). Ubiquitin enzymes, E3 ligases and DUBs contain a wide range of contain ubiquitin-binding domains (UBDs), which provide specificity for enzyme to recognize different combination of ubiquitin chains or ubiquitin like proteins. UBD bind non-covalently to ubiquitin through defined surfaces on ubiquitin, the most common being the Ile44 patch (Hicke et al., 2005). UBDs are often 20-150 amino acid in size and are categorised to 5 major classes by their structural fold (Pickart, 2001). Alpha-helical motifs are characterised by single or multiple alpha helixes. Zing finger motifs contain a Zn ion surrounded by four beta strands (Wang et al., 2003). The feature of Pleckstrin-homology motifs is a 7-stranded beta-sheet with a C-terminal alpha-helix and multiple phosphoinsitides (Rebecchi and Scarlata, 1998). Ubiquitin-conjugating-related motifs are relatively large (~150 amino acid) and are found in E2 enzymes. They consist of four helixes and a 4-stranded antiparallel beta-sheet (Pickart, 2001). Src homology 3 motifs are categorised by a beta- barrel fold and their binding to proline-rich domains (ProXXPro). However, there are other UBDs that don't fit into these categories (Randles and Walters, 2012).

After target recognition, DUB need to hydrolyse ubiquitin chain. First, DUB can cleave the chain from the distal ubiquitin chain, the end of ubiquitin chain that can be grown, which is known as exo-cleavage (Figure 1.3.2 C). On the other hand, DUB

hydrolysis that happened not at the distal end of ubiquitin chain is called endo-cleavage (Figure 1.3.2 C) (Yau and Rape, 2016). Branched and mixed ubiquitin chains can prevent cleavage from linkage specific DUBs. Unspecific DUBs may play a role in the debranching process (Figure 1.3.2 D) (Mevissen and Komander, 2017). Ubiquitin chain can be further altered by other post-translation modification. *In vitro* experiments showed that many DUBs can hydrolyse modified ubiquitin chains or mixed chains (Figure 1.3.2 E) (Mevissen and Komander, 2017; Wauer et al., 2015). Ubiquitin and UBLs can form mixed chains and specific DUBs are needed to cleave ubiquitin-UBL linkages. For example, USP7 can cleave SUMO-ubiquitin linkage (Figure 1.3.2 E) (Lecona et al., 2016).

Specificity is crucial for DUBs to recognize different substrates. There are different layers to distinguish different ubiquitin linkages and chain structures (Figure 1.3B). UBDs, including zinc finger ubiquitin-specific protease domain (ZnF-UBP domain), ubiquitin-interacting motif (UIM) and ubiquitin-associated domain (UBA domain), are abundant in DUBs. Beside the UBDs, the catalytic domains of DUBs also provide specificity (Figure 1.3B) (Pickart, 2001). DUBs interact with multiple sites in the distal ubiquitin and allow it to firmly hold the polyubiquitin chain. Ile44 patch on ubiquitin is generally important for DUB recognition. Ubiquitin-like (UBL) proteins, such as small ubiquitin-like modifier (SUMO), interferon-stimulated gene 15 (ISG15) and neuronal precursor cell expressed developmentally downregulated protein 8 (NEDD8) differ from ubiquitin though having an identical fold of ubiquitin but have

different interaction surfaces, in particular when some UBLs like NEDD8 and ISG15 have similar C-terminus to ubiquitin. Some DUBs have dual activities toward ubiquitin and ubiquitin-like proteins, in particular when some UBLs like NEDD8 and ISG15 have similar C-terminus to ubiquitin (Komander et al., 2009). The quaternary structure of different ubiquitin chains can be recognised by certain DUBs that allow them to cleave specific polyubiquitin linkages. These linkage specific DUBs work through different mechanisms however, the mechanisms still remain largely unknown (Ohtake et al., 2015).

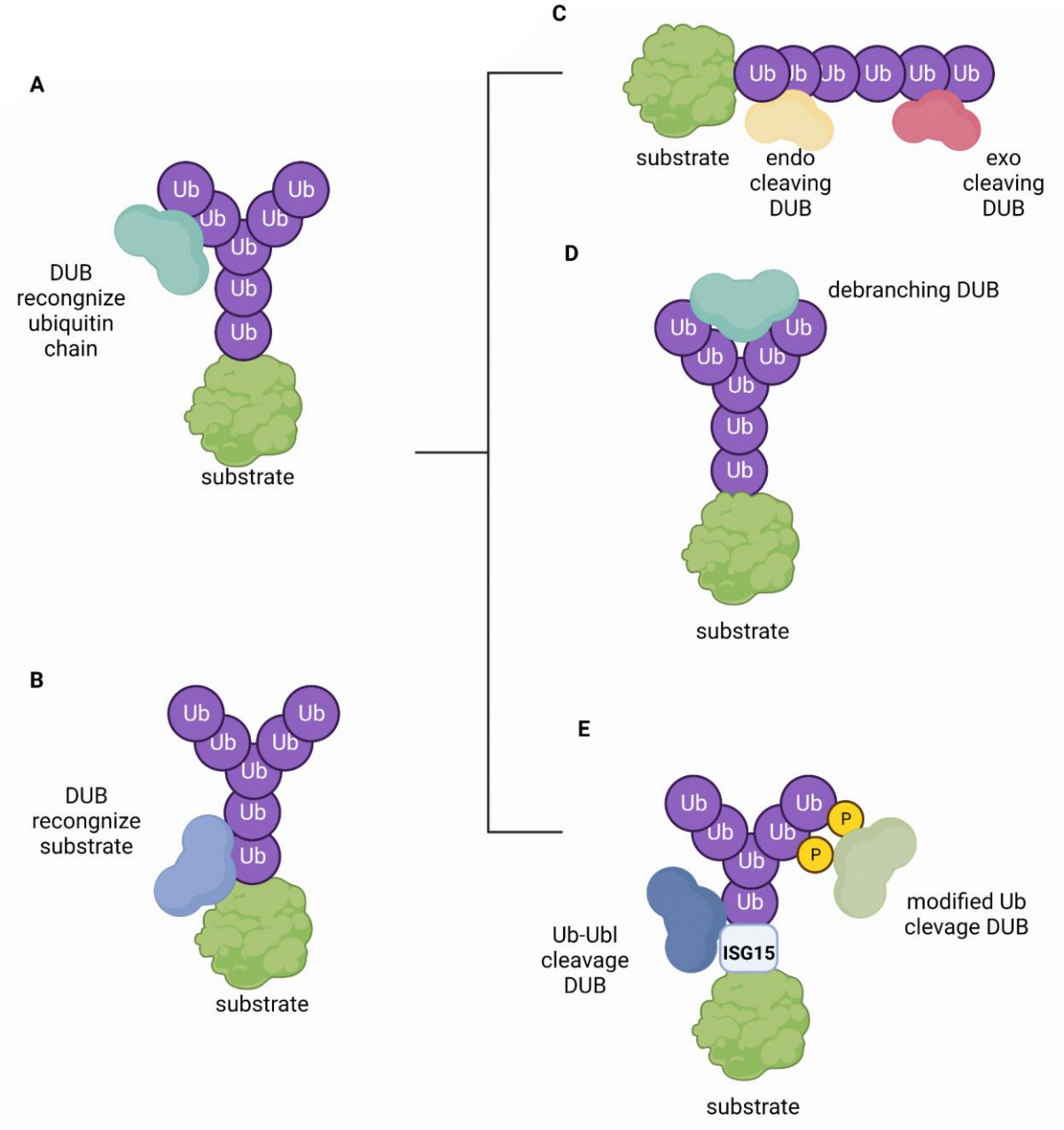



**Figure 1.3.2 Different types of DUB hydrolysis**. (A) There are DUBs that specifically bind to ubiquitin chains and (B) DUBs that recognise and bind to substrates. DUBs that bind to ubiquitin chains can further be categorised to different types according to their cleavage specificity. (C) DUBs that cleave from the distal end of ubiquitin chains (exo-cleavage) and DUBs that cleave from internal linkages (endo-cleavages). (D) There are DUBs specifically recognise branched ubiquitin chains and cleave from the branch. (E) There are DUBs that specifically recognise Ub-Ubl linkages and cleave the linkage. There are DUBs that can recognise and hydrolyse modified ubiquitin chains.

There are two major deubiquitylase families, cysteine protease and zinc metalloprotease, categorised by their mechanism of hydrolysis. The cysteine protease family contains USPs (ubiquitin-specific proteases), OTUs (ovarian tumour), Josephins, UCHs (ubiquitin carboxy-terminal hydrolase) and the motif interacting with ubiquitin (MIU) containing novel DUB family (MINDY). The zinc metalloprotease family contains JAMM/MPN+ (Mevissen and Komander, 2017; Shrestha et al., 2014).

## 1.4 Cysteine protease family DUBs

These DUBs operate through a catalytic cysteine (Komander et al., 2009). The cysteine performs nucleophilic attack by the polarizing histidine via aspartate or asparagine in catalytic triad or via other means in dyad. Nucleophile attack hydrolyses the isopeptide bond between the ubiquitin and substrate or isopeptide bond between the polyubiquitin chains (Roy et al., 2022) (Figure 1.4.1).

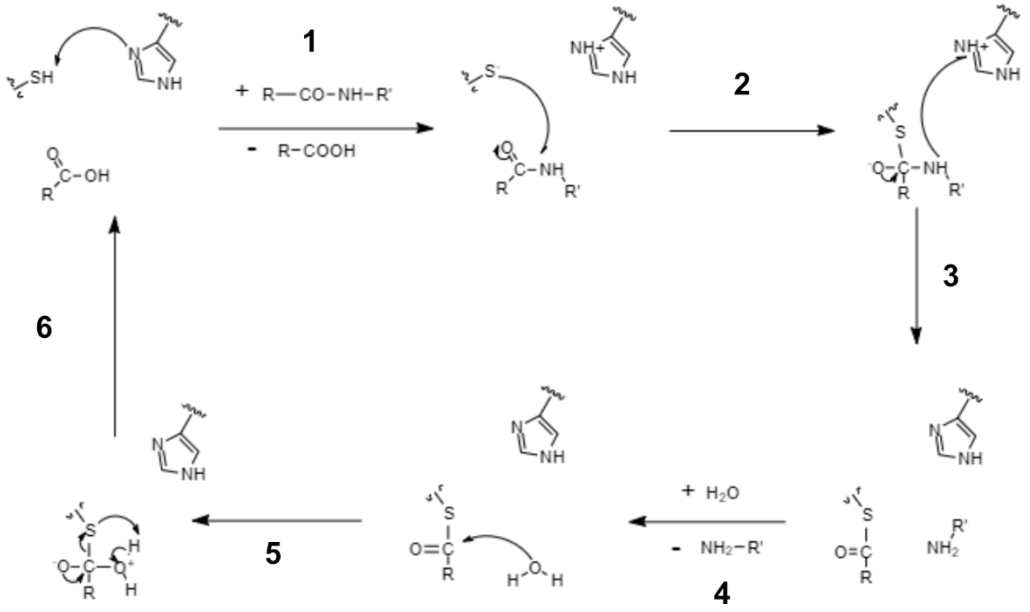



**Figure 1.4.1 The process of cysteine protease hydrolysis.** (1) The cysteine protease catalyses the deprotonation of a histidine. (2) The deprotonated cysteine attacks substrate carbonyl carbon. (3) A substrate with an amine terminus is released and the histidine residue of the enzyme is restored. A thioester linkage in the cysteine is formed (4 and 5) The thioester bond is hydrolysed (6) Finally a carboxylic acid moiety is generated and regenerating the free enzyme.

Although they share the same mechanism of hydrolysis, they can be further categorised into six families according to their catalytic domain.

*USP domains*

USP is the largest family of DUBs and is known for their role in unspecific deubiquitylation. The USP catalytic domain, which is like an open hand consisting of thumb fingers and palm. Between the thumb and fingers, lies the catalytic site (Komander et al., 2008) (the catalytic domain of CYLD is presented in 1.4.2A).

*OTU domains*

Enzymes in this family are linkage-specific DUBs. The domain contains 5 beta-strands that are in the middle of helical domains and nucleophile site of OTU has a loop that are not seen in other DUB families (Messick et al., 2008; Suresh et al., 2010) (the catalytic domain of OTU1 is presented in 1.4.2B). This domain consists of three subdomains, Otubains, A20-like OTUs and OTUDs. However, members that have the subdomains do not have the same linkage specificity. An *in vitro* screen of the OTU DUBs in digesting diubiquitin chains shows that they can be divided into four groups, depending on the number of linkage type that they can cleave. For example, in the Otubains, OTUB1 is Lys48 specific (Group I) and OTUB2 has preferential activity towards Lys63 diubiquitin chains and reduced activity towards Lys11 and 48 chains (Group III) (Mevissen et al., 2013).

*UCH enzymes*

The UCH domain is characterized by a loop covering the catalytic site. When binding to ubiquitin the loop serves as lasso straddling the ubiquitin C-terminal. It also prevents the entry of large conjugating proteins (Mevissen and Komander, 2017; Misaghi et al., 2005) (the catalytic domain of UCHL3 is presented in 1.4.2C).

*Josephins*

Josephins have preference of cleaving Lys48 and 63 linkages and have a signature helical arm at the C-terminal, which is used to bring ubiquitin chain toward the catalytic domain (Mao et al., 2005). Members of this family, Ataxin-3 (ATXN3) and Ataxin-3L, have a higher activity towards longer Lys48 and 63 ubiquitin chains (Mao et al., 2005; Zeng et al., 2020) (the catalytic domain of ATXN3 is presented in 1.4.2D).

*MINDYs*

This is a new family of DUBs and is a Lys48-specific DUB family. The best studied member is MINDY-1 (MINY1), which preferentially cleaves long polyubiquitin chain from the distal end (Abdul Rehman et al., 2016). The Cys loop regulates the enzymes catalytic activity but not linkage selectivity, by conformational changes (Rehman et al., 2021) (the catalytic domain of MINY is presented in 1.4.2E).

*ZUP family*

ZUFSP (ZUP1) is currently the only member in this family. It has no homology to other DUBs. It has highly selectivity towards Lys63 polyubiquitin chains. The ZHA binding domain (ZUFSP helical arm) that is extended from the catalytic domain helps to bind to the very far end (distal) ubiquitin. ZHA is likely to bring the distal ubiquitin toward the catalytic domain and consequently have the ubiquitin chain hydrolysed (Kwasna et al., 2018).

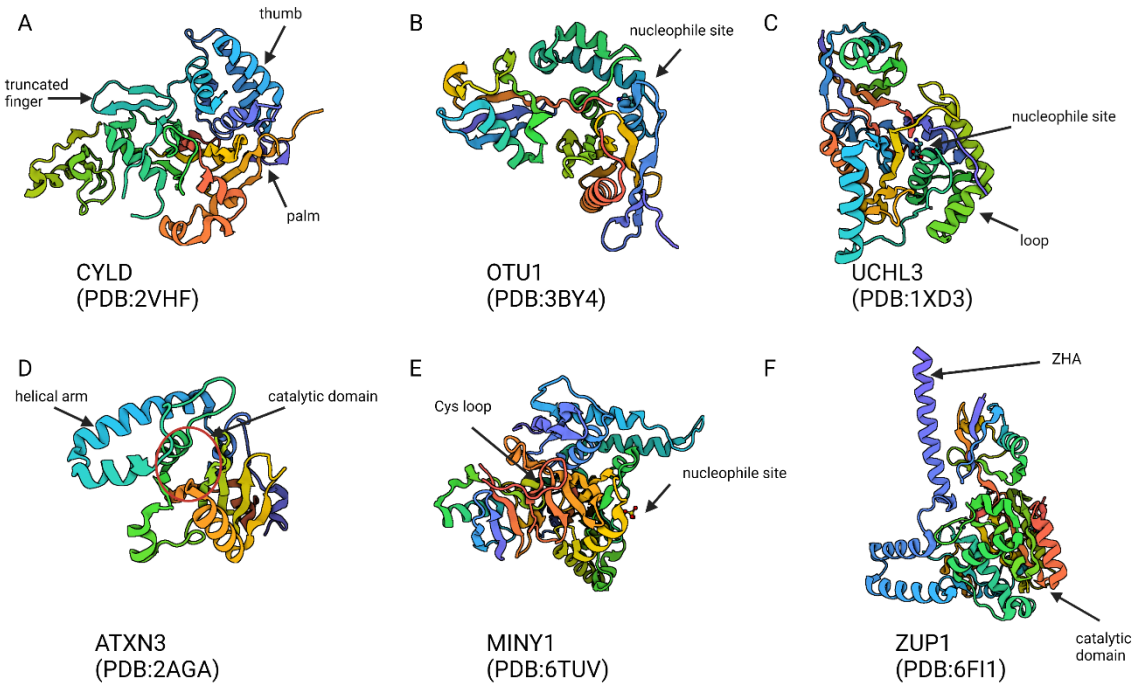



**Figure 1.4.2 Representative structure of different cysteine protease family.** All families consist of a cysteine catalytic domain, which contains a nucleophile site. (A) CYLD representing USP family. The “fingers” are used for binding and enzyme specificity. The “palm” is the cysteine protease domain. (B) OTU1 representing OTU family, with the catalytic domain containing a cysteine nucleophile site. (C) UCHL3 representing UCH family. The loop is used for selecting specific ubiquitin linkages that can be hydrolysed by nucleophile site. (D) ATXN3 representing Josephins family. The helical arm helps to bring specific chain types towards the cysteine catalytic domain. (E) MINY1 representing MINDY family. The conformational change of the cys loop will affect the activity of the nucleophile site. (F) ZUP1 representing ZUP family. The ZHA arm helps to bring longer chains towards the cysteine catalytic domain.

## 1.5 A20 sub-family DUBs

A20 sub-family belongs to the OTU (ovarian tumor) family DUB. A20, Cezanne and TRABID are known members of the A20-like subfamily. They have high level of consensus in their OTU enzymatic domain. In A20, the OTU domain is at the N terminal end (92-261) and seven Cys2-Cys2 zinc fingers regions (ZnF-A20) at C-terminal (Figure 1.5A). The fourth ZnF-A20 is predicted to be involved in E3 ligase activity (Enesa and Evans, 2014). A20 has high hydrolysis activity towards Lys48 ubiquitin chains and less hydrolysis activity towards Lys11 ubiquitin chains (Mevissen et al., 2013).

Cezanne has a ubiquitin-associated (UBA)-like domain at the N terminal (4-49) (Figure 1.5B) that binds to Lys11, 48 and 63 and Met1 ubiquitin chains (Mader et al., 2020). Cezanne OTU domain (185-365) (Figure 1.5B) provides specificity towards Lys11 diubiquitin hydrolysis (Mevissen et al., 2016). The C terminal half of Cezanne (366-919), including a ZnF-A20 domain (Figure 1.5B), assists in hydrolysis of branched ubiquitin chains (Evans et al., 2003).

Trabid has three Npl zinc finger (NZF) regions at N terminal end (Figure 1.5C). NZF1 (3-33) provides specificity towards Lys29 and 33 diubiquitins. NZF2 and 3 (84-178) assist binding to longer ubiquitin chains (Licchesi et al., 2012). Ankyrin repeat domain (260-340) provides the specificity of binding to Lys29 and 33 ubiquitin chains

and inhibits the biding of Lys63 ubiquitin chains (Figure 1.5C) (Hua et al., 2022; Licchesi et al., 2012). OTU domain (261-340) hydrolysis Lys29, 33 and 63. AnkOTU (261-592) domain preferentially cleaves Lys29 and 33 diubiquitin chain and hydrolyses Lys63 diubiquitin at a slower rate.

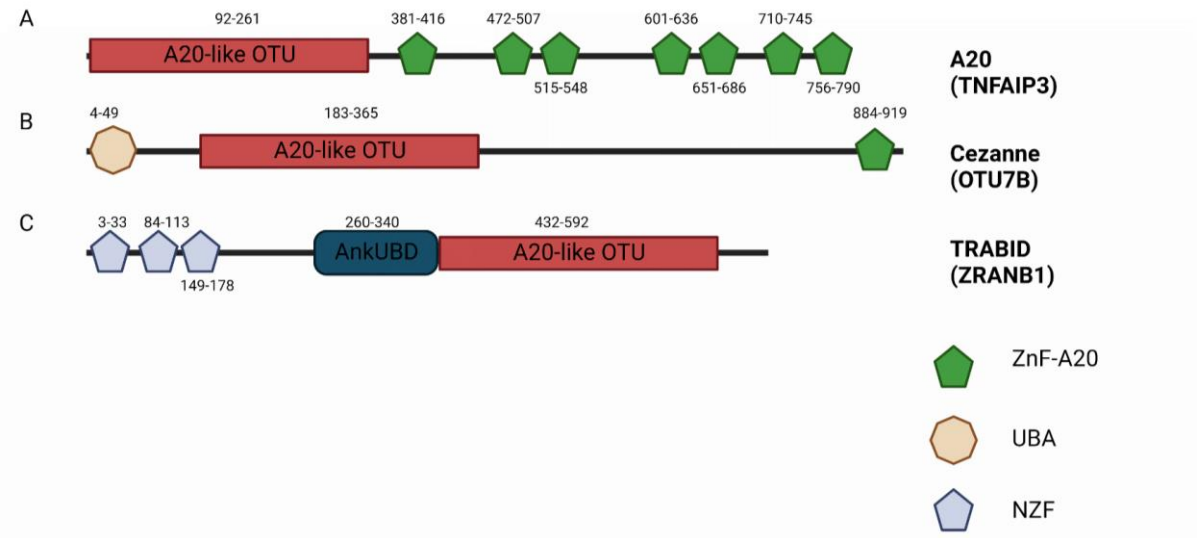



**Figure 1.5 Domain schematic of the A20 family members.** (A) A20 (TNFAIP3) has the OTU enzymatic domain at the N terminal end (92-261), which provide hydrolysis activities on Lys11 and 48. Seven zinc fingers, A20-type (ZnF-A20) follows OTU domain (381-790). (B) Cezanne (OTU7B) has a UBA domain (4-49), which provides specificity towards ubiquitin binding. The UBA is followed by OTU enzymatic domain (183-365) which can hydrolysis Lys11 ubiquitin. At the C terminal there is a ZnF-20 (884-919). (C) TRABID (ZRANB1) has three Npl4 zinc fingers (NZF) at the N terminal. NZF1 (3-33) provides specificity towards specific ubiquitin linkages (Lys29, 33 and 63). NZF2 (84-113) and NZF3 (149-178) enhance binding affinity towards longer chains. AnkUBD domain supresses the binding towards Lys63 ubiquitin chains. OTU domain provides hydrolysis activity on Lys29 and 33 ubiquitin chains.

## 1.6 TNFR1/IMD-induced NF-κB signalling

Innate Immunity is the first line of host defense, evolutionary conserved in all metazoans. NF-κB signalling is a major player in innate immunity, and the regulation of the pathway is heavily regulated by ubiquitylation and deubiquitylation. TNFR1 (*Drosophila* ortholog is Imd) pathway is the immune response for Gram-negative bacteria. When the membrane protein TNFR1 is activated, its intracellular domain will recruit TNF receptor-associated death domain (TRADD), which can further recruit adaptor proteins, including receptor-interacting protein 1 (RIP1), TNFR-associated factor 2 (TRAF2) and Fas-associated death domain (FADD) (Figure 1.6A). FADD can further recruit Caspase 8, which can release RIP1 to form a complex with transforming growth factor-β (TGF-β)-activated kinase 1 (TAK1) and TAK1-binding protein2 (TAB2) (Figure 1.6A 1 to 4). This complex needs to be ubiquitylated by TRAF6 and cIAP to further activate IκB kinase complex (IKK), which consists of two catalytic subunit IKKα and IKKβ and a regulatory subunit, NF-κB essential modulator (NEMO). IKK is also tightly regulated by ubiquitin modification. Besides the Lys63 chains from TRAF6 and cIAP2 (inhibitor of apoptosis protein2), LUBAC (linear ubiquitin chain assembly complex)-synthesised Met1 chains are also important for the activation of IKK (Figure 1.6A 5 and 6). The activation of IKK leads to the phosphorylation of the IκB-NF-κB (p65/p50) complex and results in the degradation of IκB at the C-terminal and the release of heterodimer p65/p50 into the nucleus (Figure 1.6A 7 and 8). This results in the activation and production of interleukins (IL) such as IL6 considered a hallmark of TNFR1-induced inflammation

(Al-Lamki and Mayadas, 2015; Chen and Goeddel, 2002, ; Ji et al., 2016) (Figure 1.6A).

In 1995, the first research that confirmed TNFR1 activated NF-κB signalling in mammals was published (Hsu et al., 1995). Later that year, the work of *Drosophila* immune deficiency (Imd) regulating NF-κB induced antimicrobial responses was published (Lemaitre et al., 1995). *Drosophila* IMD pathway is homologous to the mammalian TNFR1 pathway. They share a high degree of similarity in cellular components and signal regulation. Like TNFR1 activation, activation of cell membrane proteins PGRPs will recruit adaptor proteins, including Imd (ortholog of RIP1, without the kinase domain) and FADD (ortholog of FADD). The complex further recruits the caspase Dredd (ortholog Caspase8) to release Imd. Dredd need to ubiquitylated by UEV1a, Effete (Ubc5) and Bendless (Ubc13) (Figure 1.6B 1 and 2). The released Imd is further ubiquitylated by dIAP2 (ortholog cIAP2) and forms a complex with Tak1-TAB2 (ortholog TAK1 and TAB2). The Tak1-TAB2 complex is further ubiquitylated by Lys63 ubiquitin via dTRAF6 (ortholog TRAF6) (Figure 1.6B 3 and 4). The activated Tak1-TAB2 complex can further bind and phosphorylate Kenny (ortholog of IKK). Like IKK, Met1 ubiquitylation is involved in the activation of Kenny. LUBEL (ortholog of LUBAC) is the E3 ligase (Aalto et al., 2019) and CYLD is the deubiquitylase (Elliott et al., 2016) (Figure 1.6B 5 and 6). Active Kenny can further phosphorylate Relish (human ortholog IκB-p50/p65). Unlike the human IκB complex, Relish is a composite protein containing both IκB and NF-κB domains. Lys63

ubiquitylated Dredd is needed to cleave off the IκB domain of Relish, which is the C-terminal ankyrin repeat domain. Following this, the N-terminal NF- κB (Rel) domain is released to the cell nucleus. Different from the mammalian heterodimer p65/p50, Rel needs to form a homodimer in the nucleus to activate a certain set of antimicrobial peptide genes (AMPs), such as *Diptericin* and *Cecropin*. (Myllymäki et al., 2014) (Figure 1.6B 7 and 8).

Although the IMD and TNFR1 pathways are relatively similar, there are still a few differences between them. For example, in mammals, both OTULIN and CYLD targets Met1 polyubiquitin on IKK (Figure 1.6A 6). However, *Drosophila* doesn't have any gene encoding OTULIN, thus CYLD is the only known DUB cleaving the LUBEL (linear ubiquitin E3 ligase)-synthesized Met1 polyubiquitin (Aalto et al., 2019) (Figure 1.6B 6). The A20-like family DUBs also play different roles in these two pathways. A20 can bind to the Met1 chains and prohibit other enzyme processing the Met1 charged IKK signaling (Priem et al., 2019) (Figure 1.6A 9). A20 can inhibit cIAP and TRAF6 by binding to them (Lork et al., 2017) (Figure 1.6A 9). Cezanne is indicated to bindto TRAF3 and inhibits TRAF3 ubiquitylating IKK (Hu et al., 2013) (Figure 1.6A 10). TRABID is the only A20-like family DUB in Drosophila (Tran et al., 2008). It can hydrolyse Lys63 chains on Tak1 and also bind to Tak1/TAB2 complex to inhibit Imd signalling (Fernando et al., 2014) (Figure 1.6B 9).

The activation of TNFR1 or Imd induced NF-κB signalling involves a vast range of cellular components and they are competent to influence other processes, such as adaptive immunity, cell death, apoptosis and proliferation. Thus a defect in one component of the TNFR1 pathway can cause a phenotype that on the surface may seem not connected to inflammation and innate immunity (Al-Lamki and Mayadas, 2015). Studies have shown that defects in A20-like family members can induce inflammation and associated neurodegeneration (Abbasi et al., 2015; Voet et al., 2018; Wang et al., 2013). TRABID is a negative regulator of IMD signalling and knocking out the gene cause neuroinflammation and neurodegeneration in *Drosophila* (Fernando et al., 2014; Kounatidis et al., 2017).

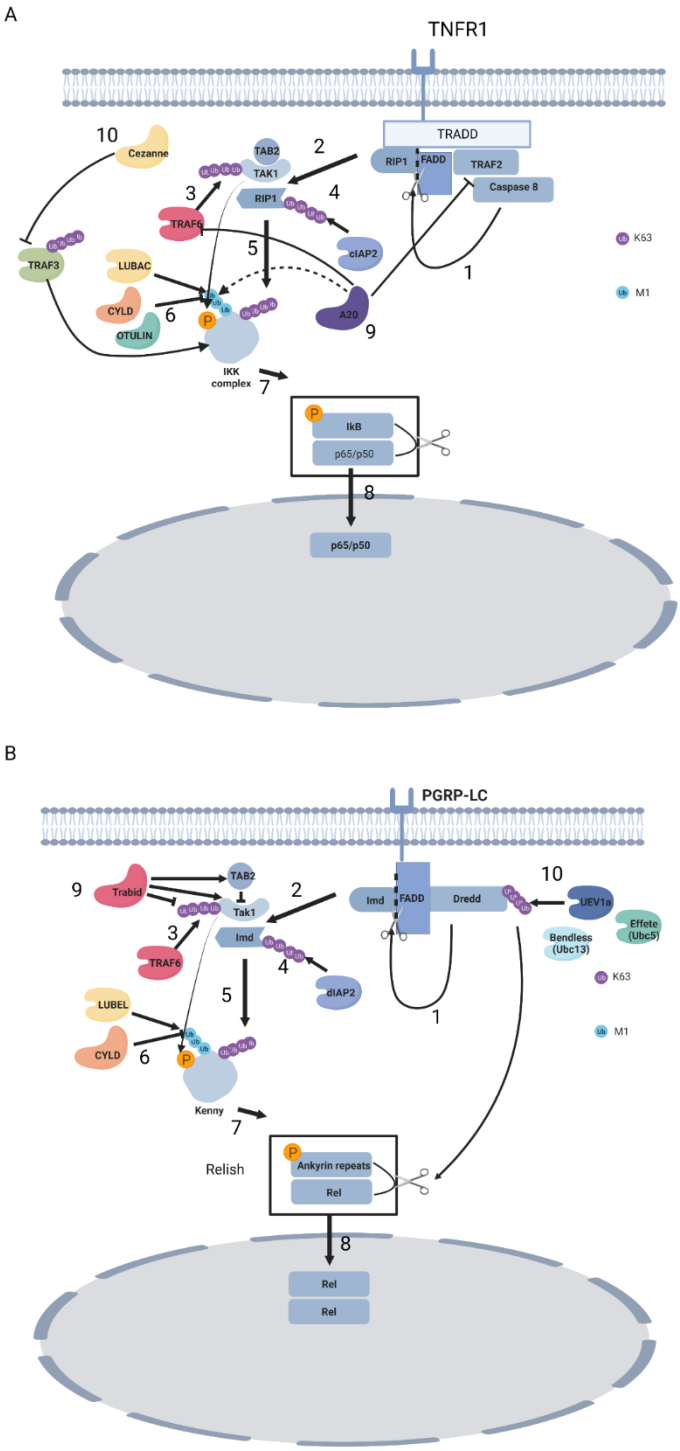



**Figure 1.6 Cartoon drawing of TNFR1 and IMD pathway activation**. (A) Human TNFR1 pathway and (B) *Drosophila* IMD pathway. (A) (1) After pathogen-stimulus signals received from TNFR1 receptor, Caspase8 cuts off RIP1 from TRADD recruited complex, including TRADD, RIP1, FADD, TRAF2 and Caspase8. (2) The released RIP1 form a new complex with TAK1-TAB2. (3 and 4) TRAF6 and dIAP2

ubiquitylates TAK1 and dIAP2 separately with Lys63 ubiquitins. (5) The ubiquitylated complex can further ubiquitylate and phosphorylate IKK complex. (6) The IKK complex can be ubiquitylated by LUBAC and deubiquitylated by CYLD and OTULIN. (7) The fully charged IKK complex will phosphorylate IκB-NF-κB (p65/p50) complex and cause the degradation of N terminal IκB. (8) p65/p50 transcriptional factor is released into the nucleus. (9) A20 is reported to bind to TRAF6 and inhibits its ubiquitylation activity. A20 also can bind to Met1 ubiquitin chains and deter the hydrolysis by OTULIN and CYLD. (B) (1) Similar to TNFR1, IMD is activated by PGRPs encountering Gram-negative bacteria. After activation, it will rapidly recruit Imd-FADD-Dredd complex and Dredd will hydrolyse Imd-FADD and release Imd. (2) Imd will bind with Tak1-TAB2 complex. (3) TRAF6 will ubiquitylate Tak1 with Lys63 ubiquitin chains and (4) Diap2 will ubiqutylate Imd. (5) The charged Tak1-TAB2 complex will phosphorylate Kenny. (6) The E3 ligase LUBEL will ubiquitylate Kenny complex with Met1 ubiquitins and CYLD is the deubiqutiylase. (7) The activated Kenny will phosphorylate Relish, which consists of ankyrin repeats at the N terminal and NF-κB containing domain Rel at the C terminal. Unlike IκB-NF-κB (p65/p50) complex, Relish need Dredd to cleave off ankyrin repeats and (8) release Rel into nucleus. (9) Trabid can cleave Lys63 ubiquitin on Tak1 to stop IMD signaling. During the process, Trabid binds to Tak1 and TAB2 and further inhibits the IMD pathway. (10) Ubiquitylation by UEV1a, Effete (Ubc13) and Bendless (Ubc5) regulates the activity of Dredd.

## 1.7 neurodegeneration, ubiquitylation and NF-κB signalling

### 1.7.1 Neurodegeneration

In a strict definition, neurodegeneration corresponds to any pathological condition that primarily affecting neurons. In practice, neurodegenerative diseases represent neurological disorders that have pathological effect on subsets of neurons. The two most common neurodegenerative disorders are Alzheimer disease (AD) and Parkinson disease, which lead to severe disability, and death, in an ageing world (Dawson et al., 2018; Johnson, 2015). Common symptoms including gait and locomotion impairment, sleep dysregulation and cognition decline. On the histology and molecular level, cerebral protein aggregations are the hall marks of AD (amyloid β (Aβ) and tau) and PD (α-synuclein) (Bombois et al., 2010; Pieruccini-Faria et al., 2021; Regional Committee for Europe, 2021).

### 1.7.2 Ubiquitylation and neurodegeneration

Aggregation of misfolded proteins, including Aβ , tau and α -synuclein, can progressively damage the nervous system and are characteristics of neurodegenerative disorders. Since the ubiquitin-proteasome system (UPS) is a major player in proteolysis, modulating the ubiquitylation level (via ligase or DUB activity), is a popular strategy in therapy development for AD and PD. Reducing the E3 ligase HRD1 mediated protein degradation can cause the accumulation of Aβ and amyloid precursor protein (APP) (Kaneko et al., 2010, p. 1). The carboxyl terminus of heat-shock cognate (Hsc)70-interacting protein (CHIP) is a E3 ligase

that can regulate ubiquitylation and degradation on tau in cell culture. Overexpressing CHIP could ameliorate the early development of tau in animal model (Sahara et al., 2005). Knocking out DUB Usp8 promotes the lysosomal degradation of α-synuclein in human cells, while knocking out Usp8 in *Drosophila*, it protects the animal from locomotor defects and cell loss (Alexopoulou et al., 2016). Moreover, knocking out DUB USP9X caused the monoubiquitylation of α-synuclein and reduced the efficiency of autophagy of α-synuclein (Rott et al., 2011).

Dysregulation of degrading misfolded proteins may not be the sole factor of pathogenesis of neurodegenerative disease. The ubiquitin-like protein — Ubiquilin 1 affects the trafficking of APP and generation of Aβ (Hiltunen et al., 2006). The E3 ligase NEDD4 is detected in degenerated tissues in several major neurodegenerative diseases. Inactivate or silencing NEDD4 can protect neurons from zinc-induced cell death and apoptosis (Kwak et al., 2012). E3 ligase — Parkin (Prkn) and ubiquitin kinase — PINK1 can provide signal for LC3 phagophore and cause mitochondria processed by autosome (Pickrell and Youle, 2015). Loss of Prkn cause aged mice to develop neurodegenerative phenotypes (Sliter et al., 2018). Parkin is also an activator of IKK/NF-κB innate immunity pathway (Henn et al., 2007).

### 1.7.3 NF-κB signalling and neurodegeneration

Since NF-κB signalling is essentially immune response, depending on the tissue,

overactivation of NF-κB can be either neuroprotection or neurodegeneration. The relationship of NF-κB and known neurodegeneration pathways is bilateral. It has been shown that in the cerebral cortex of AD patients has increased expression levels of NF-κB p65 and high level of β-site APP cleaving enzyme-1 (BACE1). The p65 subunit of NF-κB has been shown to bind the promotor region of BACE1 and subsequently induce the expression of β-secretase. β-secretase promotes the APP processing in amyloidogenic pathway and lead to the formation of amyloid fibrils, which ultimately aggregate into amyloid plaques(Hampel et al., 2021). In human neuron cells, Aβ40 peptide can induce the expression of p65/p50 heterodimers in neuron cell cultures and increases the accumulation of Aβ42 (Snow and Albensi, 2016). Furthermore, Aβ(25-35) peptide is toxic to primary neurons. It introduces high level of oxidative stress, accompanied by high level of NF-κB activation (Behl et al., 1994). Glia cells are the major immune cells of the brain. In a neuron-glia co-culture experiment, activating NF-κB signalling through Toll-like receptors (TLR) rather than TNFR1, induces several NF-κB downstream targets, including Aβ42 and TNF-α, which are activators of TNFR1 signalling (Lukiw, 2016; Sun et al., 2022). In animal models, inhibiting NF-κB signaling have been shown to influence neurodegeneration in both *Drosophila* and mice (Jin et al., 2016a; Kounatidis et al., 2017; Ou et al., 2021).

### 1.7.4 Sex dimorphism

Sex dimorphism is commonly existing in neurodegenerative diseases. For example,

about two third AD patients are females (Guo et al., 2022) and about 60% PD patients are males (Wooten et al., 2004). In AD patients' cerebral immune cells (microglia) there are more expression of inflammation genes in females (Coales et al., 2022). In expression study involving PD patient-derived astrocyte cells, a type of brain immune cells, shows X-chromosome inactivation in female patients (Booth et al., 2019). In the *Drosophila*, female and male has disparate regulation of Imd signaling (Vincent and Dionne, 2021). Moreover, proteasome mapping in mice provides evidence that ubiquitylation is sex bias in different tissues (Jenkins et al., 2020). Given the important role of ubiquitylation in neuroinflammation and neurodegeneration, it is interesting to hypothesis that sex-specific in neurodegenerative diseases is associated with disparate ubiquitylation in females and males.

## 1.8 Why TRABID?

### 1.8.1 Current known function of TRABID beside NF-κB signalling

Besides NF-κB signalling, TRABID is reported to be a positive regulator in Wnt pathway in mammalian cells and *Drosophila* via activation of TCF factors (Tran et al., 2008). Trabid has deubiquitylase activity towards APC (*Adenomatous polyposis coli*) (Tran et al., 2008). The inactivation mutation of APC is a risk factor for colorectal tumours by overacting Wnt pathway (Bienz and Clevers, 2000). In oncology, TRABID knockdown promotes hepatocellular carcinoma (HCC) growth through deubiquitylating the Lys63 ubiquitin chains on phosphatase Twist1, while Twist1

suppresses the activity of Trabid via negative regulation in Trabid's promotor region (Zhu et al., 2019). In human cells, utilizing catalytically inactive hTRABID (C443S) and hTRABID ΔOTU as probe reveal different interactors from different TRABID domains, including Lys29/48-specific E3 ligase HECTD1 and striatin-interacting phosphatase and kinase (STRIPAK) complex. TRABID is required for HECTD1 stability in cell culture. Knocking out *Trabid* in mice shows reduction in HECTD1 level in gut, liver and spleen tissues (Harris et al., 2020). Knocking out Trabid in human cells, Trabid is reported to deubiquitylate and prevent histone demethylase Jmjd2d from proteolysis. Jmjd2d can demethylate histones at the promoter region of IL-12 and IL-23, which are TLR/NF-κB induced. Expression of IL-12 and -23 can activate proinflammation T helper 1 (Th1) and Th17 cells (Jin et al., 2016). Taken together these results indicates that Trabid may have major roles in fundamental biological processes.

### 1.8.2 Current limitation in TRABID research

Previous studies mostly adopted the approach of knocking out the *Trabid* gene at cellular level. TRABID specifically hydrolyses Lys29, 33 and 63 polyubiquitin and there are other DUBs, either specific or non-specific, can process these chains. Moreover, TRABID is competent binding to various proteins (Harris et al., 2020). Knocking out *Trabid* potentially expose these target proteins to other interactions. Although knocking out *Trabid* provides valuable insight in its function, the approach may undermine the understanding of some function.

Knocking out *Trabid* in mice and *Drosophila* shows its role in neurodegeneration (Fernando et al., 2014; Jin et al., 2016), but neither study looked in to the differences between females and males in neurodegeneration phenotypes. As described in 1.7, neurodegeneration, neuroinflammation, ubiquitylation and sex dimorphism are intimately associated. However, there is rarely any *in vitro* model that could integrate these factors.

## 1.9 Thesis aim and findings

In the above context, a simple model that would integrate molecular detail with whole organism phenotypic analysis of sex-dimorphism in neurodegeneration and ubiquitylation, should be an informative research avenue to explore. The triplet of neurodegeneration, ubiquitylation and sex dimorphism is complicated to be integrated in one animal model. Genetics tools in *Drosophila* provide the opportunity for easy genome editing and a relatively short lifespan for age-dependent neurodegeneration study. Moreover, knockout *trbd* has age-related neurodegeneration phenotype. However, in knockout *tbd* flies, other DUBs may complement the function of trbd. In this study, I used enzymatic inactive *trbd* (*trbdC518A*) by editing Trabid cysteine 518 to alanine through CRISPR-Cas9, which provide a naïve loss function condition in the flies. I discovered that inactivating *Trabid* in *Drosophila* cause sex-specific neurodegeneration-related phenotypes. This

finding encouraged me to investigate the relationship of TRABID-driven ubiquitylation, neurodegeneration and sex dimorphism triplets.

In this study, I show that dTRABID has the same enzymatic activity as its human counterpart. Through CRISPR-Cas9 gene editing, I introduced a point mutation (C518A), which resulted in a null allele and an enzymatically inactive protein. This caused sex-specific changes in lifespan, behaviours, brain cell quantity, inflammation, proteome and ubiquitinome of adults. In lifespan, locomotor, and sleep assays, the *trbdC518A* mutation had more detrimental effects in males than in females. These sex dimorphism changes were underscored by brain histology, inflammation marker expression, ubiquitin/SUMO enrichment and total proteomics analysis. Some sex biases were reduced when the sex determination gene *transformer* (*tra*) was silenced in astrocytes and immunocompetent tissues (fat body, gut, and haemocytes). Our result integrates neurodegeneration, sex dimorphism and ubiquitylation in the model animal *Drosophila* with the role of the DUB Trabid.

# Chapter 2: Assessing dTRABID biochemistry, *in vitro*

## 2.1 Introduction

As stated in Chapter 1, human, mouse and *Drosophila* TRABID are involved in a wide range of cellular processes and at least two signalling pathways: Wnt and NF-κB (Fernando et al., 2014; Jin et al., 2016; Tran et al., 2008; Zhu et al., 2019). Previous studies have shown that hTRABID is a linkage-specific DUB (Licchesi et al., 2012). In this chapter, I will show how I cloned and purified the catalytic domain of dTRABID (dTRABID-AnkOTU) and tested its catalytic specificity *in vitro.*

## 2.2 Sequence alignment

To determine the potential sequence conservation between dTRABID and hTRABID, I first looked at the amino acid and structure of these two homologous proteins. I aligned the amino acid sequence of hTRABID, mTRABID (mouse TRABID) and dTRABID using Clustal Omega with default settings. Result showed that the main functional domains were conserved throughout species (Figure 1.1.2.2 A). These domains include the NZF and Ank.UBDs and OTU catalytic domain. The NZF UBDs assist TRABID for binding to longer polyubiquitin chains, Ank UBD contributes to linkage-specificity and OTU catalytic domain perform the hydrolysis activity toward ubiquitin chains (Licchesi et al., 2012). The crystal structure of hTRABID NZF and AnkOTU domain were solved by Licchesi *et al*., (Licchesi et al., 2012). AlphaFold2

predicted 3D structure of the dTRABID-AnkOTU domain (AF2: Q9VH90) was compared to the published crystal structure of its human counterpart (hTrabid-AnkOTU PDB: 3ZRH) (Licchesi et al., 2012) in Pymol. The results revealed a high degree of conservation at the structural level as the two structures overlapped (Figure 2.2 B). The hTRABID-AnkOTU domain has been shown to preferentially cleaved Lys29 and 33 chains. In this chapter I wanted to demonstrate whether dTRABID-AnkOTU had the same biochemical specificity.

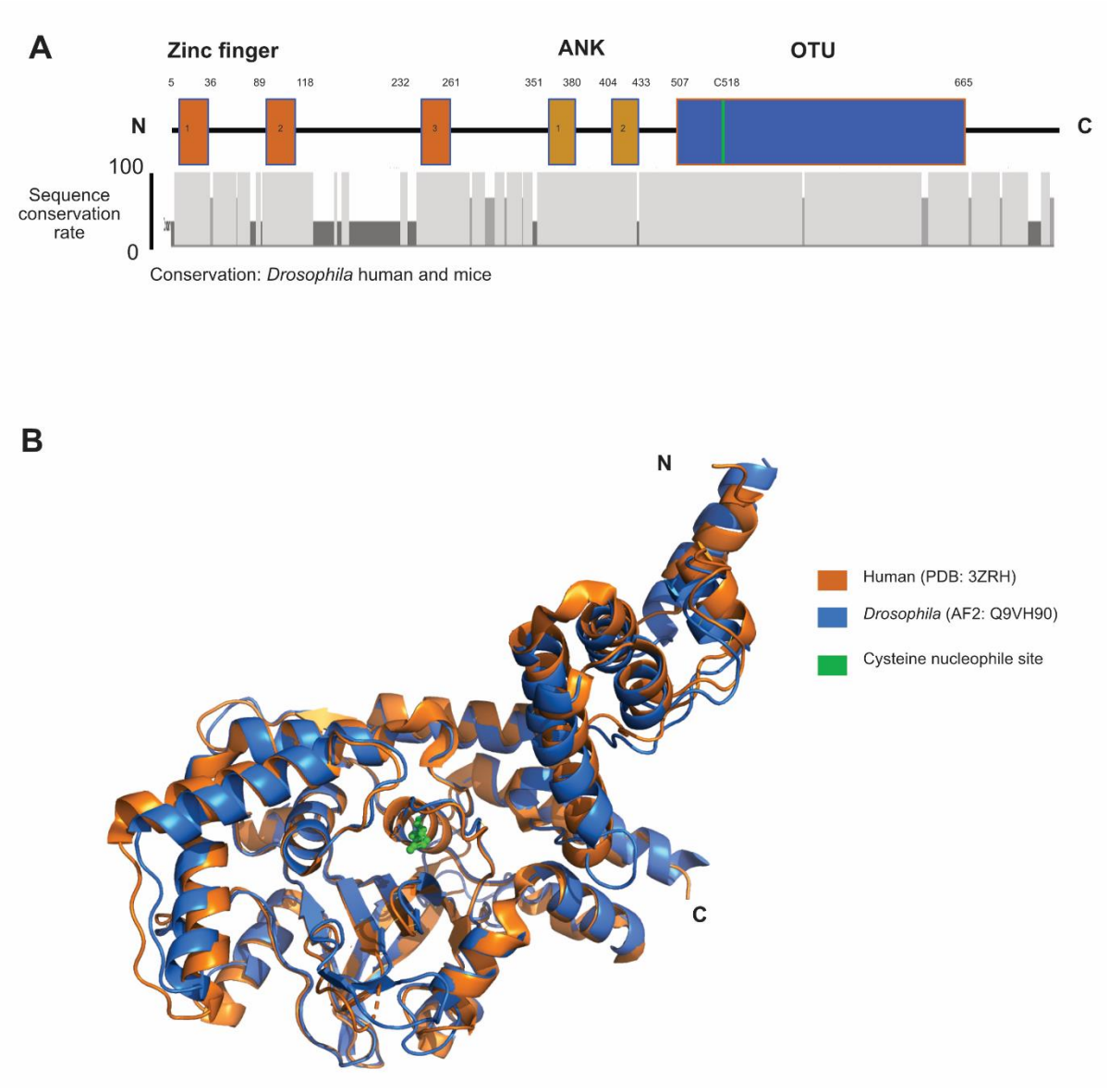



**Figure 2.2 Amino acid sequence and structure alignment of hTRABID and dTRABID.** (A) Alignment of *Drosophila* (Q9VH90), human (Q9UGI0) and mice (Q7M760) TRABID amino acid sequence and annotated domain and nucleophile site of dTRABID. The boxes demonstrate conserved domain of TRABIDs, with domain boundaries. The grey scale shows the conservation of alignment. The higher the bar, the higher the conservation of amino acid alignment. (B) Structure alignment of hTRABID-AnkOTU domain (3ZRH) and AlphaFold2 predicted dTRABID-AnkOTU (Q9VH90). The alignment shows that human and *Drosophila* TRABID has highly-conservation in their enzymatic domain structure and identical nucleophile site.

## 2.3 dTRABID has similar enzyme specificity as hTRABID

I observed that, predominantly, dTRABID-AnkOTU had a cleaving activity toward Lys29 and 33 diubiquitin chains. In detail, dTRABID-AnkOTU had a relative higher enzymatic activity toward Lys29 than Lys33 diubiquitin chains (Figure 2.3A). dTRABID-AnkOTU had a dual specificity against Lys29 and 33 ubiquitin chains. At 150 nM I did not observe hydrolysis of Lys63 chains (Figure 2.3A). However, increasing the concentration to 300 nM, hydrolysis of Lys63 diubiquitin was observed (Figure 2.3B). Hence, dTRABID's enzymatic activity was identical to its human counterpart (Licchesi et al., 2012).

Mutating hTRABID C443, the nucleophile cysteine, to serine causes the enzyme abrogated its enzymatic activity (Licchesi et al., 2012). Hence, I mutated the dTRABID-AnkOTU C518, the predicted nucleophile cysteine, to alanine (C518A). For the point mutation (C518A), 300 nM of dTRABID-AnkOTU and dTRABID-AnkOTUC518A were used for the hydrolysis of 3.5 μM Lys29 and 63 diubiquitin chain for 0, 5 and 30 minutes. The wild-type enzyme significantly cleaved Lys29 and 63 diubiquitin, while there was no enzymatic activity for the mutant enzyme towards both diubiquitin chains (Figure 2.3B). The result was in accordance with its human counterpart (Licchesi et al., 2012). Collectively, I demonstrated that human and *Drosophila* TRABID-AnkOTU shared the same biochemical characteristics *in vitro*.

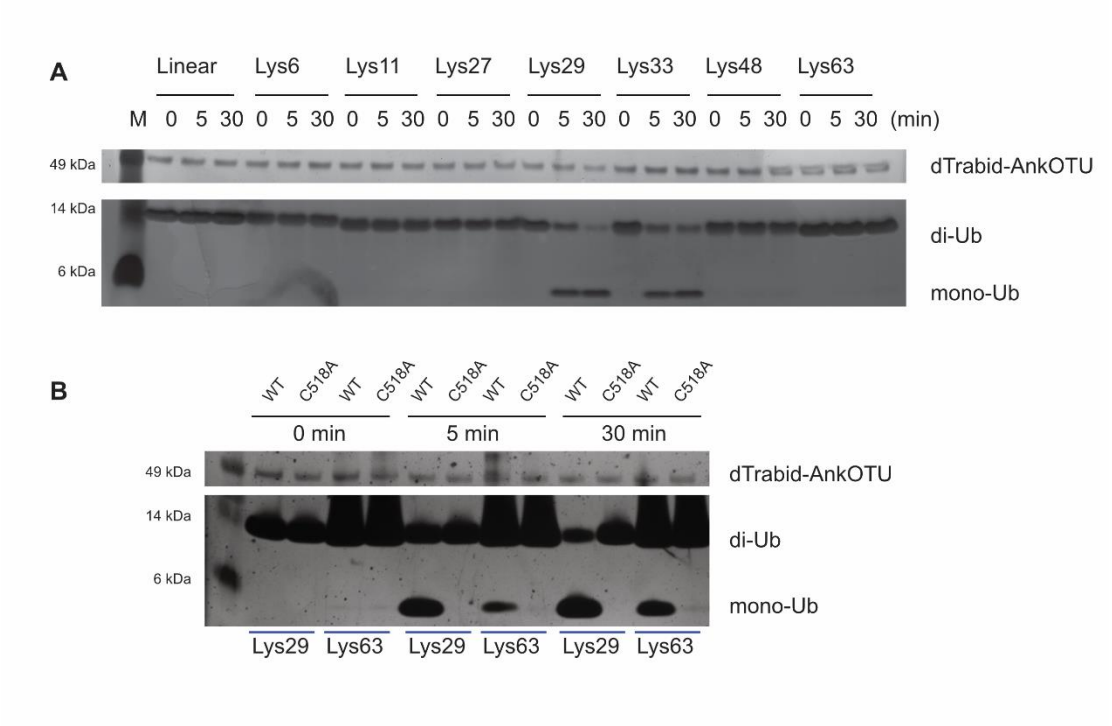



**Figure 2.3 dTRABID-AnkOTU and dTRABIDAnkOTUC518A enzymatic activities toward diubiquitins.** (A) DUB assay of 150 nM dTRABID-AnkOTU on 3.5 μM eight different diubiquitin chain for 0, 5 and 30 minutes. dTRABID-AnkOTU preferentially hydrolyses Lys29 and Lys33 diubiquitin chain. (B) DUB assay of 300 nM dTRABID-AnkOTU (WT) and dTRABID-AnkOTUC518A (C518A) on 3.5 μM Lys29 and 63 diubiquitin chain for 0, 5 and 30 minutes. WT has a relative lower enzymatic activity towards Lys63 diubiquitin chain than Lys29 diubiquitin chain. C518A mutation totally abrogates the enzymatic activity.

## 2.4 Discussion

In this chapter, I demonstrated the conservation of TRABID in human and *Drosophila* at the level of amino-acid sequence as well as at the predicted structural level. I further synthesised the dTRABID-AnkOTU enzymatic domain and the enzymatically inactive dTRABID-AnkOTUC518A. I showed dTRABID had the same biochemical features as its human counterpart, including catalytic specificity and activity. However, it is important to be aware that hTRABID-NZF domain contributes to the hydrolysis of longer Lys63 ubiquitin chains *in vitro* (Licchesi et al., 2012). Here, I did not generate a full length dTRABID or a full length dTRABID-NZF mutant to verify if the dTRABID-NZF confers the same binding function as hTRABID-NZF. In recent publication, deleting the NZF and Ank binding domains significantly reduced TRABID's deubiquitylation activity in *Drosophila* S2 cells (Hua et al., 2022). Previous *in vivo* studies of TRABID were conducted through knocking out the gene (Jin et al., 2016, Fernando et al., 2014). TRABID hydrolyses Lys63 chain ubiquitin on Tak1/TAB2 complex in *Drosophila* (Fernando et al., 2014) and hydrolyses Lys29, 33 and 63 ubiquitin *in vitro.* When knocking out TRABID *in vivo,* there are other DUBs that can substitute its role and consequently change the signal. For example, USP9X hydrolyses Lys29 and 33 ubiquitin chains and CYLD hydrolyses Lys63 chain (Komander et al., 2009), which can substitute the missing TRABID. In total, dTRABID has the same enzymatic activity and specificity as its human counterpart *in vitro*, but it is unclear about the influence of an inactive TRABID (TRABID-C518A) in an animal model.

# Chapter 3: Inactivating dTRABID *in vivo* has a different impact on males and females' locomotor activity, sleep patterns, and lifespan

## 3.1 Introduction

In the previous chapter, I demonstrated that dTRABID had the same catalytic specificity as its human counterpart *in vitro* and altering the catalytic cystine (C518A) prevented enzymatic activity. I further introduced the dTRABIDC518A (*trbdC518A*) into $w^{1118}$ *Drosophila*. Given previous results in the lab, that deletion of the *trabid* open reading frame, under *yw* background, resulted in age-dependent neurological phenotypes (Kounatidis *et al,* 2017), I investigated the effect of an enzymatically inactive Trabid. Moreover, I wanted to see the sex-specificity of these effects. In this chapter, I tested females and males of the *trbdC518A* mutants and compared them to their genetic background $w^{1118}$ in locomotor activity (climbing), sleep and lifespan. Females and males were collected separately at the day of eclosion.

## 3.2 Locomotor activity assay

Locomotion defects are symptoms and used as assessment assays in neurodegenerative diseases (Pieruccini-Faria et al., 2021). In *Drosophila,* climbing assays are generally used for evaluating the defects in locomotion. Here I adapted

an assay that can identify locomotion defects at early stages (see materials and methods) (Madabattula et al., 2015).

I recorded that *trbdC518A* males had a significantly lower climbing passing percentage than $w^{1118}$ males at day 6, 9, 12 and 18 ($p<0.0001$), while there was no statistical difference between the mutant females and wild type females (Figure 3.2C). Comparing the passing rate between sex in the same genotype, I recorded *trbdC518A* female had a higher passing rate throughout all timepoints than the males ($p<0.0001$), but there was no significant difference between wild type females and males (Figure 3.2C). This showed that locomotor activity was not sexually dimorphic in the genetic background and *trbdC518A* contributed to distinguishing males and female in climbing since locomotor defects were limited to males.

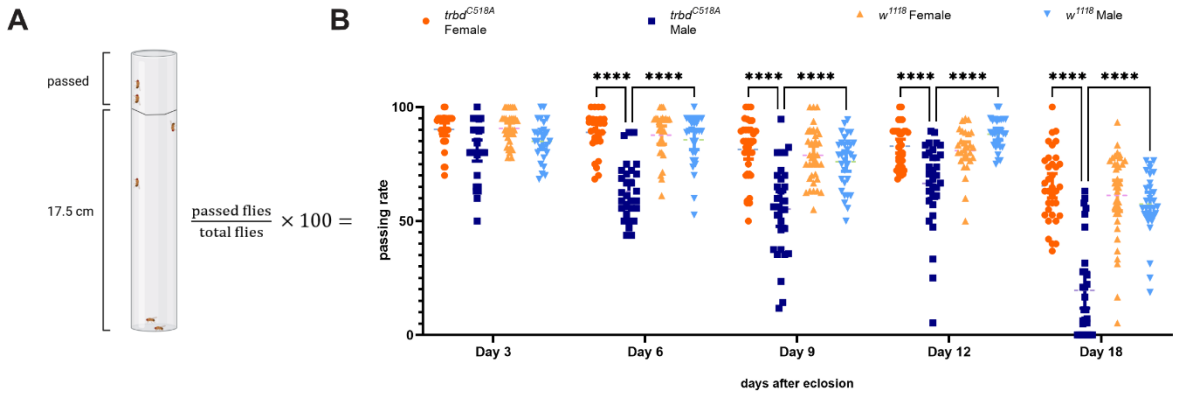



**Figure 3.2 Climbing assay showed that *trbdC518A* was more deleterious in male flies. (A)** Cartoon drawing showing in each test ~20 flies were left in a 250 ml transparent and sealed graduate cylinder. Tapping the cylinder gently for 5 times to make the flies start at the bottom and start the timer for 2 minutes count down. Flies that climbed passed 17.5 cm in 2 minutes will be scored as pass. One passing percentage is calculated by the ratio of passed flies to total flies times 100. **(B)** Climbing assay of *trbdC518A* and $w^{1118}$ on females and males at day 3, 6, 9, 12 and 18. Four comparisons were made (1) $trbd^{C518A}$ female vs $w^{1118}$ female, (2) $trbd^{C518A}$ male vs $w^{1118}$ male, (3) $trbd^{C518A}$ female vs $trbd^{C518A}$ male and (4) $w^{1118}$ female vs $w^{1118}$ male (Two-Way ANOVA with mixed model of interaction effect of time and genotype and Tukey HSD test, n=~30, 95% CI). (Day 3) There was no significant difference. (Day 6, 9, 12 and 18) Male *trbdC518A* had significant reduced climbing passing rate than *trbdC518A* female or $w^{1118}$ male (all ****p<0.0001).

### 3.3 *Drosophila* sleep monitoring

Sleep is conserved across the phylogenetic tree and sleep disruption has been closely associated with ageing and cognitive function decline (Bombois et al., 2010; Li et al., 2022; Zhang et al., 2019). Unlike humans, flies have a continuous sleep-wake cycle throughout the day, but the pattern differs between daytime and night (Cirelli and Bushey, 2008). Here, I used the *Drosophila* activity monitor (DAM) system (TriKinetics, USA) to conduct sleep analysis in light period (LP) and dark period (DP).

Looking at the difference between males and females, both *trbdC518A* and $w^{1118}$ females had less total sleep time (TST) in LP ($p<0.001$) and more TST in DP ($p<0.05$) (Figure 3.3A and B). TST was determined by total sleep episode (TSE) (Figure 3.3C and D) and mean sleep time (MST) in each episode (Figure 3.3E and F). Different sex patterns were recorded in both TSE and MST for both mutant and control in LP, with more TSE in the females (both $p<0.0001$) (Figure 3.3C) and more MST in the males (mutant $p<0.001$ and control $p<0.0001$) (Figure 3.3E). In DP, there was no significant difference between $w^{1118}$ females and males in TSE and MST, but mutant males had more TSE ($p<0.05$) and less MST ($p<0.05$) than the females (Figure 3.3D and F), indicating that in contrast to wild-type, mutant males had fragmented sleep pattern in DP, when compared to the mutant females. It further suggested *de novo* sex dimorphism in DP in the *trbdCC518A* mutants.

Introducing the *trbdC518A* mutation caused more TST in the females ($p<0.01$) (Figure 3.3A) with no change in TSE (Figure 3.3C) and more MST in LP ($p<0.01$) (Figure 3.3E). The introduction of *trbdC518A* mutation did not change the TST of males (Figure 3.3A), but increased TSE ($p<0.0001$) (Figure 3.3C) and decreased MST in LP ($p<0.0001$) (Figure 3.3E), an indication of fragmented sleep. In DP, male had reduced TST ($p<0.05$) (Figure 3.3B) but no significant change was recorded in TST and MSE (Figure 3.3D and F). In total, the *trbdC518A* mutation caused fragmented sleep pattern in males in LP, with more TSE but compensated by less MST in each TSE.

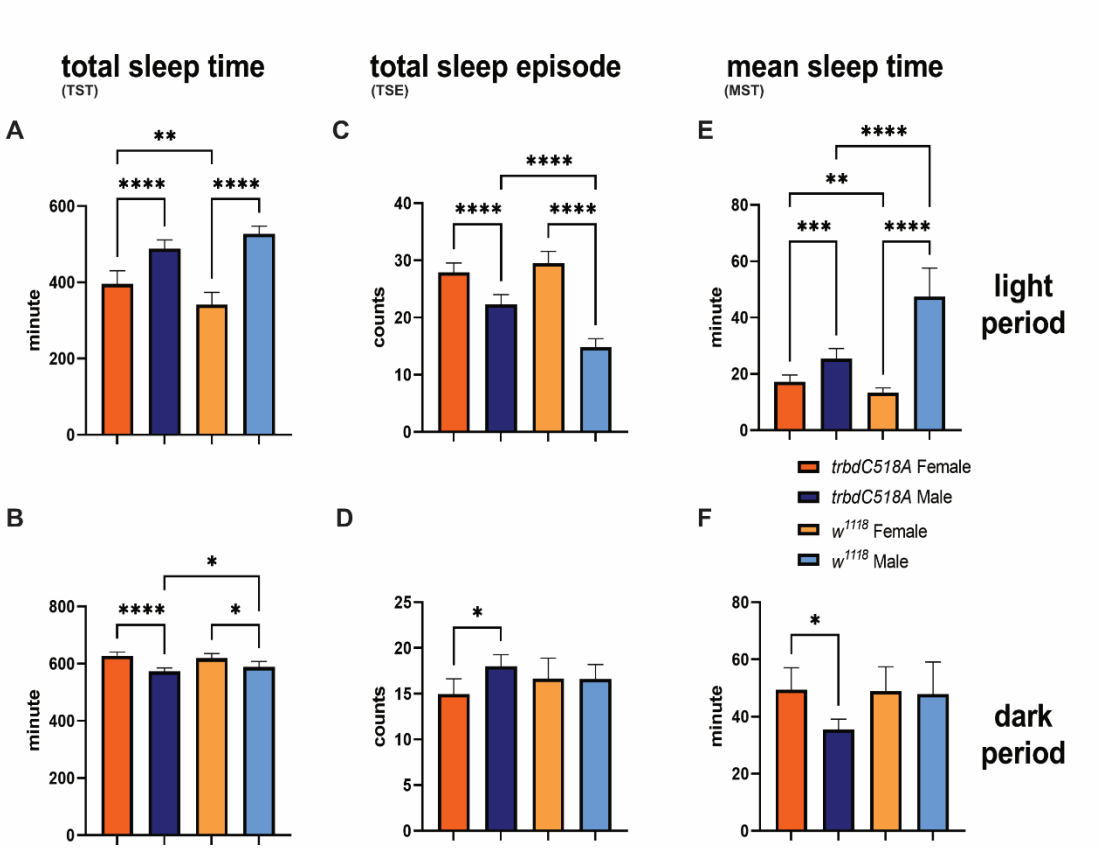



**Figure 3.3 DAM result for total sleep time (TST), total sleep episode (TSE) and mean sleep time (MST) at light period (LP) and dark period (DP)** (One-Way ANOVA Kruskal-Wallis test with uncorrected Dunn's test, n=~66, 95% CI). (A) Male had more TST than female for both *trbdC518A* and $w^{1118}$ (both ****p<0.0001) and *trbdC518A* female had increased TST than $w^{1118}$ female in LP (**p<0.01). (B) Female had more TST than male for both *trbdC518A* (****p<0.0001) and $w^{1118}$ (*p<0.05) and *trbdC518A* male had reduced TST than $w^{1118}$ male (*p<0.05), in DP. (C) Females had significant increased TSE than males in both *trbdC518A* and $w^{1118}$ (both ****p<0.0001) and *trbdC518A* male had significant increased TSE than $w^{1118}$ male (****p<0.0001) in LP. (D) *trbdC518A* male had significant reduced TSE than *trbdC518A* female (*p<0.05) in DP. (E) In LP, females had significant less MST than males in both *trbdC518A* (***p<0.001) and $w^{1118}$ (****p<0.0001). *trbdC518A* female had increased MST than $w^{1118}$ female (**p<0.01) and *trbdC518A* male had decreased MST than $w^{1118}$ male (****p<0.0001). (F) *trbdC518A* female had increased MST than $w^{1118}$ female (*p<0.05) in DP.

| Period | Measurement | Output | Conclusion |
|---|---|---|---|
| light period (LP) | total sleep time (TST) | Males has more TST than females. Introducing *trbd*$^{C518A}$ causes increase of TST in female. | *trbd*$^{C518A}$ slightly improves sleeping quality in female and significantly causes fragmented sleep in male. |
| | total sleep episode (TSE) | Males have less TSE than females. Introducing *trbd*$^{C518A}$ causes more TSE in male. | |
| | mean sleep time (MST) | Males have more MST than females. Introducing *trbd*$^{C518A}$ increases MST in female and decreases MST in male. | |
| dark period (DP) | total sleep time (TST) | Male has slightly less TST than females. Introducing *trbd*$^{C518A}$ slightly decreases TST in males. | *trbd*$^{C518A}$ causes sex difference in TSE and MST, elevating fragmented sleep in male |
| | total sleep episode (TSE) | In *trbd*$^{C518A}$, male has more TSE. | |
| | mean sleep time (MST) | In *trbd*$^{C518A}$, male has lesss MST. | |

**Table 3.3 Summary of sleep monitoring data.**

## 3.4 Lifespan assay

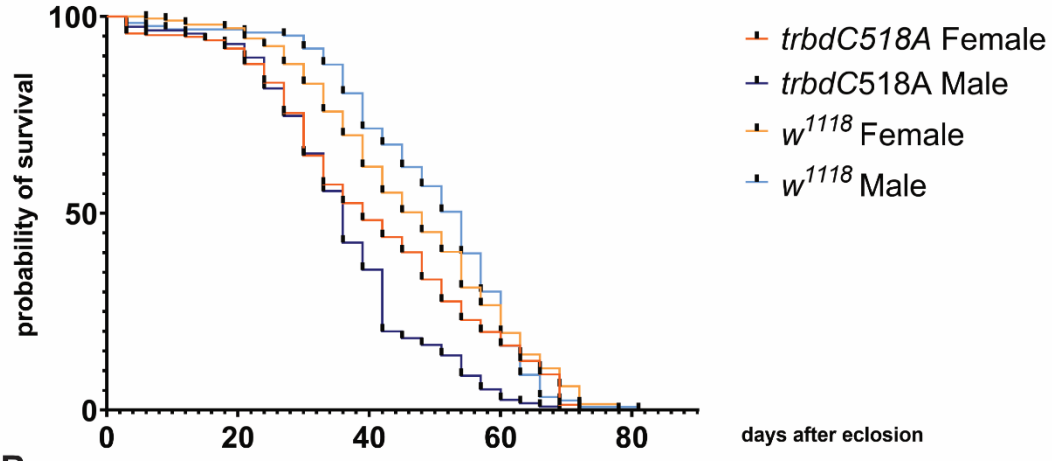
TRABID is a negative regulator of the Imd/NF-κB signalling. Loss of TRABID caused chronic brain inflammation in flies (Fernando et al., 2014; Kounatidis et al., 2017). It is well established that chronic inflammation has an important role in the ageing process (Pawelec et al., 2014). Moreover, *Drosophila* has a relative short lifespan of adult fly (~60 days), which makes it relatively convenient to use in longevity studies. Thus, I wanted to see whether the enzymatically inactive *Trabid* further to producing neurological phenotypes influenced lifespan in a sex-specific manner.

Flies were reared and collected as described (Fernando *et al,* 2014; Kounatidis *et al,* 2017) only this time flies were separated after eclosion into males and females. 20 same-sex flies were kept in a vial and food was changed every three days and dead flies were counted. The detail protocol is described in Chapter 8.2.4

There was no difference between the lifespan of wild type females and males ($p=0.0894$) (Figure 3.4A) When introducing the *trbdC518A* mutation, both female and male trbdC518A flies had significant reduction in their lifespan ($p<0.01$), but the female mutant was affected to a lesser extent than the male (Figure 3.4A). The result also reflected their median survival time, when half the population is dead. The median survival time was 39 days for *trbdC518A* female, 36 days for *trbdC518A* male, 48 days for $w^{1118}$ female and 54 days for $w^{1118}$ male (Figure 3.4B). This

suggested an inactive TRABID significantly affect the lifespan in *Drosophila* in a sex specific manner.

A




B

| Median Survival (Day) | *trbdC518A* Female | *trbdC518A* Male | $w^{1118}$ Female | $w^{1118}$ Male |
|---|---|---|---|---|
| *trbdC518A* Female | 39 | | | |
| *trbdC518A* Male | *** | 36 | | |
| $w^{1118}$ Female | ** | | 48 | |
| $w^{1118}$ Male | | **** | ns | 54 |

**Figure 3.4 Survival plot of trbdC518A and w1118 on females and males** Four comparisons were made (1) $trbd^{C518A}$ female vs $w^{1118}$ female, (2) $trbd^{C518A}$ male vs $w^{1118}$ male, (3) $trbd^{C518A}$ female vs $trbd^{C518A}$ male and (4) $w^{1118}$ female vs $w^{1118}$ male (log rank test, n=~150). (A) No significant difference between $w^{1118}$ female and male's lifespan. Male *trbdC518A* had a reduced lifespan compared to female *trbdC518A* (***p<0.001) and male $w^{1118}$ (****p<0.0001). Female *trbdC518A* had a reduced lifespan compared to female $w^{1118}$ (**p<0.01). (B) Median survival time for each genotype and survival statistical test result. The blank and stroked cells mean the comparison is not available or redundant.

## 3.5 Immunofluorescence quantification of neuron and glia

Behaviour assays suggested that there were neurodegeneration-associated symptoms in *trbdC518A* male flies. Previous data suggested, that *trbdKO* (*trbd* knockout) caused elevated vacuole numbers, an indication of neurodegeneration, in fly brain during ageing (Kounatidis et al., 2017). I sought to quantify the neuron and glia cells through immunofluorescence to gain histology evidence of effects on the numbers of brain cells. Flies were collected and raised as described in materials and methods. I dissected 18-day-old adult brains and stained them with Elav (neurons) and Repo (glia) primary antibodies in addition with DAPI to visualise nuclei (Figure 3.5A). Then, I compared signal levels (intensity and density) between control and mutant adult brains.

### 3.5.1 Projected brain area and total cerebral cell quantification

Comparing between different sexes in the same genotype, $w^{1118}$ males had a smaller projected brain area than $w^{1118}$ females ($p<0.001$). However, there was no significant difference in projected brain size between *trbdC518A* males and females (Figure 3.5B), indicating that the sex bias of brain size in $w^{1118}$ was eliminated in *trbdC518A*. The conclusion was further supported by total cell quantification by DAPI signal intensity. $w^{1118}$ male had lower DAPI signal intensity than $w^{1118}$ female ($p<0.01$) and *trbdC518A* male ($p=0.0506$) (Figure 3.5C). The smaller brain size of $w^{1118}$ male did not have a negative impact in its cell density (Figure 3.5D).

Introducing *trbdC518A* in the females caused reduction in DAPI intensity and density (both $p<0.05$) (Figure 3.5C and D), without any significant difference in projected brain size (Figure 3.5B), suggesting cerebral cell loss in the females after introducing *trbdC518A* mutation.

### 3.5.2 Glia quantification

*trbdC518A* females had stronger Repo intensity than control females ($p<0.05$) (Figure 3.5E), indicating more glia cells in the mutant females, but there was no significance in Repo density (Figure 3.5F). Comparing $w^{1118}$ males with $w^{1118}$ females and *trbdC518A* males, there was no significant difference (Figure 3.5E). Since $w^{1118}$ males had relative smaller brains, I were not surprised to record them having relative elevated Repo signal intensity than $w^{1118}$ females ($p<0.01$) and *trbdC518A* males ($p<0.05$) (Figure 3.5F). These results suggested that *trbdC518A* positively influenced glia quantity in females and negatively impacted glia densities in the males.

### 3.5.3 Neuron quantification

*trbdC518A* females had statistically indistinguishable Elav intensity ($p=0.0643$) and density compared to $w^{1118}$ females ($p=0.0599$) (Figure 3.4G and H). Though not statistically different, the p value was small enough to imply *trbdC518A* mutation

could promote neuron development in females. Meanwhile, there was no significant difference in Elav signal intensity and density between *trbdC518A* male and $w^{1118}$ male.

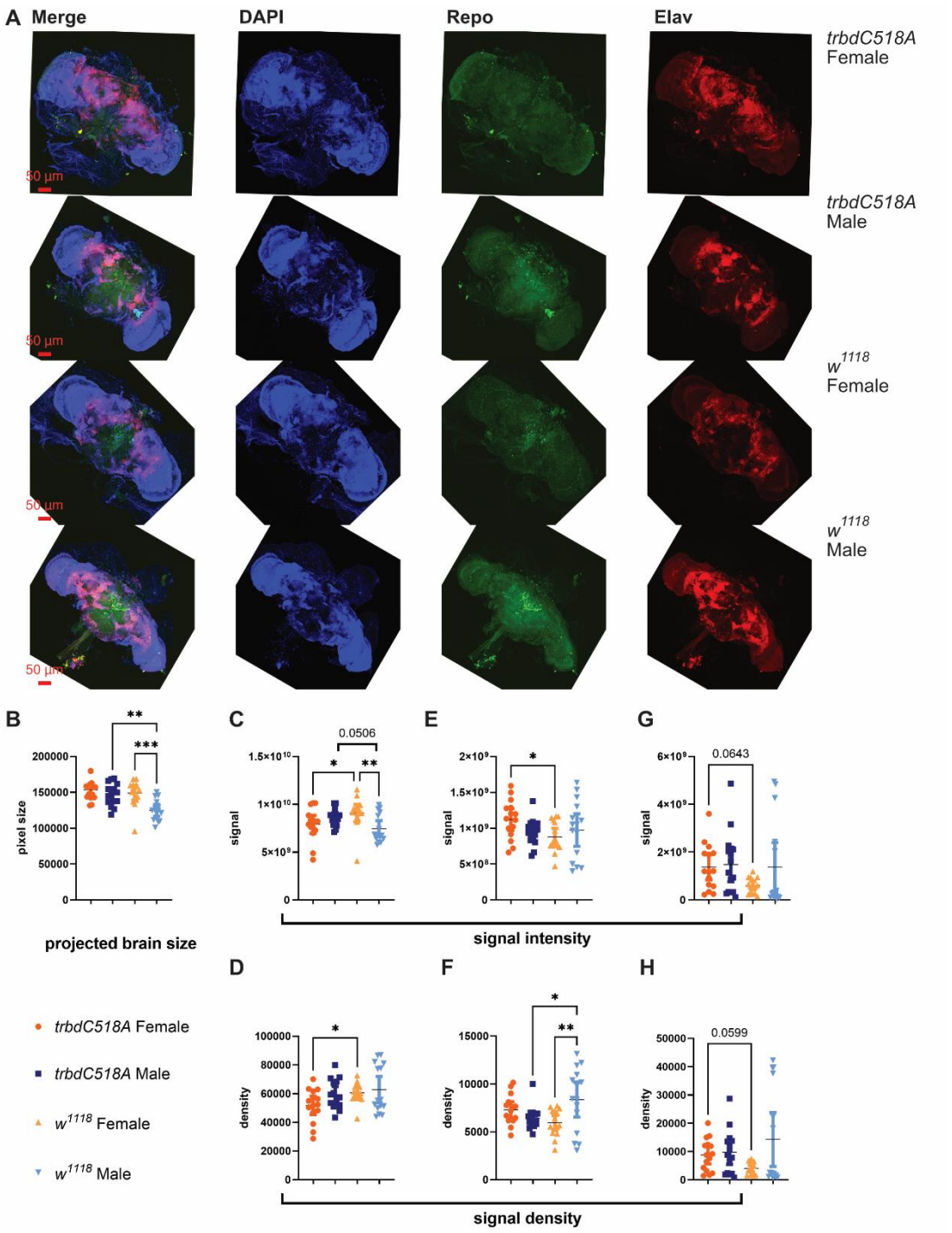

A
Merge
DAPI
Repo
Elav
trbdC518A Female
trbdC518A Male
w1118 Female
w1118 Male
50 µm
B
pixel size
projected brain size
C
signal
0.0506
E
signal
G
signal
0.0643
signal intensity
D
density
F
density
H
density
0.0599
signal density
trbdC518A Female
trbdC518A Male
w1118 Female
w1118 Male

**Figure 3.5 Immunofluorescence quantification indicated neuron and glia lost in *trbdC518A* males** (A) 18-day old *Drosophila* brains were stained by Repo and Elav primary antibody and conjugated with corresponding secondary antibody to quantify glia and neuron. DAPI was used to counterstain the nuclei (scale bar 50 $\mu m$). (B-H) Sum of fluorescence signal intensity of every Z slice, projected brain area and fluorescence signal density of projected brain area (One-Way ANOVA Kruskal-Wallis test with uncorrected Dunn's test, n=15, 95% CI). (B) $w^{1118}$ male had a significantly smaller projected brain size than $w^{1118}$ female (both ***p<0.001) and *trbdC518A* male (***p<0.01). (C) $w^{1118}$ male had a significantly weaker DAPI signal intensity than $w^{1118}$ female (**p<0.01). Though $w^{1118}$ males DAPI signals was not significantly weaker than *trbdC518A* males, but the p=0.0506. *trbdC518A* female had a significantly weaker DAPI signal intensity than $w^{1118}$ female (*p<0.05). (D) *trbdC518A* female had a significantly weaker DAPI signal density than $w^{1118}$ female (*p<0.05). (E) *trbdC518A* female had a significantly stronger Repo signal intensity than $w^{1118}$ female (*p<0.05). (F) $w^{1118}$ male had a significantly higher Repo signal density than $w^{1118}$ female (**p<0.01) and *trbdC518A* male (*p<0.05). (G) *trbdC518A* female had higher Elav signal intensity than $w^{1118}$ female (p=0.0643). (H) *trbdC518A* female had higher Elav signal density than $w^{1118}$ female.

| Measurement | Result |
|---|---|
| Projected brain size | *trbd*$^{C518A}$ increase male's projected brain size |
| Total cell signal intensity | Female has more brain cells than male in *w*$^{1118}$. In female, *trbd*$^{C518A}$ causes loss of cells. In male, *trbd*$^{C518A}$ slightly increases cell total cell number. Thus , cell number difference between male and female is eliminated in *trbd*$^{C518A}$ mutants. |
| Total cell signal density | *trbd*$^{C518A}$ causes increase in cell density in female. |
| Total glia signal intensity | *trbd*$^{C518A}$ causes increase in glia quantity in female. |
| Total glia signal density | *trbd*$^{C518A}$ causes increase in glia density in male. Hence, in *trbd*$^{C518A}$ mutants, male has higher glia density than female. |
| Total glia signal intensity | *trbd*$^{C518A}$ causes increase in cell quantity in female. |
| Total glia signal density | *trbd*$^{C518A}$ causes increase in cell density in female. |

**Table 3.5 Summary of result brain histology measurements.**

## 3.6 Discussion

In this chapter, I showed that *trbdC518A* had impacts on locomotor activity, sleep, lifespan and brain histology. Climbing assay is used for preliminary screen for neurodegeneration in *Drosophila.* Previous studies suggested knocking out *trbd* will cause climbing defects in *Drosophila* population with 1:1 female to male mix (Kounatidis et al., 2017). Here, I showed that *trbdC518A* only affect the climbing ability of males starting at day-6 after eclosion. Lifespan is a measurement for healthy ageing. Knocking out *trbd* also cause reduction in lifespan without separating females and males (Kounatidis et al., 2017). In my lifespan experiment, *trbdC518A* reduces lifespan in both females and males, but the reduces males' lifespan to a greater extent. I further used DAM assay to monitor the sleep pattern of *trbdC518A* flies. The data recorded more severe fragmented sleep, an indication of neurodegeneration (Bombois et al., 2010; Cirelli and Bushey, 2008), in male *trbdC518A* flies. Although these behaviour assays indicated *trbdC518A* has neurodegeneration-related phenotypes, they are indirect evidences and further direct evidence, such as brain histology is needed.

Previous histology study quantified the vacuoles in the brain, which is associated to neurodegeneration in *Drosophila*, through paraffin sections (Sunderhaus and Kretzschmar, 2016). I took the advantage of *Drosophila* glia and neuron primary antibodies to obtain direct quantification of neurodegeneration. I observed that *trbdC518A* promoted glia and neuron quantities. Subsequently, female's

neurological behaviours are protected from the increase of glia and neuron cells. However, I did not record any significant changes in the density of glia and neuron cells. This may cause by dTRABID promoting neuron development or preventing neurodegeneration. Furthermore, *trbdC518A* females had reduced total cerebral cell quantity and density. This indicates that, other than glia and neuron cells, *trbdC518A* is negatively affecting the quantity and density of other cerebral cells in female. In the males, I observed decrease in glia density that may explain the *trbdC518A* was more detrimental in male's neurological phenotypes. The method I adopted is not the most accurate and there are more cutting-edge techniques that can provide more detail quantification (Jiao et al., 2022). Moreover, the quantity of neurons is not the most direct evidence for neuron activity. Measuring neuron chemical signals, such as dopamine, released from the synapses using two photon microscope is the most direct evidence for neurodegeneration (Sun et al., 2018). However, my data still provided valuable hints in histology about how the inactive TRABID can impact neurodegeneration.

*Drosophila* is a model animal that provides the possibility for sex manipulation. This leads me to investigate if the newly introduced or eliminated sex dimorphism can be reversed by blocking female development in certain tissues. The sex development pathway is achieved alternative splicing through multiple repeat elements. During the process, females (XX) express high level of *sex lethal* (SXL) RNA binding protein, while Sxl is expressed in low dose in males (XY). The difference of Sxl level

will cause difference in alternative splicing in *transformer* (*tra*) mRNA, which is largely expressed in females, resulting in sex-specific form of *tra* and non-sex-specific form of *tra2. tra* is abundantly expressed in females while *tra2* is found in both males and females. In females, *tra, tra2* and other proteins work together to perform female-specific alternative splicing of *fruitless* (*fru*) and *double sex* (*dsx*). In males, *tra* work with other proteins to perform male-specific alternative splicing of *fru* and *dsx. dsx* directly controls the expressions of Yolk family proteins (Yp), which is known to be critical in sex development (Burtis et al., 1991; Butler et al., 1986; Hoshijima et al., 1991). In the next chapter, I used *UAS-tra*$^{RNAi}$ to block female development in *trbdC518A* background to verify if the sex-specific phenotypes can be eliminated.

# Chapter 4: Reversing sex in *trbd* female flies reduces sex bias in locomotor activity

## 4.1 Introduction

The gene *transformer (tra)* is a member of female somatic sexual differentiation pathway (Butler et al., 1986) and is abundantly expressed in epithelial cells. As explained in 3.6, the number of X chromosome will determine the expression of *sxl* and consequently influence the expression of *tra.* On one hand, when *tra* and *tra2* are presented, the *fru* and *dsx* pre-mRNA will be alternative spliced into the female form. On the other hand, when only *tra2* is presented, in other words, when *tra* is absent, *fru* and *dsx* will be alternative spliced into the male female (Burtis et al., 1991; Butler et al., 1986; Hoshijima et al., 1991). Hence, I used *UAS-tra*$^{RNAi}$ flies to induce tissue specific female sex development blockage. Although *tra* is a gene for female development, it is still expressed in male at a relatively low level (flybase.com).

Results in Chapter 3 showed that *trbdC518A* flies had sex-specific climbing defects, which is associated to neurodegeneration, using an early stage sensitive climbing assay (Madabattula et al., 2015), The climbing defects of *trbdC518A* male was detectable at 9-day old adult (Figure 3.2C). In this chapter, I used the *Drosophila* UAS-Gal4 system to silence *tra* in a subset of glia cells (astrocytes) or immunocompetent tissues under *trbdC518A* background and assessed the climbing

ability of 9-day old adult flies. *alrm-GAL4* was used to drive expression in astrocyte cells, which is a type of immune cells in the brain. *J6-GAL4* also known as *c546-GAL4* was used to drive expression in the gut, fat body (equivalent to the mammalian adipose tissue) and haemocytes (akin to macrophages), which are mainly located in the abdomen and thorax. Females and males can still be distinguished by their sex characteristics. The experiment explores the influence of climbing ability in *trbdC518A* flies after blocking female development in brain immune cells (astrocytes) and thorax and abdomen immune cells.

## 4.2 Reducing female development in astrocyte or immunocompetent tissues closes sex bias gap in locomotor under *trbdC518A* background

The climbing defect in males remained in control lines that had *trbdC518A* background (*trbdC518A, UAS-tra$^{RNAi}$;trbdC518A, alrm-Gal4;trbdC518A, alrm-Gal4/UAS-msd8GFP;trbdC518A* and *J6-Gal4/cyo;trbdC518A*) (Figure 4.3 A to F). When suppressing *tra* in astrocytes or immunocompetent cells, the sex bias in climbing was diminished (*alrm-Gal4/UAS-tra$^{RNAi}$;trbdC518A* and *J6-Gal4/UAS-tra$^{RNAi}$;trbdC518A*) (Figure 4.3 G and H). However, in *alrm-Gal4/UAS-tra$^{RNAi}$;trbdC518A*, females and males had promoted performance than the controls (*UAS-tra$^{RNAi}$;trbdC518A, alrm-Gal4/UAS-msd8GFP;trbdC518A* and *alrm-Gal4;trbdC518A*) (Figure 4.3 I to L) and the climbing passing rate was similar to its female counterpart. Given that *alrm-Gal4/UAS-msd8GFP* remained sexually dimorphic in climbing (Figure 4.3m) and that according to flybase expression data, *tra* is not abundantly expressed in glia, this suggested that expressing *tra$^{RNAi}$* in astrocytes positively influenced flies' locomotor activity under *trbdC518A* background.

When suppressing female development in immunocompetent cells under *trbdC518A* background, females climbing ability decreased to a level similar as the males (Figure 4.2). In general, expressing *tra$^{RNAi}$* in astrocyte elevated climbing ability in *trbdC518A* male flies to the same level as females. At the same time, climbing ability of females was reduced to the same level as males, when suppressing *tra$^{RNAi}$* in immunocompetent tissues. (Figure 4.2).

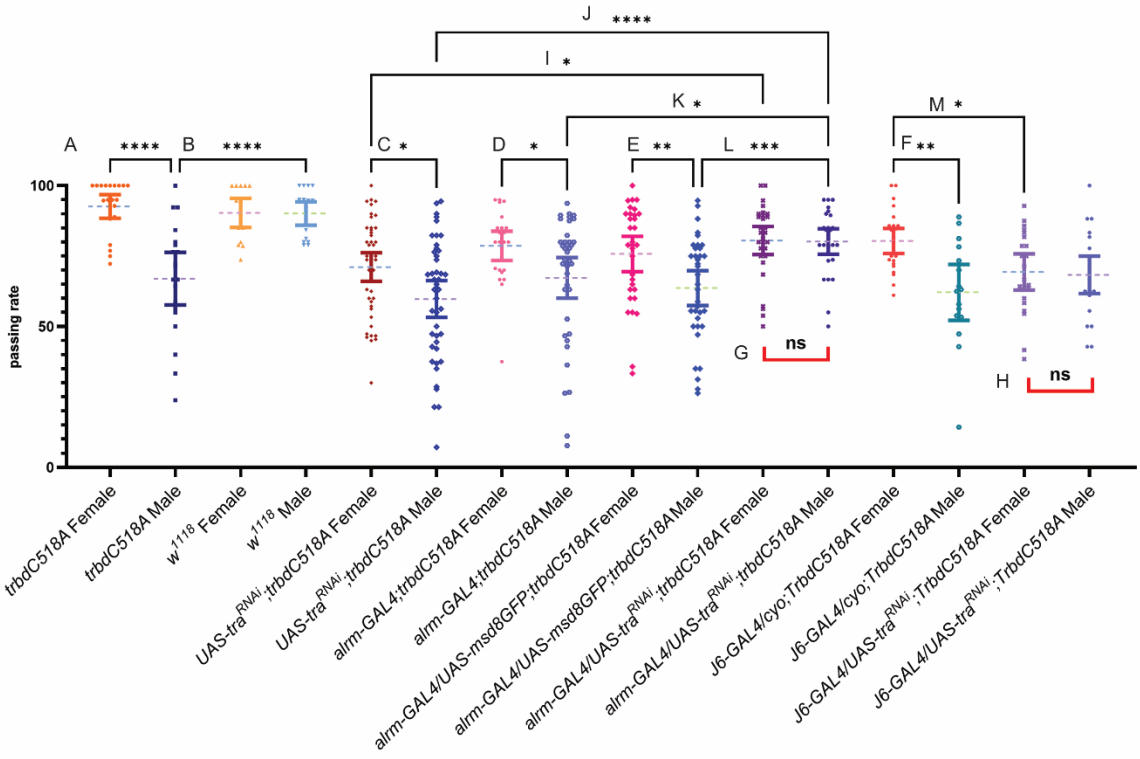



**Figure 4.2 Climbing assay of *trbdC518A*, *UAS-traRNAi/alrm-Gal4;trbdC518A* and *UAS-traRNAi/J6-Gal4;trbdC518A* with their controls** (One-Way ANOVA Kruskal-Wallis test with uncorrected Dunn's test, n>15, 95% CI). **(A)** *trbdC518A* male has lower climbing passing rate than *trbdC518A* female ($p<0.001$) and **(B)** $w^{1118}$ male ($p<0.001$). There is no significant difference between *w1118* female and males' climbing passing rate. Reduced climbing passing rate is reduced in **(C)** *UAS-tra$^{RNAi}$;trbdC518A* males, **(D)** *alrm-GAL4;trbdC518A* males, **(E)** *alrm-GAL4/UAS-msd8GFP;trbdC518A* males and **(F)** *J6-GAL4/cyo;trbdC518A* males, when compared to their female counterparts. However, there is no significant difference in female and male's climbing passing rate in **(G)** *alrm-GAL4/UAS-tra$^{RNAi}$;trbdC518A* and **(H)** *J6-GAL4/UAS-tra$^{RNAi}$;trbdC518A*. *alrm-GAL4/UAS-tra$^{RNAi}$;trbdC518A* female has elevated climbing passing rate than the control **(I)** *UAS-tra$^{RNAi}$;trbdC518A* female. *alrm-GAL4/UAS-tra$^{RNAi}$;trbdC518A* male has elevated climbing passing rate than the controls, including **(J)** *UAS-tra$^{RNAi}$;trbdC518A* male, **(K)** *alrm-GAL4;trbdC518A* males and **(L)** *alrm-GAL4/UAS-msd8GFP;trbdC518A* male. **(M)** *J6-GAL4/UAS-tra$^{RNAi}$;trbdC518A* female has significant lower passing rate than *J6-GAL4;trbdC518A* female.

## 4.3 Discussion

In this chapter, I showed that reducing female development in astrocyte or immunocompetent tissues can reduce sex bias in climbing ability under *trbdC518A* background. *trbd* is located on chromosome 3R. This restricted our choice of *UAS* and *Gal4*. Previous publication in the lab showed suppressing IMD/NF-κB in all glia cells (using *repo*-GAL4) can extend lifespan and ameliorate neurodegeneration level in *trbd* deletion mutant flies (Kounatidis et al., 2017). However, *repo-Gal4* is located on the chromosome 3, and constructing a recombinant was time consuming (see COVID19 statement), thus I used the astrocyte *alrm-Gal4,* located on the chromosome 2. Given *tra* is scarcely expressed in the brain and abundantly expressed in insect gut (flybase.com), I further used *J6Gal4.* Silencing *tra* in astrocyte significantly promoted the male climbing ability to the same level as the female and supressing *tra* in immunocompetent cell reduced the female climbing ability to the same level as the male. This indicated tissue specific effects of $tra^{RNAi}$ in the *trbdC518A* background. Since *trbd* is a negative regulator of IMD pathway (Fernando et al., 2014), these results suggested me to explore inflammatory changes in the brain.

# Chapter 5: Brain AMP expression differences

## 5.1 Introduction

Knocking out *trbd* upregulates expression of IMD/Relish-induced NF-κB mediated antimicrobial peptides (AMPs) in *Drosophila* heads and causes neuroinflammation and neurodegeneration (Kounatidis et al., 2017). Unlike knocking out *trbd* that may expose the ubiquitin chains to other DUBs, an inactive TRABID could bind and prevent the ubiquitin chains being digested by other DUBs and eventually alter the signal output, including the expression of IMD/Relish-driven AMPs. In the previous chapters, I showed sex-specific neurodegeneration phenotypes in behaviour and histology assays. Neurodegeneration is closely associated with neuroinflammation and *trbd* is a negative suppressor of Imd-induced inflammation, which is sex disparate in *Drosophila* (Vincent and Dionne, 2021). In this chapter, I used the expression of IMD-mediated AMPs as hallmarks to explore neuroinflammation of *trbdC518A* in the brain at 3- and 18-day old adult flies.

## 5.2 Difference in antimicrobial peptides and neurodegeneration maker expression in *trbdC518A* and $w^{1118}$ brains

At day 3, introducing *trbdC518A* mutation caused significant upregulation in *attacin A* (*AttA*) and downregulation in *cecropin C* (*CecC*) in the female ($p<0.05$ *trbdC518A* female vs $w^{1118}$ female) (Figure 5.2A). On the male side, introducing *trbdC518A* mutation didn't cause any significant changes (*trbdC518A* male vs $w^{1118}$ male) (Figure 5.2A). By comparing between same genotype and same sex, *attacin B* (*AttB*) was significantly downregulated in $w^{1118}$ males compared to the females ($p<0.0001$ $w^{1118}$ male vs $w^{1118}$ male) (Figure 5.2B). There was no significant change when comparing *trbdC518A* males to the females (*trbdC518A* male vs *trbdC518A* female) (Figure 5.2B).

At day 18, introducing *C518A* mutation reduced the expressions of *CecC*, *Drosocin (Dro)* and *DptA* in females ($p<0.05$ *trbdC518A* female vs $w^{1118}$ female) (Figure 5.2C). Compared to $w^{1118}$ males, the mutant males had an elevated expression in *AttA* ($p<0.05$) (Figure 5.2C *trbdC518A* male vs $w^{1118}$ male). $w^{1118}$ males had a weaker NF-κB induced AMP expression compared to $w^{1118}$ females (Figure 5.2D) that was indicated by the relative reduced expressions of *AttA*, *AttB diptericin A* (*DptA*) and *Dro* ($p<0.05$ $w^{1118}$ male vs $w^{1118}$ male). There was no significant difference when comparing *trbdC518A* female to *trbdC518A* male (*trbdC518A* male vs *trbdC518A* female) (Figure 5.2D). In total, at day 18, $w^{1118}$ male have a significantly lower AMP (*AttA*, *AttB, DptA* and *Dro*) expression than female. Introducing *trbdC518A* caused

downregulation of AMPs (*CecC, Dro* and *DptA*) in female brains and upregulation of *AttA* in males. Eventually, the sex bias in AMP expression was eliminated in the *trbdC518A* brains. It is noteworthy that the expression of *trbd* didn't change significantly in all comparisons.

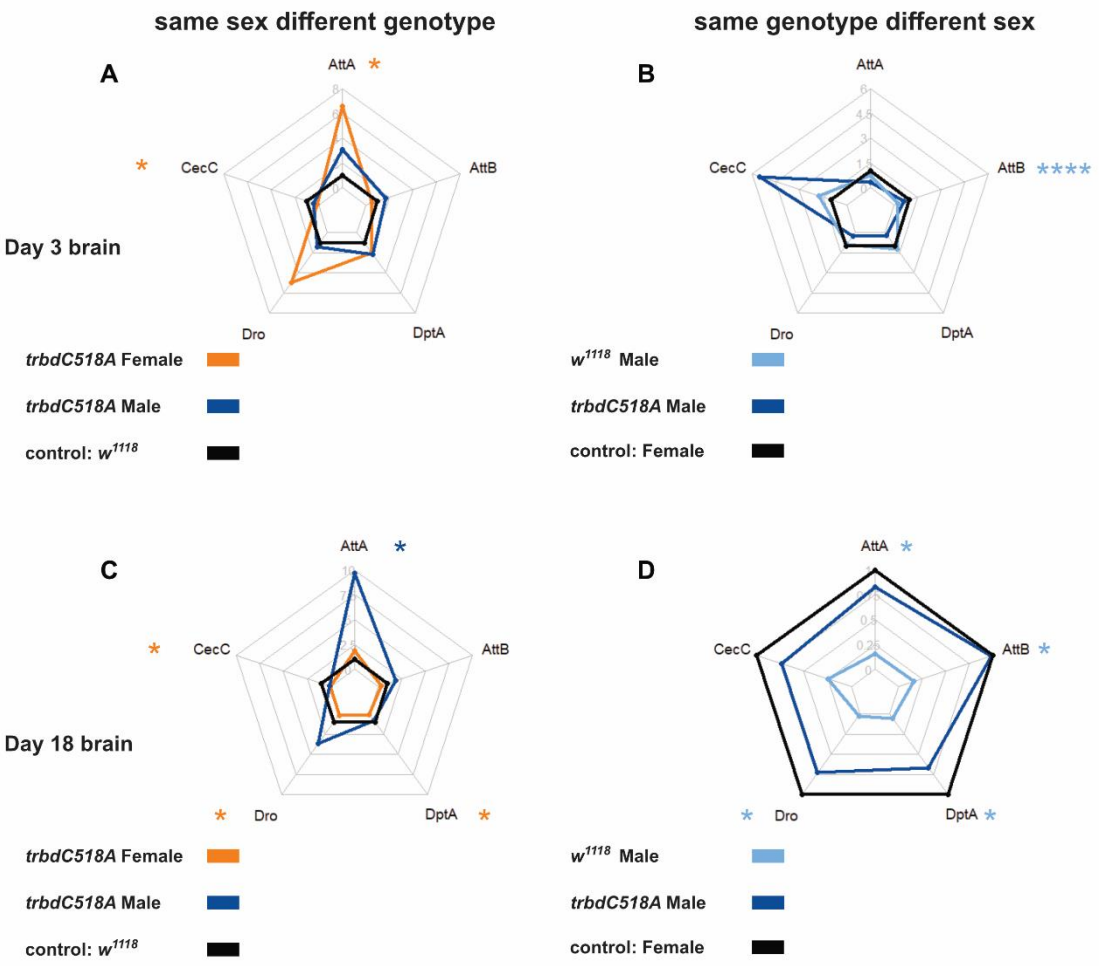



**Figure 5.2 AMPs expression in day 3 and 18 *trbdC518A* and *w*$^{1118}$ flies' brains.** (A) Relative fold change of AMPs expressions in 3-day old *trbdC518A* females' and males' brains with *w*$^{1118}$ females and males as the baseline control. (B) Relative fold change of AMPs expressions in 3-day old *trbdC518A* females' and *w*$^{1118}$ females' brains with *trbdC518A* males and *w*$^{1118}$ males as the baseline control. (C) Relative fold change of AMPs in 18-day old *trbdC518A* females' and males' brains with *w*$^{1118}$ females and males as the baseline control. (D) Relative fold change of AMPs expressions in 18-day old *trbdC518A* females' and *w*$^{1118}$ females' brains with *trbdC518A* males and *w*$^{1118}$ males as the baseline control.

## 5.3 Tissue specific blocking female development reduced sex bias in certain AMPs

I further looked into expression of AMPs in *tra*$^{RNAi}$ silenced flies that I used in chapter 4.2. Since *alrm-Gal4/UAS-tra*$^{RNAi}$*;trbdC518A* and *J6/UAS-tra*$^{RNAi}$*;trbdC518A* didn't bear the *white* eye mutation, which caused neurodegeneration (Ferreiro et al., 2018), while *UAS-tra*$^{RNAi}$*;trbdC518A* had the *white* eye mutation, hence I used *alrm-Gal4;trbdC518A* and *J6-Gal4/cyo;trbdC518A* as relative controls. If there was any sex bias expression in the controls, I expected to see a reduction of the sex bias. *Vice versa,* if there was no sex bias expression in controls, I expect to observe sex bias expression.

In 3-day old adults, no significant change was recorded in the brain of *alrm-Gal4/UAS-tra*$^{RNAi}$*;trbdC518A*, when comparing to *alrm-Gal4;trbdC518A* (*alrm-Gal4/UAS-tra*$^{RNAi}$*;trbdC518A* female vs *alrm-Gal4;trbdC518A* female and *alrm-Gal4/UAS-tra*$^{RNAi}$*;trbdC518A* male vs *alrm-Gal4;trbdC518A* male) (Figure 5.3.1A). When the comparisons were made between same genotype and different sex, no significant difference was recorded (*alrm-Gal4/UAS-tra*$^{RNAi}$*;trbdC518A* male vs *alrm-Gal4/UAS-tra*$^{RNAi}$*;trbdC518A* female and *alrm-Gal4;trbdC518A* male vs *alrm-Gal4;trbdC518A* female) (Figure 5.3.1B).

In 18-day old adults, elevated *CecC* expression was recorded in *alrm-Gal4/UAS-*

*tra*$^{RNAi}$*;trbdC518A* females brains (*alrm-Gal4/UAS-tra*$^{RNAi}$*;trbdC518A* female vs *alrm-Gal4/;trbdC518A*) (Figure 5.3.1C). No significant change was recorded comparing *alrm-Gal4/UAS-tra*$^{RNAi}$*;trbdC518A* male to *alrm-Gal4/;trbdC518A* (Figure 5.3.1C). When compared the males to the females, except increased *CecC* and decreased *DptA* expressions in *alrm-Gal4;trbdC518A* males (*alrm-Gal4;trbdC518A* males vs *alrm-Gal4;trbdC518A* females), while no other significant changes was recorded (Figure 5.3.1D). The sex disparate expression of *DptA* was eliminated, when comparing *alrm-Gal4/UAS-tra*$^{RNAi}$*;trbdC518A* female to *alrm-Gal4/UAS-tra*$^{RNAi}$*;trbdC518A* male (Figure 5.3.1D). This was cross referenced with the elevation of *DptA* in *alrm-Gal4/UAS-tra*$^{RNAi}$*;trbdC518A* female, when comparing to *alrm-Gal4/;trbdC518A* female (Figure 5.3.1C).

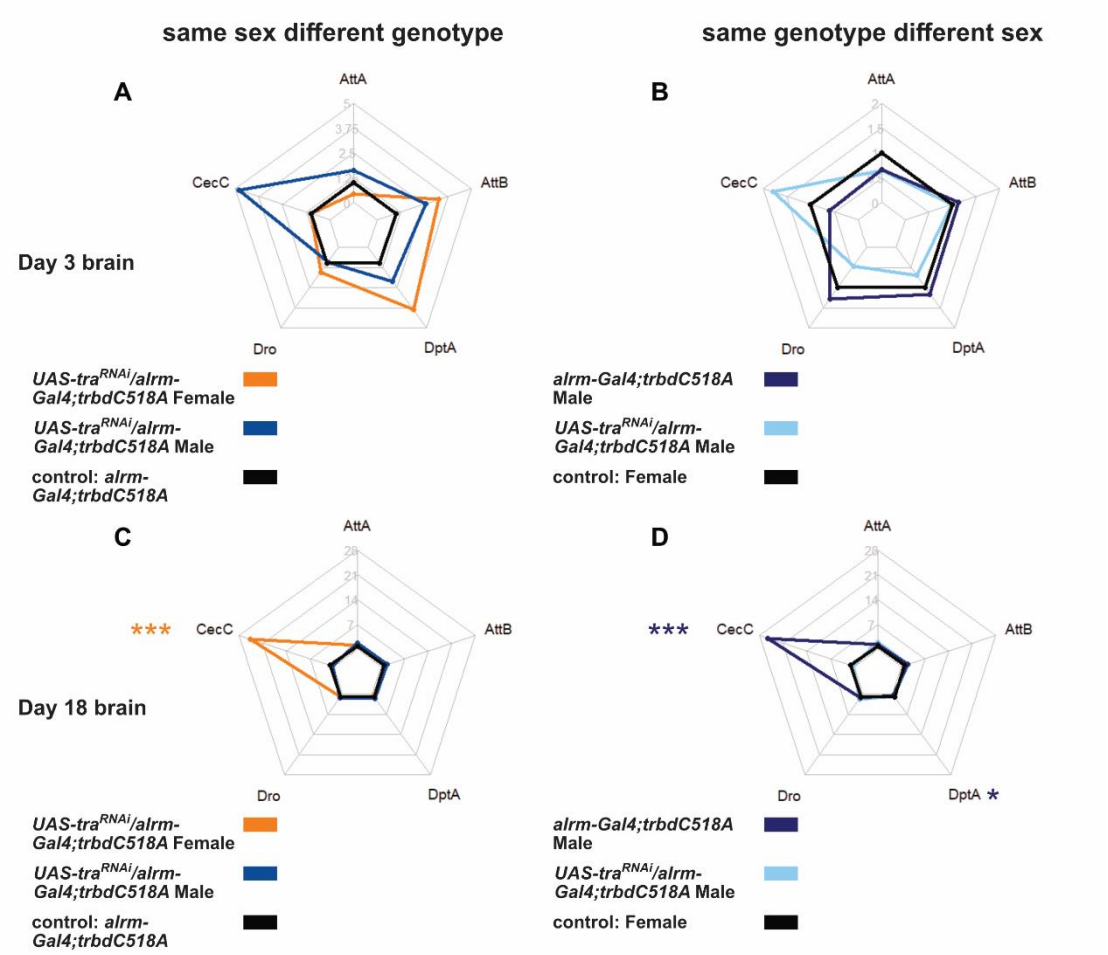



**Figure 5.3.1 AMPs expression in day 3 and 18 *alrm-Gal4/UAS-tra$^{RNAi}$;trbdC518A* and *alrm-Gal4;trbdC518A* flies' brains.** (A) Relative fold change of AMPs expressions in 3-day old *UAS-tra$^{RNAi}$/alrm-Gal4;trbdC518A* females' and males' brains with *alrm-Gal4;trbdC518A* females and males as the baseline control. (B) Relative fold change of AMPs expressions in 3-day old *UAS-tra$^{RNAi}$/alrm-Gal4;trbdC518A* females' and *alrm-Gal4;trbdC518A* females' brains with *UAS-tra$^{RNAi}$/alrm-Gal4;trbdC518A* females'males and *alrm-Gal4;trbdC518A* males as the baseline control. (C) Relative fold change of AMPs expressions in 18-day old *UAS-tra$^{RNAi}$/alrm-Gal4;trbdC518A* females' and males' brains with *alrm-Gal4;trbdC518A* females and males as the baseline control. (D) Relative fold change of AMPs expressions in 18-day old *UAS-tra$^{RNAi}$/alrm-Gal4;trbdC518A* females' and *alrm-Gal4;trbdC518A* females' brains with *UAS-tra$^{RNAi}$/alrm-Gal4;trbdC518A* males and *alrm-Gal4;trbdC518A* males as the baseline control.

Since fat body, gut and haemocytes are largely located in insect's thorax and abdomen, I explored the AMPs pattern not only in 18-day old *J6-Gal4/cyo;trbdC518A* and *J6/UAS-tra$^{RNAi}$;trbdC518A* brains but also in their thoraxes and abdomens. Since the existence of blood-brain barrier, cerebral immune response is relatively isolated from body humoral immunity (Limmer et al., 2014). Expressing *tra$^{RNAi}$* in immunocompetent tissues caused significant reduction in *CecC*, *Dro* and *AttB* expression in the male's abdomen and thorax (all $p<0.05$ *J6-Gal4/UAS-tra$^{RNAi}$;trbdC518A* male vs *J6-Gal4;trbdC518A* male) but no significant difference was recorded in the female's thorax and abdomen (*J6-Gal4/UAS-tra$^{RNAi}$;trbdC518A* female vs *J6-Gal4;trbdC518A* female) (Figure 5.3.2A). When comparison was made between males and females in abdomens and thoraxes, the background male (*J6-Gal4/;trbdC518A*) had elevated AMP expression to the control female (all $p<0.01$ *J6-Gal4/;trbdC518A* male vs *J6-Gal4/;trbdC518A* female). Significant sex-specific differences remained in *AttA*, *AttB* and *DptA* for *J6-Gal4/UAS-tra$^{RNAi}$;trbdC518A* ($p<0.01$ *J6-Gal4/UAS-tra$^{RNAi}$;trbdC518A* male vs *J6-Gal4/UAS-tra$^{RNAi}$;trbdC518A* female) (Figure 5.3.2B), but the relative fold changes between male and female were largely reduced compared to the background (*J6-Gal4/;trbdC518A*) (Figure 5.3.2B).

In conclusion, blocking female development in astrocyte caused partial changes in IMD/Relish-driven AMP expression (Figure 5.3.1 C and D). Blocking female development in immune competent tissues didn't affect the AMP expression in the

brain, but largely reduced the sex-specific AMP expression in abdomen and thorax (Figure 5.3.2 B) via decreased AMP expression in tested male groups (*J6-Gal4/UAS-tra$^{RNAi}$;trbdC518A* male vs *J6-Gal4;trbdC518A* male) (Figure 5.3.2 B).

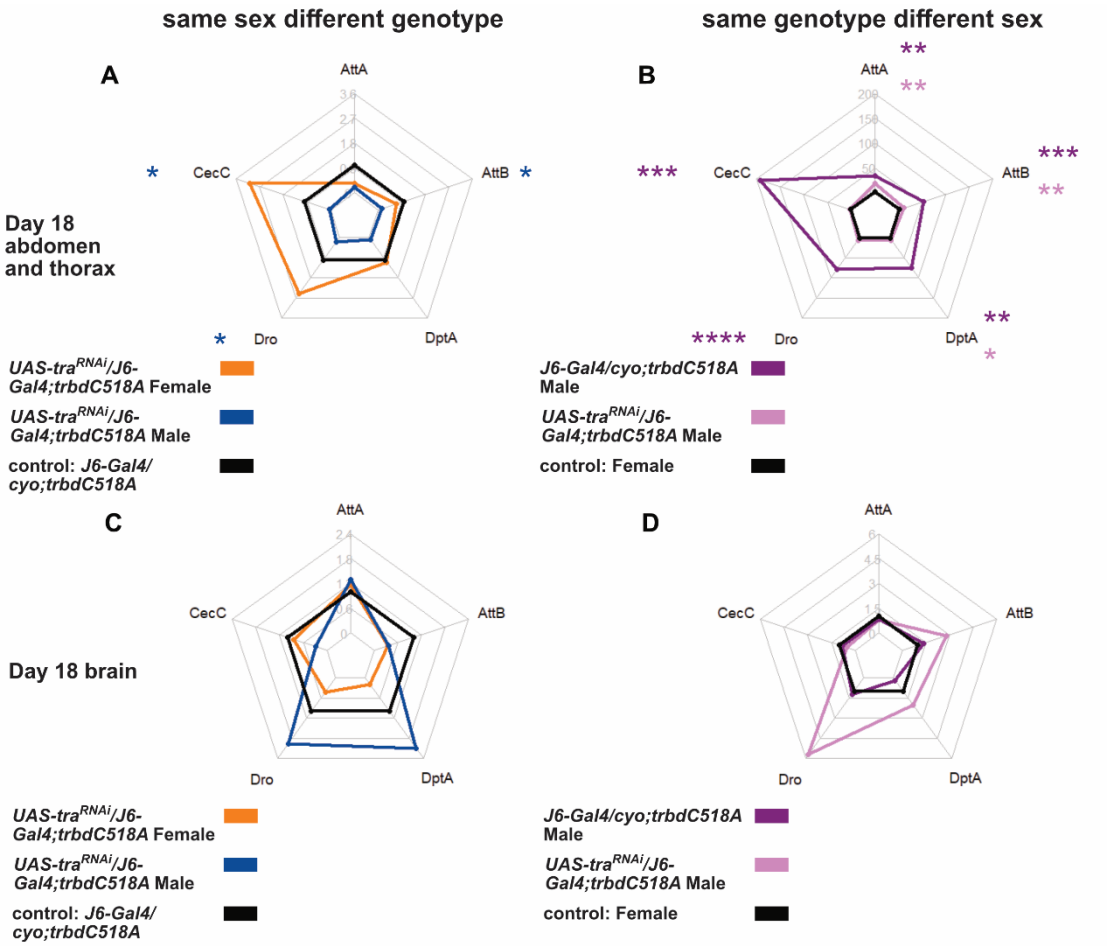



**Figure 5.3.2 AMPs expression in day 18 *J6-Gal4/UAS-tra$^{RNAi}$;trbdC518A* and *J6-Gal4;trbdC518A* flies' abdomen and thorax or brains.** (A) Relative fold change of AMPs expressions in 18-day old *UAS-tra$^{RNAi}$/J6-Gal4;trbdC518A* females' and males' thoraxes and abdomens with *J6-Gal4/cyo;trbdC518A* females and males as the baseline control. (B) Relative fold change of AMPs in 18-day old *UAS-tra$^{RNAi}$/J6-Gal4;trbdC518A* females' and *J6-Gal4/cyo;trbdC518A* females' thoraxes and abdomens with *UAS-tra$^{RNAi}$/J6-Gal4;trbdC518A* females'males and *J6-Gal4/cyo;trbdC518A* males as the baseline control. (C) Relative fold change of AMPs expressions in 18-day old *UAS-tra$^{RNAi}$/J6-Gal4;trbdC518A* females' and males' brains with *J6-Gal4/cyo;trbdC518A* females and males as the baseline control. (D) Relative fold change of AMPs expressions in 18-day old *UAS-tra$^{RNAi}$/J6-Gal4;trbdC518A* females' and *J6-Gal4/cyo;trbdC518A* females' brains with *UAS-tra$^{RNAi}$/J6-Gal4;trbdC518A* males and *J6-Gal4/cyo;trbdC518A* males as the baseline control.

## 5.4 Discussion

Knocking out dTRABID in *Drosophila* over activates IKK induced NF-κB signalling (Fernando et al., 2014; Hua et al., 2022; Kounatidis et al., 2017) and triggers neurodegeneration in brain. Neuroinflammation is strongly associated to neurodegeneration and ubiquitylation is heavily involved in NF-κB immunity and neurodegeneration. *trbd* is a negative suppressor of Imd pathway (Hua et al., 2022). My data showed divergent expression in Imd-induced AMPs in the $w^{1118}$ genetic background between males and females in brains. When introducing *trbdC518A* mutation, the sex dimorphism pattern was eliminated, with a trend of female downregulating some AMP expression (*CecC, DptA* and *Dro*) and male upregulating *AttA* expression (Figure 5.2 A). This showed that *trbdC518A* has sex bias effect in Imd NF-κB signalling. It implied that elevated Relish induced NF-κB signalling in the male brain could be neurological detrimental and reduced Relish induced NF-κB signalling in the female brain is neurological protective. Previous work has shown reducing IMD/Relish-driven NF-κB signalling in glia cells can rescue flies from neuroinflammation and neurodegeneration (Kounatidis et al., 2017). In Chapter 4, suppressing female development in astrocytes or immunocompetent tissues can rescue male-specific climbing defect in *trbdC518A.* Investigating if the neuroinflammation status is changed can provide evidence of neuroinflammation driving sex-specific neurodegeneration.

In order to find out sex bias in neuroinflammation can be reduced through blocking

female development in cerebral immune cells, I took the advantage of *Drosophila* genetics tools. *CecC* expression had sex-specific expression in the *trbdC518A* background (*alrm-Gal4;trbdC518A*) (Figure 5.3.1 D). When reducing female development in astrocyte (*alrm-Gal4/UAS-tra$^{RNAi}$;trbdC518A*), expression of *CecC* was elevated (Figure 5.3.1 C) in the female brain and the sex divergence was diminished (Figure 5.3.1 D). In *trbdC518A* background (*J6-Gal4;trbdC518A*), there were significant differences in expressions of AMPs between male and females in the thorax and abdomen (Figure 5.3.2 D). When blocking the female development in immunocompetent cells (*J6-Gal4/UAS-tra$^{RNAi}$;trbdC518A*) there were significant changes in abdomen and thorax AMP expressions in males' (Figure 5.3.2 C) and eventually the sex bias in AMP expression was largely reduced (Figure 5.3.2 D). However, the blockage of female development in the abdomen and thorax didn't influence AMP expression in the brain (Figure 5.3.2 A and B). These experiments suggest that Relish induced AMPs are sex and tissue dependent. Additionally, the data strongly suggested overexpressing *tra$^{RNAi}$* in immunocompetent tissues (*J6-Gal4/UAS-tra$^{RNAi}$;trbdC518A*) will suppress the expression of Relish-induced AMPs in male abdomen and thorax (Figure 5.3.2 C and D). Canonically, *tra* is only considered to affect female sex development, but recent publication suggest the expression of *tra* will affect cell development (Rideout et al., 2015). In total, the AMP expression result is hard to explain the climbing result from Chapter 4. Given the sophistication of neurological behaviours, more molecular evidence is needed to delineate global role of TRABID in the model of sex-specific neurodegeneration.

# Chapter 6: TRABID has sex-specific impacts in ubiquitination accumulation and protein ubiquitination *in vivo.*

## 6.1 Introduction

Creating a null *trbd* mutant caused multiple sex-specific and neurodegenerative related phenotypes. DUBs are important players in post-translation modification. The phenotypes reported in previous chapters have suggested that inactivating Trabid cause sex-specific phenotypes in ageing and neurodegeneration. Literatures have provided insight in *trbd'*s affect in specific pathways, such as Imd (Fernando et al., 2014), Wnt (Tran et al., 2008), TLR (Jin et al., 2016a), and ultimately influences development, ageing, inflammation and neurodegeneration. However, the global affect remained unclear for TRABID in an animal model. Moreover, previous works used *trbd knockout* animals (Fernando et al., 2014; Hua et al., 2022; Jin et al., 2016a; Kounatidis et al., 2017; Tran et al., 2008), in this study, an enzymatically inactive *trbd* was generated through CRISPR-Cas9 point mutation. When TRABID is missing, other DUBs may substitute its role for hydrolysing target ubiquitin chains (Lys29, 33 and 63) and binding to substrates (such as Tak1/TAB2) (Fernando et al., 2014; Licchesi et al., 2012a). When the inactive TRABID (TRABIDC518A) is present, it is still able to bind to target ubiquitin chains and substrate proteins. Furthermore, the phenotypes recorded in previous chapters may cause by direct or indirect regulations by *trbdC518A.*

Although neuroinflammation is a pathogenesis of neurodegeneration, there are other pathogeneses for neuroinflammation, including mitochondria damage, apoptosis and aggregation of misfolding proteins(Jack et al., 2017; Priem et al., 2019; Xu et al., 2021). Moreover, beside regulating Imd pathway, TRABID is implied in other pathways, including Wnt and Twist1-induced oncology (Tran et al., 2008; Zhu et al., 2019). Hence, expanding the role of TRABID in neurodegeneration, beside Imd activation can provide global insights for pathogenesis for neurodegeneration.

In order to provide global insights about TRABID associated regulation, I took advantage of rapid and deep-scale ubiquitylation (Udeshi et al., 2020) and total proteome profiling to explore the global and sex-specific regulation of inactive TRABID in 18-day old adult *Drosophila* heads. I used GlyGly ubiquitin enrichment to perform my ubiquitinome experiment. Trypsin protease hydrolysis after GlyGly amino acids. Different ubiquitylation at Lys residue will generate different peptide sequences that has GlyGly residue at the C terminal. GlyGly antibody is capable to pull down the GlyGly motif after trypsin protease digestion. Further conducting mass spectrum profiling, it is possible to quantify the proteins that are ubiquitylated and the distinct GlyGly peptide sequence that can be used to distinguish ubiquitin linkages. I identified the significant expressed and ubiquitylated proteins by comparing different genotype with same sex (*trbdC518A* female vs *w1118* female and *trbdC518A* male vs *w1118* male) and different sex with same genotype

(*trbdC518A* male vs *trbdC518A* female and *w1118* male vs *w1118* female). The differential genes in each comparison were subjected to gene ontology (GO) pathway analysis in STRING database, which provides objective insights. Moreover, from ubiquitylation profiling, I discovered sex-specific accumulation of Lys 6, 27 and 29 linkage chains. The analysis not only provided *de novo* pathways that are affected by *trbdC518A* and provided omics data to explain the phenotypes that are recorded in previous chapters.

## 6.2 Genes and pathways enriched in STRING database search

### 6.2.1 Hsc70-4 is sex-specifically regulated

When comparisons were made for different genotype with same sex (*trbdC518A* female vs *w1118* female and *trbdC518A* male vs *w1118* male), Hsc70-4, which was involved in protein folding and participated in several neurodegenerative pathogenesis in flies (Iijima-Ando et al., 2005; Johnson et al., 2020), was the only protein that had a diverse regulation by ubiquitin modification, (Figure 6.3.1A). It was downregulated in *trbdC518A* males and upregulated in the females. In mouse, it coordinated the homeostasis of microtubule and tau accumulation (Fontaine et al., 2015). In human cells, the E3 ligase CHIP and chaperone Hsc70 complex and ubiquitin-conjugating Enzyme H5b (UbcH5B) selectively modify phosphorylated Tau, which is pathogenesis for AD (Shimura et al., 2004).

| behaviour | neuron : | immune system: |
|---|---|---|
| GO:0050896 | GO:0007411 | DME-168256 |
| DME-432626 | GO:0007413 | DME-168249 |
| GO:0009605 | GO:0061564 | DME-1280215 |
| GO:0040011 | GO:0030424 | DME-1280218 |
| | GO:0030182 | DME-5676590 |
| **UPS:** | GO:0043005 | DME-5607761 |
| DME-209360 | GO:0031175 | DME-1169091 |
| DME-209461 | GO:0001505 | DME-209459 |
| | | DME-450321 |
| | | DME-450282 |
| | | DME-450294 |

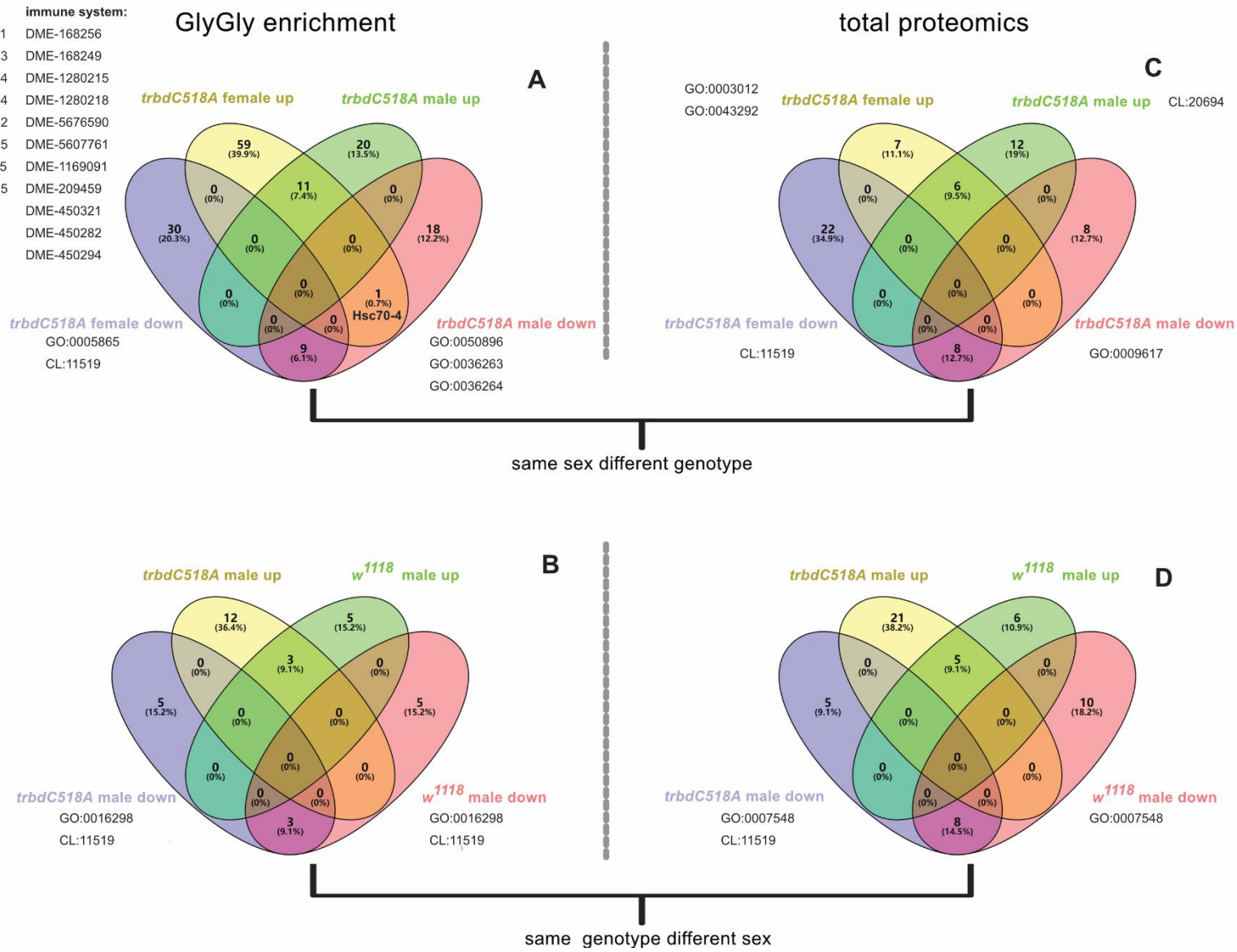


**Figure 6.2.1 Ubiquitinomics and proteomics analysis reveals sex bias in gene ontology and interactome enrichment in the heads of *trbdC518A* and *w$^{1118}$***(A) Ubiquitin GlyGly enrichment Venn analysis by comparing differentially expressed protein hits ($p<0.05$ and $log2<-1$ or $>1$) between *trbdC518A* female or male to *w$^{1118}$* female or male. (B) Ubiquitin GlyGly enrichment Venn analysis by comparing differentially expressed protein hits ($p<0.05$ and $log2<-1$ or $>1$) between *trbdC518A* or *w$^{1118}$* males to *trbdC518A* or *w$^{1118}$* female. (C) Total proteomic Venn analysis by comparing differentially expressed protein hits ($p<0.05$ and $log2<-1$ or $>1$) between *trbdC518A* female or male to *w$^{1118}$* female or male. (D) Total proteomic enrichment Venn analysis by comparing differentially expressed protein hits ($p<0.05$ and $log2<-1$ or $>1$) between *trbdC518A* or *w$^{1118}$* males to *trbdC518A* or *w$^{1118}$* female.

### 6.2.2 Female specific Yp family proteins and related pathways

Between the females and males (*trbdC518A* male vs *trbdC518A* female and *w1118* male vs *w1118* female), the gene ontology (GO) and STRING cluster (CL) related to “lipase activity” (GO:0016298 and CL:11519) were enriched in the females in the GlyGly list (Figure 6.2.1A and Table 6.4.2.2A and B) and sex differentiation (GO:0007548) was enriched in the total proteome list (Figure 6.3.1D and Table 6.4.2.2H). These two GOs and one CL mainly consisted Yp (Yolk) family proteins, which were involved in female sex differentiation (Belote et al., 1985). Noteworthy, comparing the mutant females and wild type females (*trbdC518A* female vs *w1118* female), the Yp proteins (CL:11519) were less enriched in the mutants in both lists (Figure 6.2.1A and C and Table 6.4.2.2B and F). However, comparing result in males between the mutant and wild type (*trbdC518A* male vs *w1118* male), I didn’t observe the difference in Yp protein related pathway enrichment (Figure 6.2.1A and B). This implied the mutant females were more like males on proteome level in the head.

### 6.2.3 Sex bias in pathways related to locomotor activity

I found “muscle component” (GO:0005865) was less ubiquitylated in the female mutants than female controls (*trbdC518A* female vs *w1118* female) (Figure 6.3.1A and Table 6.4.2.2B) and detected enrichment of “muscle process” (GO:0003012 and GO:0043292) in total proteome list (Figure 6.3.1B and Table 6.4.2.2F). This suggested that female mutants can retain the same level of locomotor activity (Figure 3.2) may lead by less ubiquitylation of muscle component and consequently

enhanced muscle function. When inactivating TRABID, proteins related to “response to stimulus” (GO:0050896) was less ubiquitylated in the male mutants and enriched in the female mutants (Figure 6.3.1A and Table 6.4.2.2A and B). The result was limited to female *trbdC518A* flies and could explain why *trbdC518A* had a more deleterious impact in male flies (Figure 3.2).

### 6.2.4 Female specific ubiquitylation in circadian rhythm

Inactive TRABID caused more serious fragmented sleep pattern in males than in females (Figure 3.3 and Table 3.3). When compared to $w^{1118}$ females, reactome (DME) term “circadian clock pathway” (DME-432626) was relatively enriched in *trbdC518A* females (*trbdC518A* female vs *w1118* female) (Figure 6.3.1A and Table6.4.2.2B) in the ubiquitinome analysis, suggesting when TRABID was inactivated, ubiquitylation in female “circadian clock pathway” may ameliorate the negative influence in sleep pattern. These terms were not observed in *trbdC518A* (*trbdC518A* male vs *w1118* male) and protein expression comparisons. The result indicated that the sex-specific sleeping pattern was associated with sex-specific ubiquitylation.

### 6.2.5 Sex dimorphism in neuron development and neurotransmitter

Histology study indicated sex-specific changes in cerebral cells’ quantities (Figure 3.5). When introducing *trbdC518A* in female flies (*trbdC518A* female vs *w1118*

female), GOs that were related to axon (GO:0007411, GO:0007413, GO:0061564 and GO:0030424) and neuron (GO:0030182, GO:0043005 and GO:0031175) were enriched by ubiquitin modification (Figure 6.3.1A). This could explain the observation of increased glia and neuron quantities and densities in mutant females (Figure 3.5E-G). I noticed that the GO “regulation of neurotransmitter levels” (GO:0001505) was enriched by ubiquitylation (Figure 6.3.1A and Table 6.4.2.2B), when introducing the mutation in female. GOs related to dopamine monooxygenase (DBH) activity (GO:0036263 and GO:0036264) were less ubiquitylated in *trbdC518A* males compared to *w1118* males (Figure 6.3.1A). DBH is involved in the synthesis of the neurotransmitter norepinephrine. Sex specificity in ubiquitin modification of neurotransmitters could explain the sex bias in neurological behaviours, such as locomotor activity and sleep pattern. The sex-specific difference in locomotor activity and cerebral histology difference after introducing *trbdC518A* can be associated by sex-specific neuron/glia cell or neurotransmitter changes.

### 6.2.6 Divergence in immunity between males and females

Sex bias in Relish/NF-κB induced AMP expression in brain was reported in chapter 5 (Figure 5.2). No immune related pathway was significantly enriched when comparing same genotype between sexes (*trbdC518A* male vs *trbdC518A* female and *w1118* male vs *w1118* female) (Figure 6.3.1B and D). Introducing the null mutation in female flies (*trbdC518A* female vs *w1118* female), reactome (DME) hits that related to immunity (DME-168256, DME-168249, DME-1280215 and DME-

1280218), including NF-κB signalling (DME-5676590, DME-5607761 and DME-1169091) Imd (DME-209459) and JNK-MAPK (DME-450321, DME-450282 and DME-450294), were relatively enhanced by ubiquitylation (Figure 6.3.1A). Given the fact ubiquitylation was heavily involved in immune related pathways, it was not surprising to find ubiquitylation related proteins were dominant components in these hits. Introducing *trbdC518A* did not change any immune-related pathway in male flies (*trbdC518A* male vs *w1118* male).

At the total proteome level, immune-related pathways and proteins were only indicated in the comparison of *trbdC518A* male vs *w1118* male. Hits associated to bacterium (GO:0009617) was downregulated (Figure 6.3.1C and Figure 9.1.1F) and AMP, *AttA* or *AttB,* was upregulated for mutant males (Figure 9.1.1F). Elevation of *AttA* was recorded in male mutant brain's qPCR assays (Figure 5.2C). *Drosophila* Sting pathway was reported to co-regulate Relish-induced AMP signal with the canonical Imd pathway (De Gregorio et al., 2002; Martin et al., 2018). Three Tot family protein and the protein Sting were matched in GO:0009617 (Figure 6.3.1C and Figure 9.1.1F), suggesting the Sting pathway may be upregulated when *trbdC518A* was introduced in male.

In total, ubiquitylation had a larger influence in immune regulation when the inactive *trbd* was introduced in the female flies than in the male flies, but the output of total

proteome suggested immune response related proteins were altered in the male but not in the female.

### 6.2.7 Sex dimorphism in ubiquitin linkages and ubiquitin-proteasome system (UPS)

Since sex-specific ubiquitylation was recorded, thus if there is change in ubiquitylation system remain interesting and insightful. Ubiquitin-proteosome system (UPS) associated reactome hits, including DME-209360 (ubiquitination and proteolysis of phosphorylated CI) and DME-209461 (ubiquitination and degradation of phosphorylated ARM), in female mutants, when the control was $w^{1118}$ female (Figure 6.3.1A and Figure 9.1.1A). Polyubiquitin (Ubi-p63E), ubiquitin thioesterases (CG4603 and CG4968), E2 enzyme (eff) and component of proteasome (Rpn8 and Prosbeta3) were UPS related protein (Figure 9.1.1A). This indicated that inactive TRABID could elevate the UPS activity in female heads. When introducing *trbdC518A* (*trbdC518A* male vs *w1118* male), there was no significant pathway associated to ubiquitination in males (Figure 6.3.1A), but polyubiquitin (Ubi-p63E) accumulation was recorded (Figure 9.1.1B). The finding strongly suggested that sex-specific ubiquitylation took place under an inactive TRABID.

The GlyGly enrichment-mass spectrum approach allowed me to relatively compare ubiquitin linkages between two samples, except Met1 and Lys29 linkages, due to

their low existence. After normalizing the data set against the proteins that were uniquely presented in proteome (excluding the proteins that were ubiquitylated from proteome dataset, see chapter 8.5 for detail), I found Lys6, 27 and 33 linkages were accumulated in the mutant females' heads ($p<0.05$, Figure 6.3.7A, C and D), when introducing the null mutation (*trbdC518A* female vs *w1118* female). Given Lys29 and 33 chains were the primary substrates for TRABID hydrolysis *in vitro* (Figure 2.3), it is not surprising to find accumulation of Lys33 chains. Accumulation of Lys6 and 27 chains are likely be indirect effect from *trbdC518A,* since they are not substrate for TRABID from unbiased *in vitro* DUB assays (Licchesi et al., 2012 and Figure 2.3 A). The accumulation was not observed in the males (*trbdC518A* male vs *w1118* male). This hinted that the *trbdC518A* mutation had a sex-specific impact in Lys6, 27 and 33 linkage homeostasis.

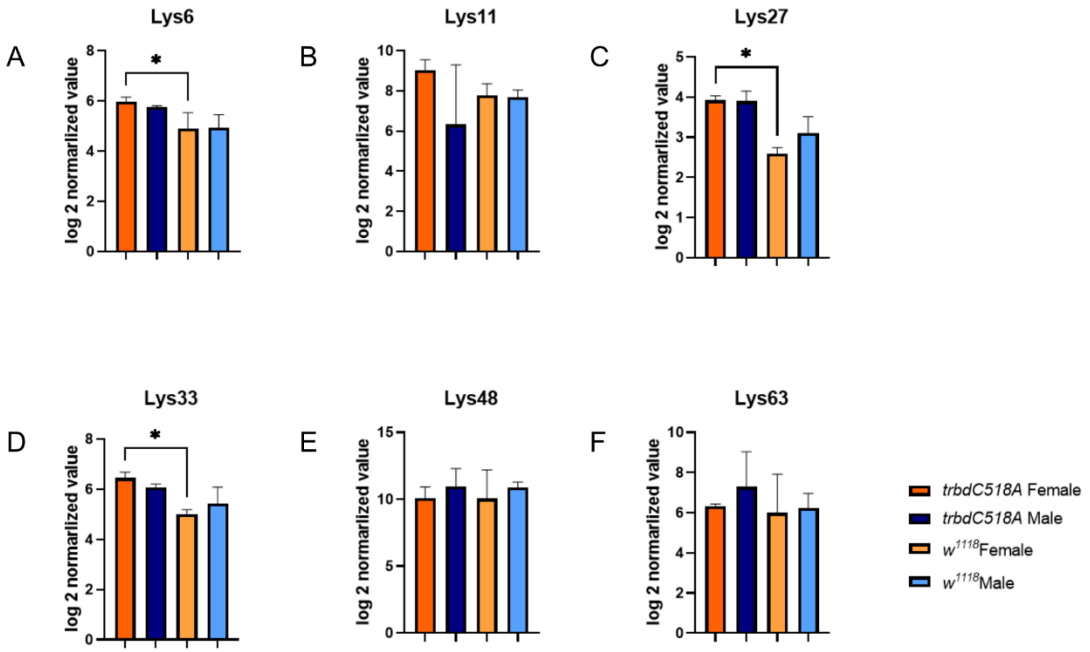



**Figure 6.2.7 *trbdC518A* influences Lys6, 27 and 33 homeostasis.** (A) *trbdC518A* female had higher Lys6 ubiquitins than $w^{1118}$ female in the head (One-Way ANOVA Kruskal-Wallis test with uncorrected Dunn's test, n=2, SD). (B) *trbdC518A* female had higher Lys11 ubiquitins than $w^{1118}$ female in the head (One-Way ANOVA Kruskal-Wallis test with uncorrected Dunn's test, n=2, SD). (C) *trbdC518A* female had higher Lys27 ubiquitins than $w^{1118}$ female in the head (One-Way ANOVA Kruskal-Wallis test with uncorrected Dunn's test, n=2, SD). (D) *trbdC518A* female had higher Lys33 ubiquitins than $w^{1118}$ female in the head (One-Way ANOVA Kruskal-Wallis test with uncorrected Dunn's test, n=2, SD). (E) *trbdC518A* female had higher Lys48 ubiquitins than $w^{1118}$ female in the head (One-Way ANOVA Kruskal-Wallis test with uncorrected Dunn's test, n=2, SD). (F) *trbdC518A* female had higher Lys63 ubiquitins than $w^{1118}$ female in the head (One-Way ANOVA Kruskal-Wallis test with uncorrected Dunn's test, n=2, SD).

### 6.2.8 *In silicon* analysis of dTRABID directly regulated pathways

Harris et al., generated proteomic data for TRABID interacting proteins from cells. They provided the information of proteins that directly interacting with TRABID in human cells, by using an inactive TRABID (Harris et al., 2020). Obtaining the GOs of these TRABID direct interacting proteins from STRING protein database and cross referencing with GOs that generated from glygly enriched proteins in *Drosophila trbdC518A* females and males provided insights in pathways that were directly regulated by TRABID in *Drosophila* head. In female cytoplasm (GO:0005737), cellular process (GO:0009987), cellular catabolic process (GO:0044248), organonitrogen compound catabolic process (GO:1901565), organonitrogen compound metabolic process (GO:1901564), intracellular anatomical structure (GO:0005622) and cellular anatomical entity (GO:0110165) were likely pathways that were directly regulated by TRABID. Cytosol (GO:0005829) was the cellular component that was likely to be regulated by TRABID directly in *Drosophila* male head.

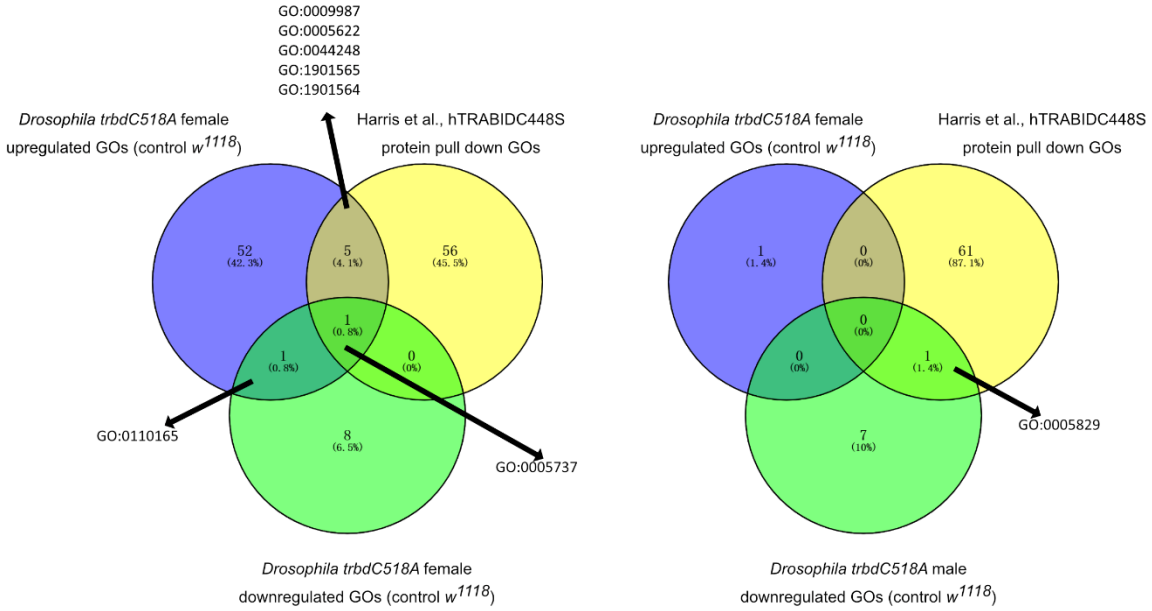



**Figure 6.2.8 Venn diagram of cross referencing GOs generated by Harris et al., and GOs from our GlyGly enrichment.** The figure provide information about common pathways (GOs) that is likely regulated by TRABID in *Drosophila* and human cell culture. Venn analysis of GOs that are found in ubiquitylation upregulation and downregulation (GlyGly pull down) in *trbdC518A Drosophila* female and male (control $w^{1118}$) with GOs enriched by hTRABIDC448S pull down in human cell culture. The left diagram shows there are five common GO between *trbdC518A* upregulation and hTRABIDC443S. One common GO in *trbdC518A* female upregulation, *trbdC518A* female downregulation and hTRABIDC443S. In the right diagram, there is one GO is in common between *trbdC518A* male downregulation and hTRABIDC443S.

## 6.3 Discussion

In this chapter I looked into ubiquitinomes and proteomes to seek molecular hints about how *trbdC518A* has sex bias impact in neurodegeneration. The *trbdC518A* mutation triggered relative more ubiquitin modification in female heads, including pathways that were annotated for behaviour, neuron immune system and ubiquitin-proteosome system (Figure 6.1.2A). However, the ubiquitylation regulation didn't significantly affect protein expression or degradation (Figure 6.1.2C). This indicates that the less server neurodegeneration impact, including locomotor activity, ageing, fragmented sleep, neuron and glia cell quantities, that was observed in female flies can be related to alteration in ubiquitylation in associated pathways rather in protein expression or degradation. However, how an inactive *trbd* can cause the female-specific changes remains for future investigation.

On the male side, *trbdC518A* male has relatively less ubiquitin modification than *trbdC518A* female (Figure 6.1.2A), when comparing to the *w1118* controls. On the protein expression level, immune related genes are overexpressed in *trbdC518A* males (Figure 6.1.2C), including AttA/AttB and Sting/cGAS antivirus pathway (Figure 9.1.1B), indicating neuroinflammation may drive *trbdC518A* male flies to more server neurodegeneration impact. Sting/cGAS can activate Relish induced AMP expression and overactivation of IMD/Relish can cause neurodegeneration in flies (Holleufer et al., 2021; Kounatidis et al., 2017), indicating inactivating *trbd* can cause inflammation in male flies through activation of cGAS/String-Relish activation and

subsequentially cause neurodegeneration. However, in this study, I was not able to verify the hypothesis.

Currently, most neurodegeneration studies focuses on the regulation of cerebral aggregated proteins and neuroinflammation, including their accumulation and degradation, which focus on the proteasome degradation signal related Lys48 linkage ubiquitin and Met1 and Lys63 linkage ubiquitins in immune signalling (Atkin and Paulson, 2014; Jack et al., 2017; Kwak et al., 2012; Li et al., 2018). More and more researches underlined the role atypical ubiquitin linkages (Lys6, 11, 27, 29, 33) have important role in cellular signalling (Kulathu and Komander, 2012). The finding in accumulation of Lys6, 27 and 33 ubiquitin linkages in *trbdC518A* females provides critical insight for rare ubiquitin linkages.

Although the omics data is too complicated to interpret under current knowledge, it still provided interesting finding about an inactive autosomal DUB having sex-specific influence in neurodegenerative phenotypes and provides important information for future studies.

# Chapter 7 Conclusion and discussion

## 7.1 Conclusion

Here I demonstrate that dTRABID has a similar biochemical specificity as hTRABID *in vitro*. When introducing *trbdC518A* mutation, it caused abrogation of dTRABID enzymatic activity *in vitro* biochemical assay. *In vivo, trbdC518A* caused sex-specific impact in lifespan, locomotor activity, sleeping pattern and brain histology. Although both sexes are affected, the *null trbd* is more deleterious in males' neurological behaviours. Moreover, suppressing female development in certain tissues (astrocytes and immunocompetent tissues), the sex bias in locomotor activity and Relish/NF-κB induced AMP expressions can be partially reduced. The study further provided evidence in ubiquitinome and proteome showing that *trbdC518A* had sex bias influence in various pathways that are associated with the phenotype recorded, including, muscle component and function, circadian rhythm, react to stimulus, neurological signalling and development, NF-κB immunity, UPS and ubiquitin linkage homeostasis. In total, the study discovered that inactivating an autosomal deubiquitylase, *trbd*, generated sex-specific neurodegenerative phenotypes and underlined by ubiquitinome and proteome.

## 7.2 Discussion

### 7.2.1 Biochemistry

In this study, I demonstrated the dTRABID-AnkOTU domain has the same catalytic

activity towards Lys29 and 33 ubiquitin linkages *in vitro.* The result aligns with hTRABID enzyme specificity *in vitro* and dTRABID enzyme specificity *in vivo* (Hua et al., 2022; Licchesi et al., 2012a). In *Drosophila* studies TRABID interacts with Tak1/TAB2 complex and inhibits IMD driven NF-κB activation (Fernando et al., 2014; Hua et al., 2022). In human cells, hTRABID interact with HECTD1 and STRIPAK complex (Harris et al., 2020). From the PhosphoSitePlus (https://www.phosphosite.org/homeAction.action) (Hornbeck et al., 2015), TRABID has several predicted phosphorylation and ubiquitylation sites (Figure 7.2). It is not uncommon for phosphorylation regulating DUB's activity. For example, phosphorylation of Ser177 in OTUB5's OTU domain is necessary for the enzyme activation (Huang et al., 2012). Noteworthy, in the OTU enzymatic domain, there are three predicted phosphorylation sites (Figure 7.2), which may play an important role regulating the enzyme's activity. It is possible that STRIPAK complex, which is a kinase and phosphatase complex that interact with TRABID in human cell culture (Harris et al., 2020), can phosphorylate TRABID and regulates its activity, but needs further study to verify the hypothesis.

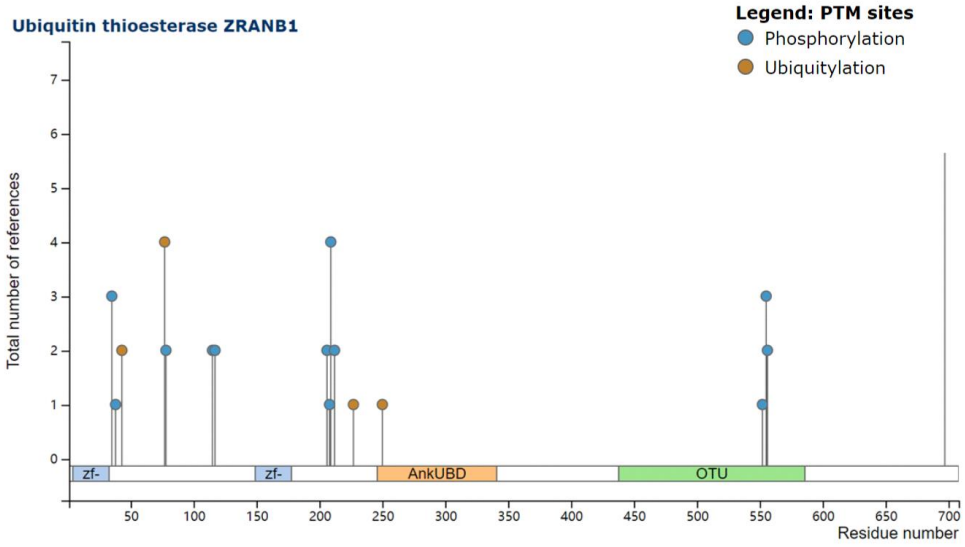



**Figure 7.2.1 Phosphorylation and ubiquitylation site of TRABID**. Phosphosite summerised the phosphorylation (blue) and ubiquitylation sites that are discovered from available publication and databases.

### 7.2.2 Cellular biology

Even though *Drosophila* is a canonical animal model for biological studies, there is still significant difference between the invertebrate and vertebrate. One apparent issue for dTRABID is that Trabid is the only A20 family protein in *Drosophila* (Tran et al., 2008). Knocking out dTrabid over activates IKK induced NF-κB signalling (Fernando et al., 2014; Hua et al., 2022; Kounatidis et al., 2017). In vertebrates, A20 is well known for its role as a negative regulator of IKK/NF-κB activation (Lork et al., 2017). Hence, It is tempting to hypothesize that dTrabid is substituting A20's role in *Drosophila* and its loss triggers inflammation induced neurodegeneration (Kounatidis et al., 2017).

In human cell culture and mouse model, TRABID is dispensable for TNFR1/IKK-induced NF-κB signalling (Evans et al., 2001; Jin et al., 2016), while TRABID is a negative regulator for IMD/Relish-driven NF-κB signalling (Fernando et al., 2014; Hua et al., 2022). A20 mediates Met1, Lys48 and Lys63 ubiquitin chains to regulate inflammation (Lork et al., 2017; Wertz et al., 2015), while *in vitro* DUB assays showed that hTrabid specifically hydrolyses Lys29 and 33 chains (Licchesi et al., 2012) (Figure 2.3), and less active towards Lys63 chains. In the context of TNFR1 or IMD-mediated NF-κB signaling, A20 and TRABID can regulate Lys63 ubiquitin to inhibit the pathway. However, in TNFR1 or IMD-regulated immunity can TRABID substitute A20's role in vertebrate system and *vice versa* can A20 substitute TRABID role in invertebrate system remains unclear.

Given Lys29 and 33 linkages are the primary substrate for TRABID and *trbdC518A* mutation led to Lys33 ubiquitin accumulation in female heads (Lys29 cannot be detected due to technical barriers), indicating the unique role in regulating ubiquitin homeostasis *in vivo.* It is reported that Lys29 chains is involved in activation of ASK1 and subsequentially activation antiviral immunity (Yu et al., 2016). Lys33 facilitates post-Golgi transportation via regulation of CRN7 (Baumann, 2014). Lys29 and 33 ubiquitins are atypical chain types and are not well studied. My ubiquitinome and proteome date provided critical insight about pathways that are likely regulated by TRABID with relative accumulation of Lys33 chains. However, molecular and functional studies are needed to verify potential regulations.

Accumulations of Lys6 and 27 chain in female *Drosophila* head are likely due to indirect influence of inactivating TRABID. Since Lys 6 and 27 polyubiquitins are closely linked to mitochondrial activity (Birsa et al., 2014; Gersch et al., 2017) and dysfunction of mitochondria plays important role in pathogenesis of neurodegenerative diseases (Xu et al., 2021). Currently, there is no direct findings of TRABID affecting mitochondrial health. Functional study of TRABID in mitochondrial function is prospect for future studies.

### 7.2.3 Neurobiology

Neurodegenerative diseases, such as AD and PD, have sex bias risks (Guo et al., 2022; Wooten et al., 2004). I created a *trbdC518A Drosophila* mutant and assessed lifespan and neurodegenerative behaviours in both females and males. Results showed that *trbdC518A* is more deleterious to male fly's lifespan, locomotor ability and sleeping (Figure 3.2, Table 3.3 and Figure3.4). Further cerebral histology analysis indicated the null mutation had sex differential impact in brain size, total cell, glia and neuron quantities and densities (Table 3.5). Female and male flies have sexual dimorphism in cerebral cellular quantities (Jiao et al., 2022). Though our quantitation method was not the most direct and accurate, it hinted that introducing *trbdC518A*, reduced sex difference in brain size, total cell number and glia cell density. Reduced level of neurons doesn't result in direct reduction of neuron transmitters, which are critical chemical substance for neuronal signals. A more direct way to quantify neurodegeneration is to quantify neurotransmitters, which is possible through quantifying different types of neurotransmitters (Sun et al., 2018).

Given the complexity of neuron system, the pathogenesis of neurodegenerative diseases may not be directly linked to the loss of total cerebral cells or neurons or glia cells. The more direct pathogenesis of neurodegenerative diseases is likely to be defects in neurotransmitters, such as dopamine (Rangel-Barajas et al., 2015). In our GO analysis, I obtained hits that hints *trbdC518A* has sex dimorphism in neuron development and neurotransmitter processing. It is tempting to select genes from

these GO hits and generate double mutant *Drosophila* with *trbdC518A* for epistasis analysis, such as Hsc70-4, which will be explained in the next paragraph.

In the GOs that related to neuron development and were relatively upregulated in *trbdC518A* female (control $w^{1118}$) ubiquitinome contained several genes in common, including *draper (drpr), basket (bsk), chromosome bows (chb), arp3, raspberry (ras), pathetic (path)* and *Hsc70-4. drpr* encodes a single-pass transmembrane receptor and is involved in glial phagocytosis. Draper offers neuron protection against Aβ42-induced toxicity, in a *Drosophila* model that expresses human Aβ42 (Ray et al., 2017). *bsk* encodes a JNK pathway kinase. Overexpression of *bsk* in *Drosophila* neurons protects the animal from 1-octen-3-ol-mediated dopamine neurotoxicity (Inamdar et al., 2014). *chb* is critical for microtubule dynamics in kinetochore attachment and central spindle formation. In a *Drosophila* model expressing human Tau protein, there is genetic interaction between *chb* (human ortholog *CLASP1/CLASP2*), *CLIP-190* (human ortholog *CLIP1/CLIP2*) and *Tau.* In human, *CLASP1/CLASP2* and *CLIP1/CLIP2* encode microtubule plus-end tracking proteins and coordinate with Tau proteins, which control microtubule end proteins, to regulate the dynamics of microtubules (Feuillette et al., 2020; Ramirez-Rios et al., 2017). In *Drosophila* model PD, α-synuclein impair maturation of autophagosome through Arp2/3 complex (Sarkar et al., 2021). Downregulation of RAS-MAPK-MSK1 is shown to decrease ATXN1 level and suppress neurodegeneration in *Drosophila* and mice (Park et al., 2013). *path* plays an important role for extreme dendrite growth in

*Drosophila* sensory neurons (Lin et al., 2015). As mentioned in Chapter 6.3.1, Hsc70-4 is the only gene that had divergent regulation in *trbdC518A* males and females. The interaction of Hsc70-4 and *ataxin-3* facilitates the Ataxin-3 aggregation and ultimately cause the neurodegenerative disorder spinocerbellar ataxia type 3 (SCA3) in *Drosophila* (Johnson et al., 2020). Understanding the role of ubiquitylation in these candidates can provide insight in female-specific neurodegeneration.

### 7.2.4 Omics studies

This study generated high quality of ubiquitinomics and proteomics data in *trbdC518A Drosophila* heads and cross referenced with proteomic data that was generated recently Harris et al., (Harris et al., 2020), I was able to predict direct regulatory pathways of TRABID in *Drosophila* heads, mostly in cellular development, metabolic and trafficking. Moreover, the cross reference also found sexual dimorphism in the predicted pathways (Chapter 6.3.8).

I only did our proteomics studies in 18-day old adult fly heads. Given ageing is a major risk for neurodegeneration and our brain AMP expression data showed differences between 3-day old adult fly and 18-day old adult fly a later time point will also be informative. Moreover, *trbdC518A* mutation may have different impact in different cells or tissues. In the future, temporal (day 3, 18 and 30) and spatial (head and abdomen) omics studies in *trbdC518A* model animals or cells can provide

significant insight on TRABID targets.

## 7.3 Limitation of the study

*Drosophila* is a model animal that is widely used in biological research. Introducing *trbdC518A* mutation in *Drosophila* provided us the platform to look into sex-specific difference in behaviour, brain histology and NF- κB induced inflammation and head ubiquitinomics and proteomics. It also offered the genetics tools for tissue-specific suppression of female development in certain tissues. However, the biological gap between human and *Drosophila* should be underscored.

Although 75% of human disease genes can be found in *Drosophila, Drosophila* and mammals only share 40% similarity in sequence (Yamaguchi and Yoshida, 2018). This leads to variances in some pathways. For example, in the deubiquitylation process of *Drosophila* IMD/NF-κB pathway, *Drosophila* does not have *A20*, *Cezanne* and OTULIN genes, which are important DUBs involved in the human TNFR1/NF-κB pathway. Moreover, *Drosophila* does not encode the gene for Aβ, tau and α-synuclein, which are known aggregate proteins in human neurodegenerative disorders. The *Drosophila* model for Aβ, tau and α-synuclein are all achieved by introducing human ortholog genes into the animal via transgenic means (Auluck et al., 2002; Crowther et al., 2005; Wittmann et al., 2001). However, lacking the indigenous pathways may undermine the results. Like innate immunity, adaptive

immunity can be neuronal protective or detrimental (Mayne et al., 2020). *Drosophila* does not have an adaptive immune system. In the *Trabid* knockout mouse model, TRABID is reported to deubiquitylate and prevent histone demethylase Jmjd2d from proteolysis. Consequently, Jmjd2d can demethylate histones at the promoter region of IL-12 and IL-23, which are TLR/NF-κB induced. Expression of IL-12 and -23 can activate proinflammation T helper 1 (Th1) and Th17 cells (Jin et al., 2016). In total, the knowledge gap between our invertebrate model and other vertebrate models is still significant.

## 7.4 Significance of the study

Previous studies have showed bilateral association between (1) ubiquitylation and neurodegenerative diseases, (2) ubiquitylation and sexual dimorphism and (3) sex bias and neurodegeneration (Fisher et al., 2018; Jenkins et al., 2020; Schmidt et al., 2021). Findings in this study draw insight into the combination of the three namely, sex, neurodegeneration and ubiquitylation in *Drosophila* via deactivating the enzymatic activity of an evolutionary conserved *Drosophila* DUB – Trabid. Suppressing female sex development in certain tissues can partially reduce the sex bias in neurodegeneration, behaviour and inflammation. This study provided high quality ubiquitinomics and proteomics data to support our behaviour and histology data and identify potential targets of Trabid. The *in vivo* ubiquitin linkage homeostasis data underlines the enzymatic specificity of TRABID that is found *in vitro.*

# Chapter 8: Materials and methods

## 8.1 dTRABID-AnkOTU and dTRABID-AnkOTU cloning and protein purification

### 8.1.1 Cloning dTRABID-AnkOTU and dTRABID-AnkOTUC518A into pOPIN vectors.

For cloning dTRABID-AnkOTU into poPINS plasmid, Primer "GCGAACAGATCGGTGGTGACACCCTGCAAGAGCGTCAAGAGAG" and "ATGGTCTAGAAAGCTTTATTCTTCGTCGGAGTCGCCGTCGG" were used to amplify dTRABID-AnkOTU domain (PCR: 98 ℃ for 20 sec denature, 65 ℃ for 30 sec annelation and 72 ℃ for 30 sec amplification) The dTRABID gene was synthesized with codon optimization to *Spodoptera frugiperda* (*S. frugiperda*) (Sigma, UK) and cloned into HindIII and KpnI (NEB, UK) digested pOPINS plasmid (Figure 8.1.1A). Colonies were selected by X-gal and confirmed by Sanger sequencing (Sourcebioscience, UK) (Figure 8.1.1B).

I used "TTCTGCTGGCGACGCCCTGCTGGACTCTGC" and "TGCATAGCAGAGTCCAGCAGGGCGTCGCCA" to create the C518A point mutation with the original cloning primers (PCR: 98 ℃ for 20 sec denature, 65 ℃ for 30 sec annelation and 72 ℃ for 30 sec amplification). The sequence was confirmed by Sanger sequencing (Sourcebioscience, UK) (Figure 8.1.1C).

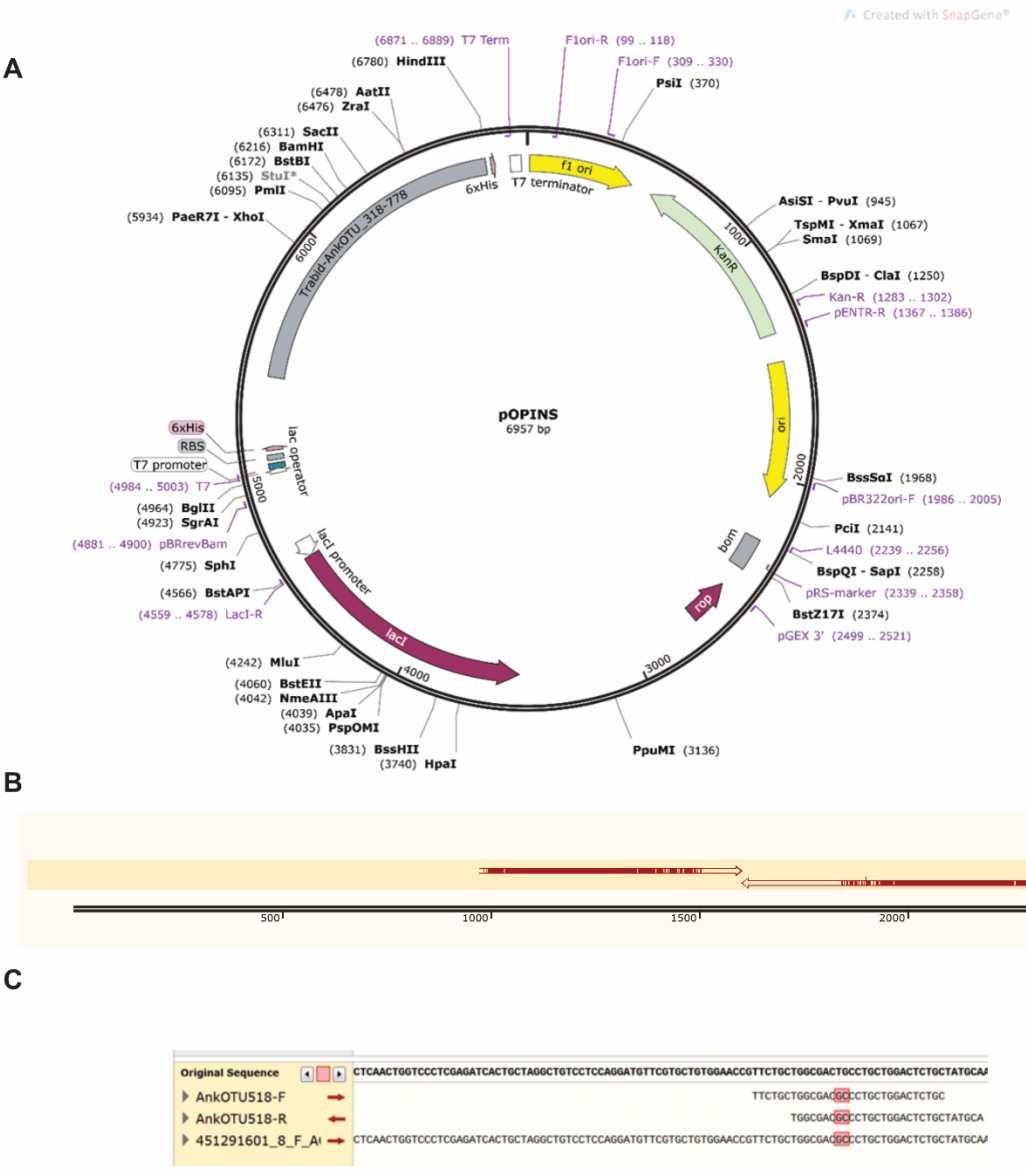



**Figure 8.1.1 Molecular data for cloning dTRABID-AnkOTU and dTRABID-AnkOTUC518A.** (A) pOPINS plasmid backbone inserted with dTRABID-AnkOTU sequence with codon optimized to *S. frugiperda*. (B) Sanger sequence result of dTRABID-AnkOTU with *S. frugiperda* codon optimization. (C) Sanger sequence result of dTRABID-AnkOTUC518A with *S. frugiperda* codon optimization.

### 8.1.2 Protein expression and purification

Plasmid (dTRABID-AnkOTU or dTRABID-AnkOTUC518A) was transformed into Rosetta II *Escherichia coli* (*E. coli*) competent cells and selected on kanamycin and chloramphenicol LB plate. Respectively, all colonies selected from the LB plate were made into 300 ml overnight LB liquid preculture which contains 30 µg/ml kanamycin and 34 µg/ml chloramphenicol. Every liter of 2xTY media were inoculated with 15 ml overnight preculture with 30 µg/ml kanamycin and 34µg/ml chloramphenicol. The cultures were incubated at 30 ℃ for 3 hours and temperature was lowered to 18 ℃ and 400 µg of isopropyl β-D-1-thiogalactopyranoside (IPTG) were added. The cultures were incubated overnight, harvested and stored in -80 ℃.

Harvested cell pellets were defrosted at room temperature (23 ℃) and sonicated for 2 minutes at 30 amp (15 seconds impulse and 15 seconds rest) in lysis buffer (20 mM tris, 300 mM NaCl, 20 mM imidazole, 2 mM ethanethiol and pH 8). Lysate was centrifuged for 30 minutes at 15000 rpm at 4 ℃. Lysate was subjected to Ni-column (GE, UK) purification and eluted with 20 mM tris, 300 mM NaCl, 500 mM imidazole and 2 mM ethanethiol (pH 8) (Figure 2.2.2.1 A). Elution was dialyzed with anion wash buffer (20 mM Tris (pH 7.5) and 4 mM DTT) with 1 mg SUMO protease at 4 ℃ for overnight.

Ni-column purified elutes were subjected to ResourceQ anion exchange chromatography (GE, UK). The wash buffer contained 20 mM Tris (pH 7.5) and 4 mM DTT and elution buffer contained 20 mM Tris (pH 7.5), 4 mM DTT and 1 M NaCl. Elution fractions were analyzed by SDS-PHAGE gel (12%) running in MES buffer (Thermo Fisher, UK) for 40 mins at 180 V. Fragments that were about 48 kDa were collected and concentrated (Figure 2.2.2.1 B and C).

Concentrated fragments were subject to SuperDex75 gel filtration chromatography (GE, UK). The gel filtration buffer contained 20 mM Tris (pH 7.5), 4 mM DTT and 750 mM NaCl. Filtered fragments were analysed by SDS-PAGE gel. Fragments that contained solo band that were 48 kDa were pooled, concentrated and snap freeze for long term storage. I used this method to purify dTRABID-AnkOTU (Figure 8.1.2.1 A-E). For dTRABID-AnkOTUC518A (Figure 8.1.2.2 A-G), a SuperDex200 gel filtration chromatography (GE, UK) was applied before SuperDex75 gel filtration chromatography (GE, UK).

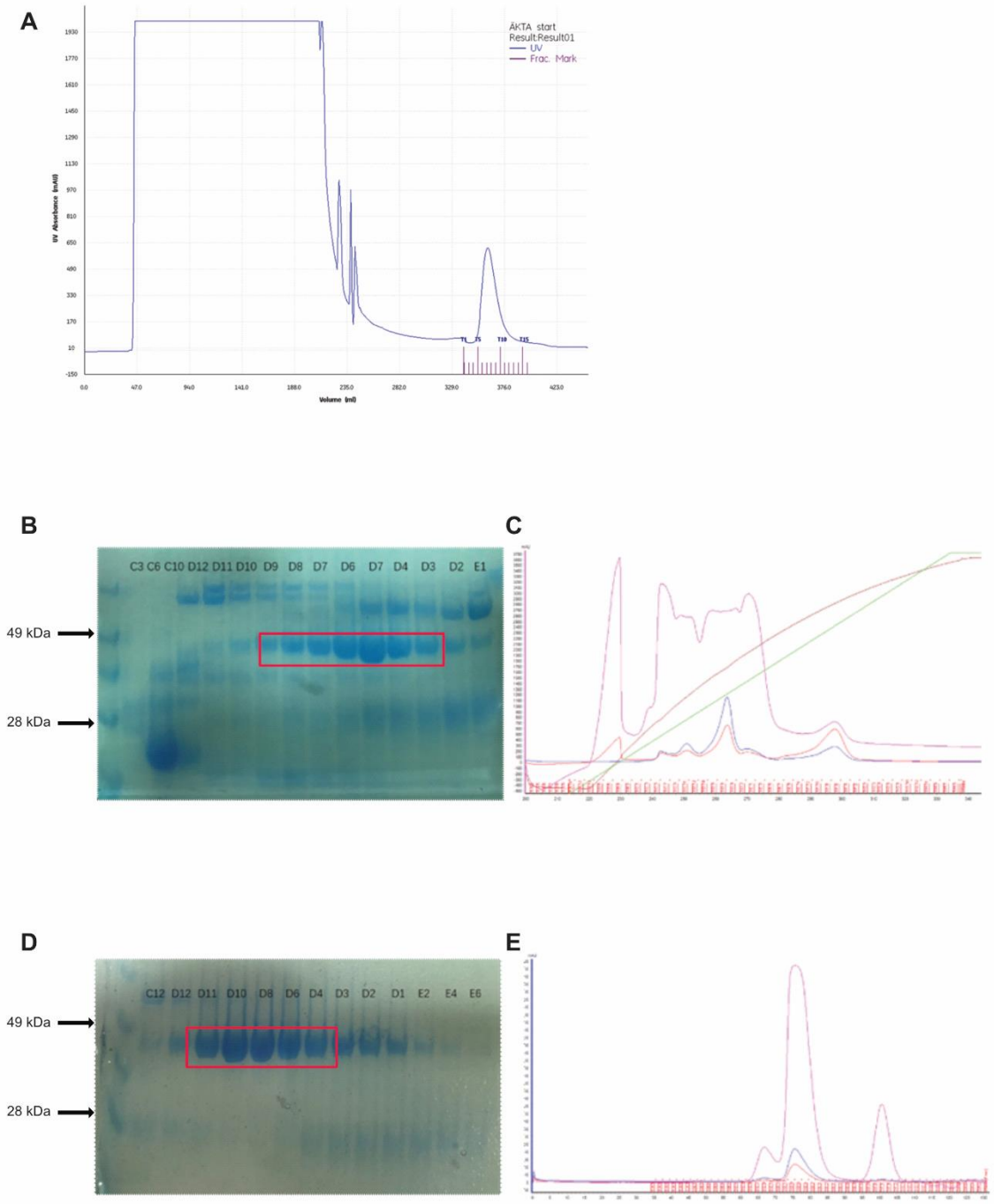



**Figure 8.1.2.1 Chromatography result for dTRABID-AnkOTU** (A) Ni column chromatography graph for dTRABID-AnkOTU. (B) 12% SDS gel electrophoresis result for selected aliquots of ResourceS column filtered elutes. Gel was stained by Coomassie Blue. Elutes from cell D3-D8 were pooled together for next step(red box). (C) ResourceS chromatography graph for dTRABID-AnkOTU. (D) 12% SDS gel electrophoresis result for selected aliquots of SuperDex200 column filtered elutes.

Gel was stained by Coomassie Blue. Elutes from cell D4-D11 were pooled together for next step (red box). (E) SuperDex200chromatography graph for dTRABID-AnkOTU.

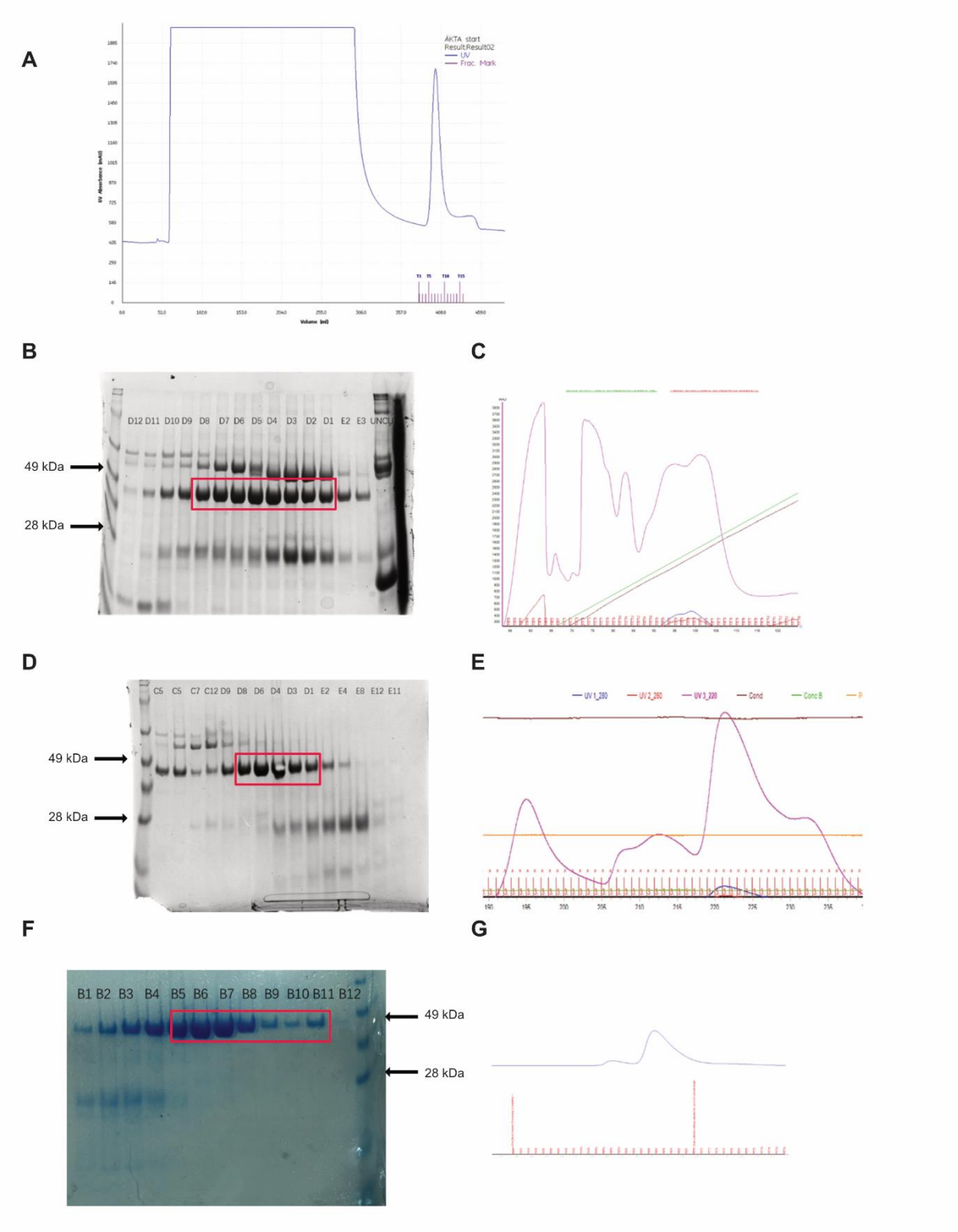



**Figure 8.1.2.2 Chromatography result for dTRABID-AnkOTUC518A** (A) Ni column chromatography graph for dTRABID-AnkOTU. (B) 12% SDS gel

electrophoresis result for selected aliquots of ResourceS column filtered elutes. Gel was stained by Coomassie Blue. Elutes from cell D1-D8 were pooled together for next step (red box). (C) ResourceS chromatography graph for dTRABID-AnkOTU. (D) 12% SDS gel electrophoresis result for selected aliquots of SuperDex75 column filtered elutes. Gel was stained by Coomassie Blue. Elutes from cell D1-D8 were pooled together for next step (red box). (E) SuperDex75 chromatography graph for dTRABID-AnkOTU. (F) 12% SDS gel electrophoresis result for selected aliquots of SuperDex200 column filtered elutes. Gel was stained by Coomassie Blue. Elutes from cell B5-B11 were pooled together for next step (red box). (G) SuperDex200chromatography graph for dTRABID-AnkOTU.

### 8.1.3 Deubiquitylase assays

Deubiquitylases were diluted to 300 or 600 nM using gel filtration buffer (20 mM Tris (pH 7.5), 4 mM DTT and 750 NaCl). The final reaction concentration will be 150 or 300 nM. 10x DUB buffer that contained 500 mM, 500 mM NaCl and 50 mM fresh DTT. 2x master mix that 18 µl water, 6 µl 10 x DUB buffer and 0.6 µg/ml diubiquitin chains was prepared for each ubiquitin chain type and time point. I used 150 nM dTRABID-AnkOTU to hydrolyse all eight diubiquitin chains for 0, 5 and 30 minutes. I used 300 nM dTRABID AnkOTU and dTRABID-AnkOTUC518A to hydrolysis Lys29 and 63 diubiquitin chains for 0, 5 and 30 minutes. The result was visualized by silver staining (bio-rad, UK).

## 8.2 Behaviour and brain histology assays

### 8.2.1 Fly husbandry and crossing

The flies were generated by CRISPR-Cas9 (RainbowGene, USA). Balancer chromosomes are used to obtain heathy stocks in lethal mutations and tracking chromosomes in genetic mating schemes. Here I crossed it to a Tm3sb/Dr background, which has a double balancer on the third chromosome and is used to trace the *trbdC518A* mutation. The crossing progeny trbdC518A/Tm3sb was self-crossed and homozygous *trbdC518A* flies were checked by sequencing (Figure 8.2A and B). Flies were reared in 25℃ and 34% humidity. Fly foods were prepared using 1.5 kg organic cornmeal, 600 g yeast, 900 g molasses, 162 g agar, 33.6 g Tegosept, 101 ml 100% propionic acid, and 168 ml 100% ethanol in 20 L of hot

water. I collaborated with Biochemistry media kitchen team, especially with Mr. Tony Bywaters. Foods were changed every three days to reduce microbial infection to the animal.

### 8.2.2 Locomotor activity assay

Flies needed to climb 17.5 cm in a transparent graduate cylinder in 2 minutes to pass the assay (Madabattula et al., 2015) (Figure 8.2C).. All tests were carried out between 1 pm-5pm. Around 20 flies were tested each time and the passing ratio was calculated by the equation:

$$\text{passing ratio} = \frac{\text{number of flies passed the assay}}{\text{total flies}} \times 100$$ (Figure 3.2B).

Flies were collected at the day of eclosion. 10 to 20 flies were kept in a vial with same sex and food was changed every 3 days. I assessed our flies at day 3, 6, 9, 12 and 18. 5 biological replications were conducted with at least 5 repeats. In GraphPad Prism 9.2.0, normal distribution was checked for each group and two-way ANOVA was performed, using mixed-effects model with Tukey's multiple comparison correction.

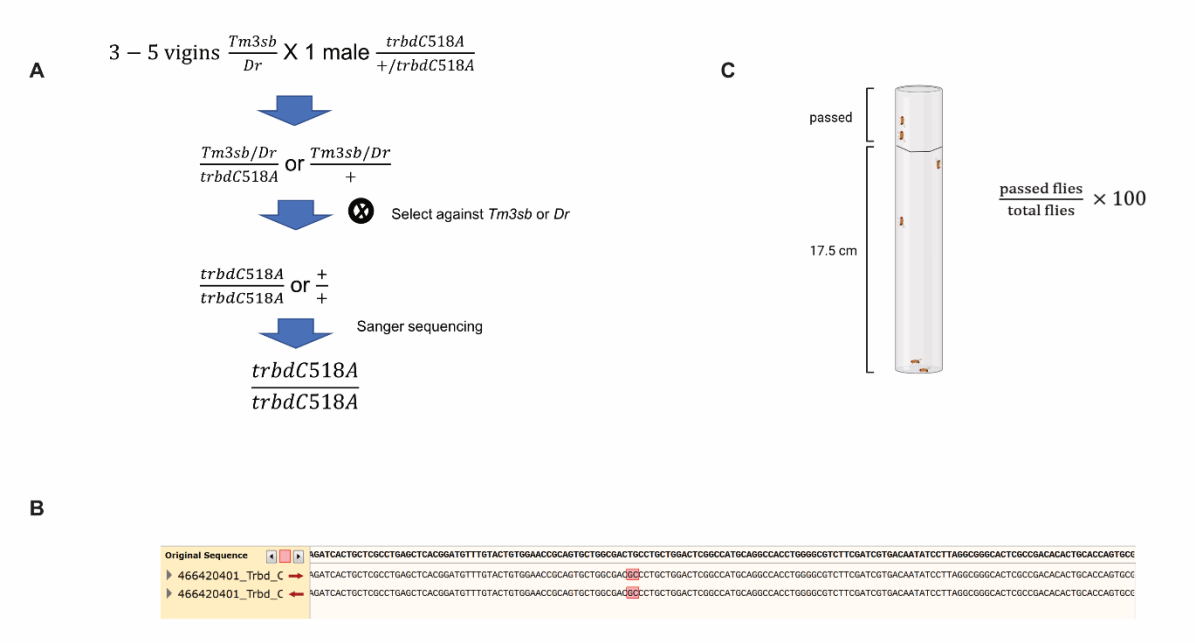



**Figure 8.2 Generating homozygous trbdC518A fly and climbing assay.** (A) Crossing strategy for obtaining homozygous *trbdC518A* flies. (B)Sequence confirmation of *trbdC518A* in *Drosophila* homozygous progenies. (C) Illustration of the assay and how the passing rate was calculated.

### 8.2.3 *Drosophila* activity monitoring (DAM)

Flies were collected at the day of eclosion and ~20 flies were kept in a vial. Food was changed every three days. On day-5, flies were anesthetized on ice and loaded on DAM with fresh food. The incubators were set at 25℃. The recording starts on day 6, with the LP starting from 8 am and DP starting from 8 pm. The recording lasted for at least 3 days. I chose the second day (7 days after eclosion) data for analysis. 3 biological replication was conducted with at least 15 repeats in each replication. In GraphPad Prism 9.2.0, normal distribution was checked for each group. Since some group didn't pass the normality test, thus Kruskal-Wallis with uncorrected Dunn's test was applied for others. Multiple comparisons were conducted and plotted out.

### 8.2.4 Lifespan assay

Flies were reared and collected as described on precious context. 20 flies were kept in a vial and food was changed every three days and dead flies were counted. Food change lasted until the last fly's death in the vial. Every biological replication contained at least 10 repeats for each genotype. Three biological replications were conducted and data was pooled together. In GraphPad Prism 9.2.0, I used built-in survival analysis to perform Mantel-Cox (Log-rank) test, calculate the median survival and visualize the result.

### 8.2.5 *Drosophila* brain immunofluorescence assay

Dr Jeff Lee helped me to design the experiment. Three biological replications were prepared in total, and each replication had at least 10 brains. Flies were anesthetized on ice at day-18 after eclosion and dissected in PBS. PBTX solution (PBS and 0.3% Tween 80) and 4% PFA were used to prepare fix solution. Brains were moved to fix solution and fixed at room temperature for 30 minutes incubation. Samples were washed for 3 times in PBXT and transferred to Intercept (PBS) blocking buffer (Li-Cor, UK) for an hour incubation at 4 degrees with gentle rocking. Primary antibodies (1%, Rat-Elav-7E8A10 anti-elav and 8D12 mouse anti-Repo, DSHB, USA) in PBTX was used to replace the blocking solution and incubated at 4 degrees for overnight with gentle rocking. On the second day, samples were washed with PBTX for three times and replaced with secondary antibody (1%, goat anti-mouse Alexa Fluor 488 and goat anti-rat Alexa Fluor 568, ThermoFisher UK) and 1 ug/ml DAPI solution. After 45 minutes, samples were washed in PBTX solution for 3 times and incubated in PBXT solution for more than 45 minutes. Samples were incubated in Vectashield mounting media (2BScientific, UK) for more than 30 minutes and mounted on glass slide with cover slip.

Specimens were imaged on an Olympus SpinSR10 spinning disk confocal system equipped with Prime BSI sCMOS camera. 20x dry objective (0.8NA, UPLXAPO20X) was used to acquire the images. The microscope was driven using Olympus cellSens Dimension software. The image data were uploaded and stored in the

Department of Biochemistry, University of Oxford OMERO server. Images were analysed in FIJI-ImageJ. I summed fluorescence intensity across Z slices to quantify immunofluorescence signal (Figure 3.5 A).

In each biological replication, five samples were selected for the analysis for each phenotype and three biological replications were prepared. Raw images were background subtracted with the rolling ball subtraction method in ImageJ prior to the intensity calculation. Brain areas were calculated by outlining the DAPI channel signals. In each channel, the area and raw integrated density (RID) of the brain and background were measured. The signal intensity of the brain (foreground) of each channel was calculated by the equation:

$$\text{Foreground Signal} = \text{Foreground RID} - \frac{\text{Background RID}}{\text{Background Area}} \times \text{Foreground Area}.$$

The foreground signal density of the brain was calculated by the equation:

$$\text{Foreground Signal Density} = \frac{\text{Foreground Signal}}{\text{Foreground Area}}.$$

I used GraphPad Prism built-in normality test to test the distribution. Since some group didn't pass the normality test, thus Kruskal-Wallis with uncorrected Dunn's test was applied for others. Multiple comparisons were conducted and plotted out.

## 8.3 Method of reducing female development in *trbdC518A* background

I used the *Drosophila* UAS-Gal4 system to reduce the female sex development in astrocytes (*alrm-Gal4*) and immunocompetent cells (fat body, gut, haemocytes) (*J6-Gal4*) under the *trbdC518A* background and carried out the climbing assay 9 days after eclosion to explore if the sex bias can be reduced. I obtained and integrated *UAS-tra$^{RNAi}$* (VDRC#2560), *trbdC518A*, *alarm-Gal4*, and *J6-Gal4* into *gla/cyo;TM6B/pri*. The detail crossing process was illustrated in Figure 7.3A. I checked the *C518A* mutation in *gla/cyo;trbdC518A/TM6B* by Sanger sequencing (Figure 7.3B) (Sourcebioscience, UK). *gla/cyo;trbdC518A/TM6B* was used to cross with *UAS-tra$^{RNAi}$/cyo;TM6B/pri*, *UAS-msd8GFP$^{i}$/cyo;TM6B/pri alrm-Gal4/cyo;TM6B/pri* and *J6-Gal4/cyo;TM6B/pri* to generate *UAS-tra$^{RNAi}$/cyo;TM6B/trbdC518A*, *UAS-msd8GFP/cyo;TM6B/trbdC518A*, *alrm-Gal4/cyo;TM6B/trbdC518A* and *J6-Gal4/cyo;TM6B/trbdC518A*. I tried to obtain *UAS-tra$^{RNAi}$;trbdC518A, UAS-msd8GFP;trbdC518A alrm-Gal4;trbdC518A* and *J6-Gal4;trbdC518A* via selfing, but *J6-Gal4;trbdC518A* female was infertile. Thus I used *J6-Gal4/cyo;trbdC518A* for future experiment. The UAS and Gal4 lines that had *trbdC518A* mutation were crossed to generate *UAS-msd8GFP/alrm-Gal4;trbdC518A, UAS-tra$^{RNAi}$/alrm-Gal4;trbdC518A* and *UAS-tra$^{RNAi}$/J6-Gal4;trbdC518A.* I applied the climbing assay that was mentioned in Chapter 3 to assess the locomotor activity.

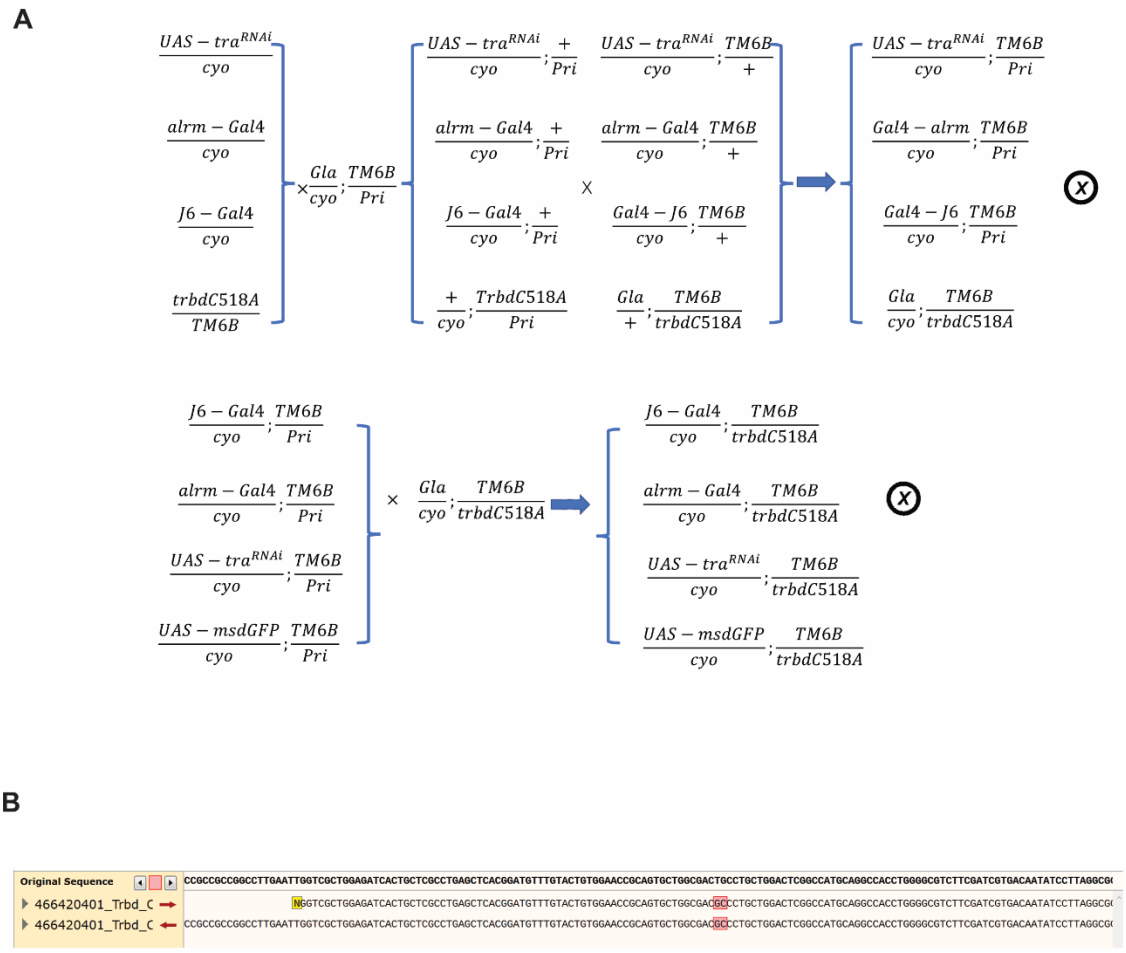



**Figure 8.3 Strategy of integrating tissue specific *tra*$^{RNAi}$ into trbdC518A background.** (A) Crossing map of generating astrocyte- and immunocompetent cells-specific *tra*$^{RNAi}$ *Drosophila* lines and their controls into *trbdC518A* background. (B) Sanger sequence confirmation of *trbdC518A* in *Gla/Cyo;trbdC518A*.

| lines | experiment |
|---|---|
| $w^{1118}$ | climbing |
| | sleep monitoring |
| | brain histology |
| | ubiquitinome and proteome |
| $trbd^{C518A}$ | climbing |
| | sleep monitoring |
| | brain histology |
| | ubiquitinome and proteome |
| *Tm3sb/Dr* | Third chromosome balancer for checking $trbd^{C518A}$ homogeneity |
| $UAS\text{-}tra^{RNAi}/cyo$ (VDRC#2560) | Initial UAS parent line for female blocking experiment |
| *alrm-Gal4/cyo* | Initial Gal4 parent line for female blocking experiment |
| *J6-Gal4/cyo* | Initial Gal4 parent line for female blocking experiment |
| *Gla/cyo;TM6B/Pri* | Double balancer for generating lines for female blocking experiment |
| $J6\text{-}Gal4/cyo;TM6B/trbd^{C518A}$ | Immunocompetent tissue specific Gal4 line under $trbd^{C518A}$ background |
| $alrm\text{-}Gal4/cyo;TM6B/trbd^{C518A}$ | Astrocyte specific Gal4 line under $trbd^{C518A}$ background |
| $UAS\text{-}tra^{RNAi}/cyo;TM6B/trbd^{C518A}$ | $UAS\text{-}tra^{RNAi}$ line under $trbd^{C518A}$ background |
| $UAS\text{-}msdGFP/cyo;TM6B/trbd^{C518A}$ | *UAS-msdGFP* control line under $trbd^{C518A}$ background |

**Table 8.3 *Drosophila* lines used in animal experiments.**

### 8.4 Sample preparation for *Drosophila* brain AMPs expression

Brains or abdomens and thoraxes were dissected in PBS and RNA was isolated immediately using TRIzol Plus RNA Purification System (ThermoFisher, UK). Samples were stored in -80 ℃. I used Superscript III cDNA synthesis kit (ThermoFisher, UK) to synthesize cDNA.

I used SensiFast qPCR master mix (Bioline, UK) to carry out the qPCR reaction. Gene *sdha* was used as the house keeping gene. The primers were listed in table 8.4. I used CFX Connect Real-Time PCR system (Bio-rad) to collect ct values. 45 amplification cycles were conducted for each run. I followed the manufacture protocol of SensiFast qPCR master mix (with annealing temperature of 60 and amplification time of 15 sec) and used the R package “qpcr” (https://cran.r-project.org/web/packages/qpcR/qpcR.pdf) to perform “ddct-test” analysis and “relative expression” following the user manual. I used the R package “fmsb” to present the relative expression in spider plots. The relative gene expression of control group was normalized to “1” and used as baseline for the relative expression of the test group.

| | |
|---|---|
| CTCCTGCTGGAAAACATC | attacin A forw |
| GCTCGTTTGGATCTGACC | attacin A rev |
| GTGGTAGGTCAGGTTTTCGC | attacin B forw |
| CCAATGGCTTCGAGTTCCAG | attacin B rev |
| TGTAAGCTAGTTTATTTCTATGG | cecropin C forw |
| GATGAGCCTTTAATGTCC | cecropin C rev |
| CACCCATGGCAAAAACGC | drosocin forw |
| TGAAGTTCACCATCGTTTTCCTG | drosocin rev |
| CATGCTGCTGTGTTCCGCGA | Sdha forw |
| ACCATCCAGGGGCTTGCTGA | Sdha rev |
| ATGACCATGAAGCCCACTCC | DptA forw |
| TCCTCCCAAGTGGTGTCCAT | DptA rev |

**Table 8.4 Primers for qPCR assay.**

## 8.5 Sample preparation for GlyGly enrichment and LC-MS

Flies were collected and reared as described in previous chapters. 20 flies were kept in a vial and food was changed every 3 days. Flies were flashed frozen by dry ice on day-18. In each genotype, ~150 fly heads were cut off and placed into lysis buffer from PTMScanHS Ubiquitin/SUMO Remnant Motif Kit Protocol (#59322, Cell Signaling, UK), that contained 5% SDS in triethylammonium bicarbonate (TEAB) buffer (T7408, SigmaAldrich, Germany). Samples were homogenized by an electric motor pestle for 2 minutes at room temperature, sonicated following protocol instruction and centrifuged for 15 minutes at 12000 rpm. The supernatant was transferred into a new 1.5 ml microcentrifuge. The concentration of protein was measured by Pierce 660 assay (ThermoFisher, UK) with Ionic Detergent Compatibility Reagent (ThermoFisher, UK). Protein samples were flashed froze for further GlyGly ubiquitin enrichment experiment.

Dr Adan Pinto Fernandez and Dr Andreas Damianou helped me with ubiquitin enrichment and liquid chromatography-mass spectrometry (LC-MS). The concentration of lysate was measured by Pierce 660nm assay with ionic detergent compatibility reagent (ThermoFisher, UK). I normalized all samples' input to 1 mg. I followed the protocol of PTMScan HS Ubiquitin/SUMO Remnant Motif Kit protocol (#59322, Cell Signaling, USA) to perform the reduction and alkylation of protein and S-trap clean-up protease digestion. After trypsin digestion, 50 μl (~30 μg) of aliquot was taken from the resuspension and used for total protein LC-MS, which served as

a control for ubiquitin enrichment. In case of ubiquitylation success, I should observe different protein hits in both PTMScan processed samples and the aliquots that were not PTMScan processed. I continued to perform immunoaffinity purification (IAP) following the protocol.

Tryptic peptides were analysed using a Dionex Ultimate 3000 nano UPLC (Thermo Scientific) coupled to an Orbitrap Fusion Lumos Tribid mass spectrometer (Thermo Scientific). Briefly, peptides were trap on a PepMap C18 trap columns (Thermo) and separated on an EasySpray column (50cm, P/N ES803, Thermo) over a 60-minute linear gradient from 2 % buffer B to 35 % buffer B (A: 5 % DMSO, 0.1 % formic acid in water. B: 5 % DMSO, 0.1 % formic acid in acetonitrile) at a flow rate of 250 nL/min. The instrument was operated in data-independent acquisition mode as previously described in Steger M. et al. 2021 (Steger et al., 2021).

1388 ubiquitylated proteins and 2583 total proteins were detected. I kept the reads that had valid values in both biological replications and resulted in 944 ubiquitylated proteins and 2455 total proteins. Principal component analysis (PCA) showed that two biological replicates were similar to each other after log2 transformation (Figure 8.5.1A and B), indicated that there were limited variabilities between biological replications. Since I only had two biological replicates, hence I chose to filter out proteins that had only one reads from a single biology replicate. In our case, this

method was more conservative than data imputation. Distributions for all data sets were largely normal distributions after normalizing (Figure 7.5.1C and D). I tried using data imputation, but the outputs were not normal distributions and according to Perseus user manual, the situation was not fit for further analysis (data not shown).

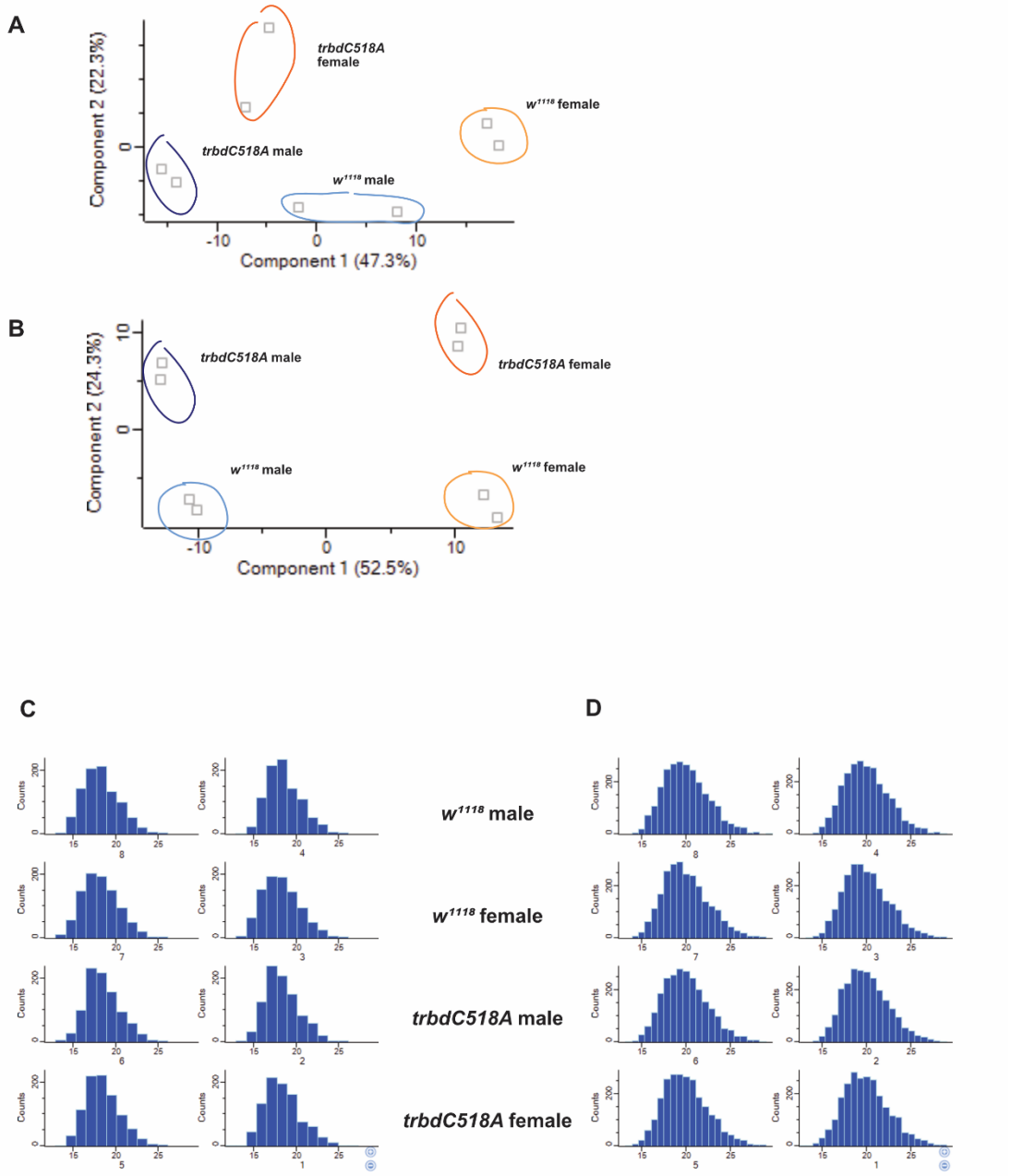



**Figure 8.5.1 Quality control of ubiquitinomics and proteomics data.** (A) PCA of protein reads for each sample from ubiquitin GlyGly enrichment after normalization. Biological replications of same genotype were grouped together (emphasised by same colour of circles). (B) PCA of protein reads for each sample from total proteomics after normalization. Biological replications of same genotype were grouped together (emphasised by same colour of circles). (C) Distribution of ubiquitin GlyGly enrichment protein reads after missing data filtration. The distribution of every sample was normal distributed. (D) Distribution of total protein reads after missing data filtration. The distribution of every sample was normal

distributed.

Two sample t-test was performed, and proteins that were p>0.05 and log foldchange<-1 or >-1 were plotted out in volcano plots (Figure9.1.1A-H). Further Venn diagram analysis was conducted on these proteins. The Venn diagram analysis was performed in Venny 2.1 (https://bioinfogp.cnb.csic.es/tools/venny/) (Table 9.1.2.1A-D). I summarised all significant different gene for “upregulation in *trbdC518A* male (control $w^{1118}$ male)”, “downregulation in *trbdC518A* male (control $w^{1118}$ male)”, “upregulation in *trbdC518A* female (control $w^{1118}$ female)”, and “downregulation in *trbdC518A* male (control $w^{1118}$ female)” in ubiquitin enrichment and total protein lists. Results were further searched in STRING databank (https://string-db.org) (Table 9.1.2 A-H).

Dr Adan Pinto Fernandez searched ubiquitin glygly residues in our glygly enrichment list. Prof Gunner Dittmar (Luxembourg Institute of Health) provided suggestion for the data normalization. I did a Venn diagram analysis on glygly enriched proteins and total proteins. I selected the 1550 proteins that were exclusive to total proteins and adding the ubiquitin linkages result for width adjustment normalization analysis (Figure 8.5.2).

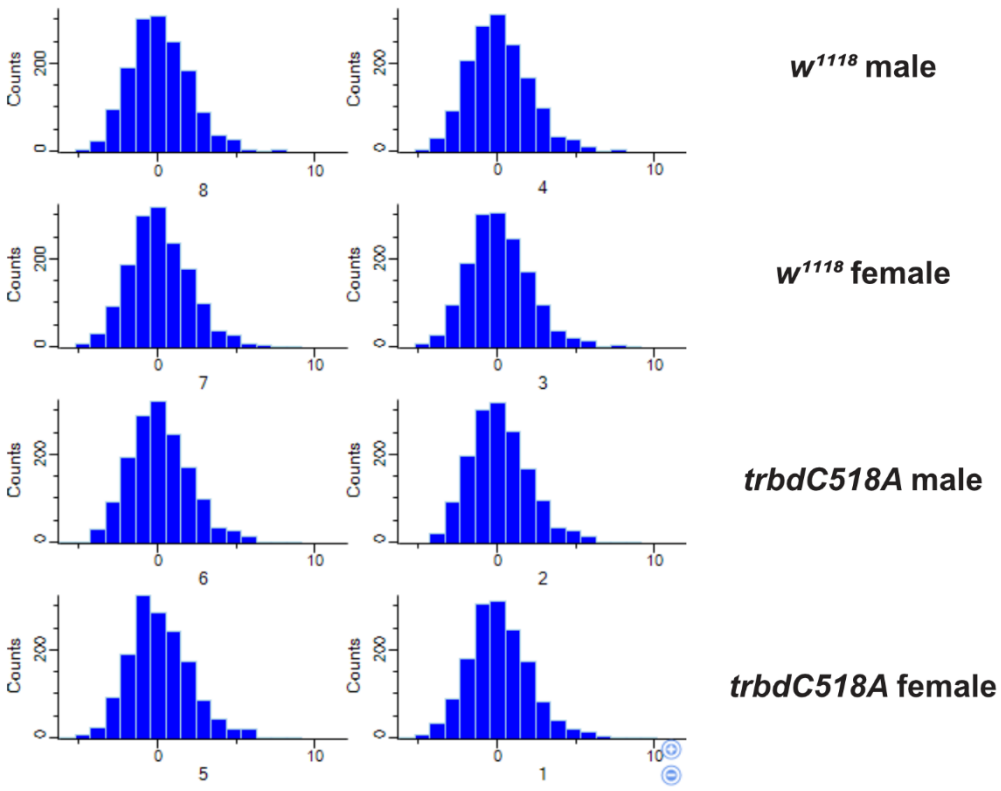



**Figure 8.5.2 Distributions of total protein exclusive protein reads (total protein reads – GlyGly protein reads) after log transformation and width adjustment normalisation. All samples' distribution is normal distribution.**

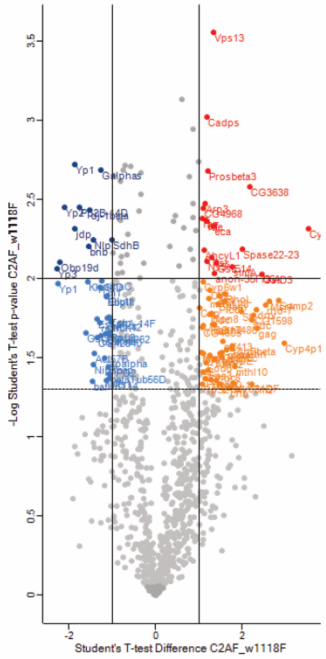
# Chapter 9: Appendices

## 9.1 Supplement figures and tables for LC-MS

### 9.1.1 Volcano plots and table

This section shows the t-test result of ubiquitin enriched proteins and total proteins. I presented the result in volcano plots and tables.

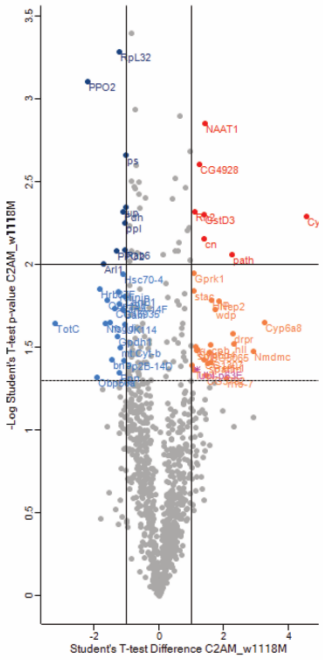
A




| Log Student's T-test p-value | Student's T-test Difference | Genes | Log Student's T-test p-value | Student's T-test Difference | Genes |
|---|---|---|---|---|---|
| 1.32218 | -1.00376 | Aladin | 1.3121 | 1.70096 | chb |
| 1.35404 | -1.46507 | baf | 1.33272 | 1.47918 | v |
| 1.35606 | -1.13961 | UK114 | 1.3341 | 2.21929 | Tm2 |
| 1.36842 | -1.06983 | Nfs1 | 1.33486 | 1.06426 | RpS27A;Ubi-p63E |
| 1.39795 | -1.08405 | betaTub56D;betaTub60D | 1.34189 | 1.77769 | Myo31DF |
| 1.4403 | -1.09151 | PPO2 | 1.35775 | 1.3863 | lolal |
| 1.45916 | -1.44543 | Nipsnap | 1.36174 | 1.26333 | Hsc70-1;Hsc70-4 |
| 1.5009 | -1.18259 | Atpalpha | 1.37294 | 1.13642 | Pde6 |
| 1.52841 | -1.42037 | Act57B;Act79B;Act88F | 1.39405 | 1.01335 | Exd2 |
| 1.62699 | -1.34925 | CG42540 | 1.4136 | 1.10232 | Zdhhc8 |
| 1.63816 | -1.27555 | up | 1.4243 | 1.20517 | Fas3 |
| 1.64013 | -1.06062 | Mfe2 | 1.44841 | 1.82059 | mthl10 |
| 1.64988 | -1.17063 | CG12262 | 1.45968 | 1.00157 | sls |
| 1.65872 | -1.62739 | GstS1 | 1.47084 | 1.15838 | Sod3 |
| 1.66497 | -1.08594 | RpL3 | 1.49328 | 1.35186 | Arpc2 |
| 1.72083 | -1.30229 | retinin | 1.50658 | 1.52706 | cn |
| 1.72771 | -1.02546 | ND-42 | 1.5148 | 1.24296 | Hrb98DE |
| 1.7441 | -1.3585 | Est-6 | 1.52908 | 1.0882 | wat |
| 1.75019 | -1.12707 | CanA-14F;Pp2B-14D | 1.52959 | 1.47623 | Lis-1 |
| 1.76036 | -1.08226 | Tctp | 1.53504 | 1.04571 | mts |
| 1.88603 | -1.14078 | EbpIII | 1.53736 | 1.52318 | OtopLc |
| 1.89631 | -1.11924 | Glut1 | 1.55511 | 1.62497 | mask |
| 1.94492 | -1.29522 | Tm1;Tm2 | 1.5569 | 1.76019 | spartin |
| 1.96854 | -2.26163 | Yp1 | 1.57398 | 1.76576 | rdgBbeta |
| 1.98075 | -1.56748 | Klp68D | 1.59304 | 2.9578 | Cyp4p1 |
| 1.98951 | -1.24148 | ninaC | 1.60366 | 1.55034 | olf413 |
| 2.06299 | -2.29397 | Yp3 | 1.687 | 2.34497 | gag |
| 2.10282 | -2.21494 | Obp19d | 1.69613 | 1.06479 | CG4603 |
| 2.45272 | -2.12121 | Yp2 | 1.70385 | 1.08781 | Ythdf |
| 2.31612 | -1.87829 | jdp | 1.71023 | 1.30641 | CG17486 |
| 2.72207 | -1.86502 | Yp1;Yp2 | 1.71029 | 1.35003 | mon2 |
| 2.45484 | -1.76199 | Pp2B-14D | 1.74118 | 2.2188 | Sdc |
| 2.2081 | -1.54264 | bnb | 1.77241 | 2.26626 | CG1598 |
| 2.43376 | -1.53506 | dj-1beta | 1.77621 | 1.2489 | Ddc |
| 2.24843 | -1.44058 | Nlp | 1.7837 | 1.29704 | Rpn8 |
| 2.68758 | -1.26249 | Galphas | 1.79236 | 1.98091 | SK |
| 2.24646 | -1.02101 | SdhB | 1.80581 | 2.32753 | drpr |

**Figure 9.1.1 Volcano plots and tables for t-tests (A)** t-test result (p<0.05, FDR=0.01) for ubiquitin GlyGly enriched proteins in *trbdC518A* female with control $w^{1118}$ female (*trbdC518A* female vs control $w^{1118}$ female). Hits that were relatively enriched in control group ($w^{1118}$ female), in similar terms downregulated in the test group (*trbdC518A* female), were on the left side and coloured in blue in both volcano plot and table. Hits that were relatively enriched in test group (*trbdC518A* female), in similar terms downregulated in the control group ($w^{1118}$ female), were on the left side and coloured in orange in both volcano plot and table.

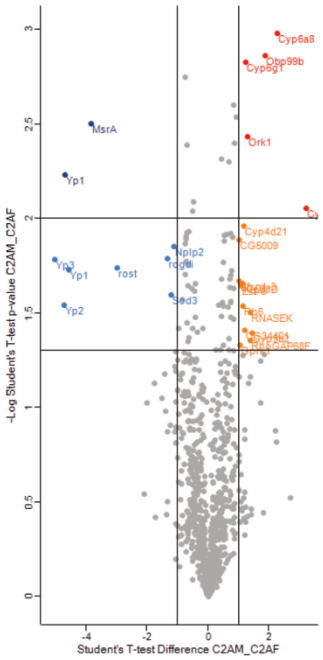
**B**




| Log Student's T-test p-value | Student's T-test Difference | Genes | Log Student's T-test p-value | Student's T-test Difference | Genes |
|---|---|---|---|---|---|
| 2.66586 | -1.02156 | ps | 1.78023 | 1.84465 | Nep2 |
| 2.08999 | -1.05888 | Rab6 | 2.15901 | 1.39087 | cn |
| 1.94308 | -1.11123 | Hsc70-4;Hsp68 | 1.41034 | 1.57867 | Tret1-1 |
| 3.28765 | -1.24204 | RpL32 | 1.31509 | 2.07153 | rho-7 |
| 1.80913 | -1.06284 | LanB1 | 1.47353 | 1.57067 | CG5065 |
| 1.5653 | -1.27553 | Gpdh1 | 1.78527 | 1.61962 | HIP;HIP-R |
| 1.49922 | -1.21099 | mt:Cyt-b | 1.42887 | 1.39647 | CG1307 |
| 2.3509 | -1.01974 | up | 2.31859 | 1.09301 | Rh2;ninaE |
| 2.00784 | -1.71007 | Arl1 | 1.36752 | 1.19184 | Ubi-p63E |
| 1.42449 | -1.46817 | bnb | 1.94872 | 1.08481 | Gprk1 |
| 2.31868 | -1.10907 | Fdh | 1.50702 | 1.13061 | Klc |
| 1.85569 | -1.83199 | Hrb87F | 1.51576 | 1.57626 | cpb |
| 1.78383 | -1.6007 | Obp19d | 1.4752 | 2.91282 | Nmdmc |
| 1.72975 | -1.11703 | Cam | 1.39302 | 1.0038 | RhoL |
| 1.41931 | -1.08333 | Pp2B-14D | 1.65176 | 3.25976 | Cyp6a8 |
| 1.7658 | -1.22139 | CanA-14F;Pp2B-14D | 1.36558 | 1.07856 | Tre1 |
| 1.34682 | -1.22761 | Ppn | 1.48085 | 1.15567 | spt4 |
| 1.64767 | -3.22911 | TotC | 1.5196 | 2.30475 | hll |
| 2.25219 | -1.07082 | ppl | 2.29125 | 4.56657 | Cyp4p1 |
| 1.64259 | -1.06122 | UK114 | 1.84432 | 1.07018 | stac |
| 2.08691 | -1.31218 | PPO2 | 1.48652 | 1.19615 | Cyp6d4 |
| 3.10787 | -2.22055 | PPO2;PPO3 | 2.30613 | 1.40164 | GstD3 |
| 1.73852 | -1.36847 | CG16935 | 1.33052 | 1.45313 | CG3792 |
| 1.32017 | -1.93019 | Obp56a | 1.40283 | 1.50198 | spartin |
| 1.64429 | -1.66511 | Nfs1 | 2.06377 | 2.25718 | path |
| 1.83542 | -1.26157 | retinin | 1.58166 | 2.28631 | drpr |
| 1.64916 | -1.51889 | rogdi | 1.73281 | 1.73579 | wdp |
| | | | 2.85213 | 1.42977 | NAAT1 |
| | | | 2.60986 | 1.23357 | CG4928 |

**Figure 9.1.1 (B)** t-test result (p<0.05 FDR=0.01) for ubiquitin GlyGly enriched proteins in *trbdC518A* male (*trbdC518A* male vs $w^{1118}$ male). Hits that were relatively enriched in control group (control $w^{1118}$ male), in similar terms downregulated in the test group (*trbdC518A* male), were on the left side and coloured in blue in both volcano plot and table. Hits that were relatively enriched in test group (*trbdC518A* male), in similar terms downregulated in the control group control ($w^{1118}$ male), were on the left side and coloured in orange in both volcano plot and table.

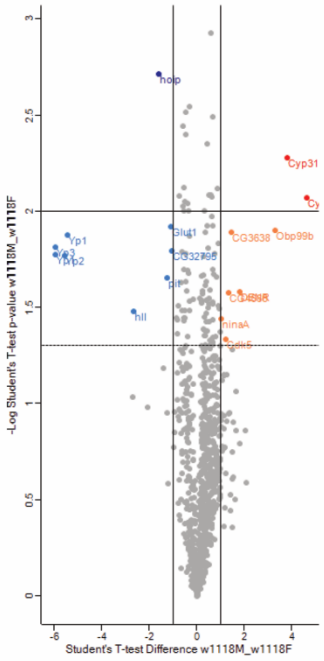
C




| -Log Student's T-test p-value | Student's T-test Difference | Genes | -Log Student's T-test p-value | Student's T-test Difference | Genes |
|---|---|---|---|---|---|
| 1.73791 | -2.98653 | rost | 1.53684 | 1.14613 | Rh6 |
| 2.23186 | -4.70472 | Yp1 | 1.64556 | 1.06784 | Est-6 |
| 1.73032 | -4.56189 | Yp1;Yp2 | 1.33171 | 1.03725 | Gprk1 |
| 1.54115 | -4.71512 | Yp2 | 1.65781 | 1.12892 | Klp68D |
| 1.78143 | -5.04364 | Yp3 | 2.9797 | 2.27079 | Cyp6a8 |
| 2.50414 | -3.84816 | MsrA | 1.88893 | 1.00521 | CG5009 |
| 1.59425 | -1.20433 | Sod3 | 1.50293 | 1.38631 | RNASEK |
| 1.85412 | -1.13848 | Nplp2 | 2.43248 | 1.27376 | Ork1 |
| 1.79065 | -1.3539 | rogdi | 1.39486 | 1.42571 | Cyp9b2 |
| | | | 2.82807 | 1.22995 | Cyp6g1 |
| | | | 2.86072 | 1.87286 | Obp99b |
| | | | 2.05424 | 3.22019 | Cyp313a1 |
| | | | 1.9613 | 1.1572 | Cyp4d21 |
| | | | 1.35455 | 1.38385 | RhoGAP68F |
| | | | 1.41111 | 1.18247 | CG34401 |

**Figure 9.1.1 (C)** t-test result (p<0.05, FDR=0.01) for ubiquitin GlyGly enriched proteins in *trbdC518A* male (*trbdC518A* male vs *trbdC518A* female). Hits that were relatively enriched in control group (*trbdC518A* female), in similar terms downregulated in the test group (*trbdC518A* male), were on the left side and coloured in blue in both volcano plot and table. Hits that were relatively enriched in test group (*trbdC518A* male), in similar terms downregulated in the control group (*trbdC518A* female), were on the left side and coloured in orange in both volcano plot and table.

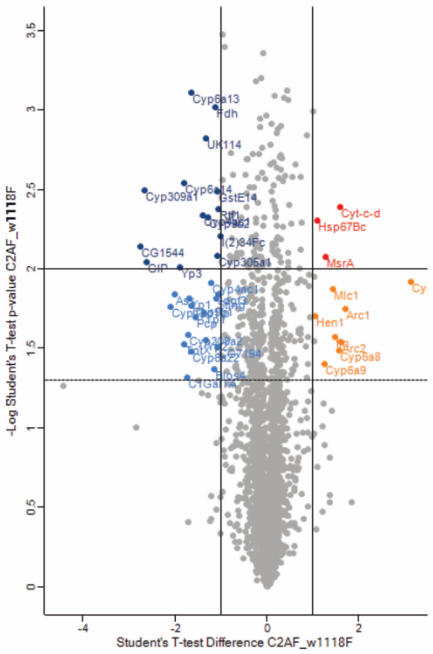
**D**




| -Log Student's T-test p-value | Student's T-test Difference | Genes | -Log Student's T-test p-value | Student's T-test Difference | Genes |
|---|---|---|---|---|---|
| 1.77473 | -5.96237 | Yp1 | 1.44298 | 1.00314 | ninaA |
| 1.88082 | -5.4484 | Yp1;Yp2 | 1.3364 | 1.20223 | Cdk5 |
| 1.7706 | -5.57932 | Yp2 | 1.90206 | 3.30438 | Obp99b |
| 1.81346 | -5.99139 | Yp3 | 2.28084 | 3.78913 | Cyp313a1 |
| 1.92253 | -1.09266 | Glut1 | 2.0723 | 4.64089 | Cyp4d21 |
| 1.79477 | -1.07924 | CG32795 | 1.58344 | 1.79047 | DENR |
| 2.71525 | -1.62832 | hoip | 1.57755 | 1.32987 | CG4666 |
| 1.4815 | -2.66868 | hll | 1.89284 | 1.44892 | CG3638 |
| 1.65574 | -1.26439 | pit | | | |

**Figure 9.1.1 (D)** t-test result (p<0.05, FDR=0.01) for ubiquitin GlyGly enriched proteins in *w*$^{1118}$ male (*w*$^{1118}$ male vs *w*$^{1118}$ female). Hits that were relatively enriched in control group (*w*$^{1118}$ female), in similar terms downregulated in the test group (*w*$^{1118}$ male), were on the left side and coloured in blue in both volcano plot and table. Hits that were relatively enriched in test group (*w*$^{1118}$ male), in similar terms downregulated in the control group (*w*$^{1118}$ female), were on the left side and coloured in orange in both volcano plot and table.

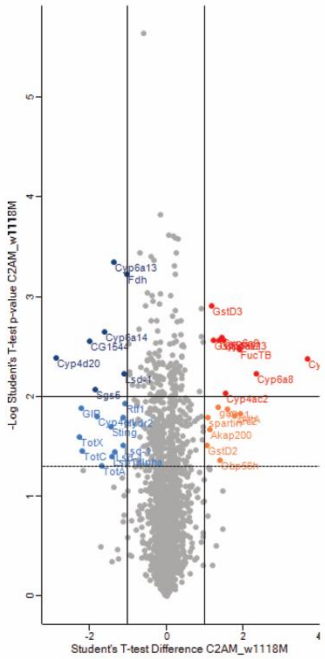
**E**




| -Log Student's T-test p-value | Student's T-test Difference | Genes | -Log Student's T-test p-value | Student's T-test Difference | Genes |
|---|---|---|---|---|---|
| 1.81862 | -1.10104 | Sting | 2.39279 | 1.59403 | Cyt-c-d |
| 1.84388 | -2.00587 | Ass | 1.87343 | 1.42743 | Mlc1 |
| 1.81848 | -1.70056 | Yp1 | 2.08022 | 1.28197 | MsrA |
| 1.72291 | -1.38913 | Yp1;Yp2 | 1.9515 | 1.01306 | gag |
| 1.55485 | -1.32879 | Yp2 | 2.30936 | 1.0956 | Hsp67Bc |
| 2.04298 | -2.62811 | GIP | 1.57759 | 1.46723 | fln |
| 2.01068 | -1.91058 | Yp3 | 1.5475 | 1.01595 | Obp28a |
| 1.70103 | -1.56299 | Pcp | 1.48715 | 1.56114 | Cyp6a8 |
| 1.45894 | -1.00136 | Cys | 1.40317 | 1.25609 | Cyp6a9 |
| 3.02177 | -1.12721 | Fdh | 1.53999 | 1.6145 | Arc2 |
| 1.76542 | -2.11661 | Cyp12d1-p | 1.70762 | 1.05484 | Hen1 |
| 1.58652 | -1.72568 | Cyp309a2 | 1.75407 | 1.70616 | Arc1 |
| 2.48904 | -1.09029 | GstE14 | 1.9247 | 3.13624 | Cyp4p1 |
| 1.32273 | -1.74774 | C1GalTA | | | |
| 1.52565 | -1.82135 | TotX | | | |
| 1.8398 | -1.05819 | Idgf3 | | | |
| 2.82211 | -1.32656 | UK114 | | | |
| 2.20714 | -1.01193 | l(2)34Fc | | | |
| 1.773 | -1.64852 | Cyp9b1;Cyp9b2 | | | |
| 2.32789 | -1.28429 | Cyp9b2 | | | |
| 2.5433 | -1.822 | Cyp6a14 | | | |
| 3.11358 | -1.65186 | Cyp6a13 | | | |
| 1.48151 | -1.65727 | Cyp6a22 | | | |
| 2.14273 | -2.75674 | CG1544 | | | |
| 1.91232 | -1.22664 | Cyp4ac1;Cyp4ac3 | | | |
| 2.34312 | -1.39927 | Cyp4ac1 | | | |
| 2.49704 | -2.66665 | Cyp309a1 | | | |
| 1.507 | -1.0768 | CG7194 | | | |
| 1.37352 | -1.14541 | Blos4 | | | |
| 2.08431 | -1.08435 | Cyp305a1 | | | |
| 2.38017 | -1.06833 | Rtf1 | | | |

**Figure 9.1.1 (E)** t-test result (p<0.05, FDR=0.01) for total proteomic analysis in *trbdC518A* female (*trbdC518A* female *w*$^{1118}$ female). Hits that were relatively enriched in control group (*trbdC518A* female), in similar terms downregulated in the test group (*w*$^{1118}$ female), were on the left side and coloured in blue in both volcano plot and table. Hits that were relatively enriched in test group (*w*$^{1118}$ female), in similar terms downregulated in the control group (*trbdC518A* female), were on the left side and coloured in orange in both volcano plot and table.

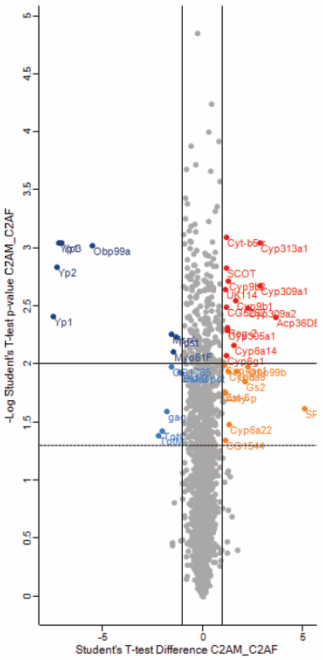
**F**




| -Log Student's T-test p-value | Student's T-test Difference | Genes | -Log Student's T-test p-value | Student's T-test Difference | Genes |
|---|---|---|---|---|---|
| 1.69713 | -1.45414 | Sting | 1.89187 | 1.33724 | gag |
| 1.88426 | -2.2311 | GIP | 1.82665 | 1.92687 | AttA;AttB |
| 2.06872 | -1.84673 | Sgs5 | 2.23383 | 2.34631 | Cyp6a8 |
| 1.3963 | -1.43026 | Lsp1alpha | 2.56325 | 1.36668 | Cyp6a21;Cyp6a8 |
| 3.23207 | -1.0299 | Fdh | 2.59419 | 1.44432 | Cyp6a9 |
| 1.79302 | -1.13451 | Hydr2 | 1.81294 | 1.77601 | Arc2 |
| 1.59776 | -2.27793 | TotX | 1.87199 | 1.57879 | Arc1 |
| 1.45943 | -2.18699 | TotC | 2.37571 | 3.68292 | Cyp4p1 |
| 1.3022 | -1.69165 | TotA | 2.56327 | 1.48835 | Cyp6a23 |
| 1.79857 | -1.81055 | Cyp4g1 | 1.35745 | 1.39505 | Obp56h |
| 2.65199 | -1.61144 | Cyp6a14 | 2.56474 | 1.21375 | GstD4 |
| 3.35449 | -1.36541 | Cyp6a13 | 2.90932 | 1.17823 | GstD3 |
| 2.55595 | -1.99151 | CG1544 | 1.50754 | 1.04942 | GstD2 |
| 2.2284 | -1.11322 | Lsd-1 | 2.47252 | 1.91023 | FucTB |
| 1.44681 | -1.35658 | Lsd-1 | 1.67252 | 1.1281 | Akap200 |
| 1.51312 | -1.13811 | Lsd-1 | 2.03809 | 1.54104 | Cyp4ac2 |
| 2.38489 | -2.8856 | Cyp4d20 | 1.79247 | 1.07446 | spartin |
| 1.93127 | -1.07791 | Rtf1 | | | |

**Figure 9.1.1 (F)** t-test result (p<0.05, FDR=0.01) for total proteomic analysis in *trbdC518A* male (*trbdC518A* male vs $w^{1118}$ male). Hits that were relatively enriched in control group ($w^{1118}$ male), in similar terms downregulated in the test group (*trbdC518A* male), were on the left side and coloured in blue in both volcano plot and table. Hits that were relatively enriched in test group (*trbdC518A* male), in similar terms downregulated in the control group ($w^{1118}$ male), were on the left side and coloured in orange in both volcano plot and table.

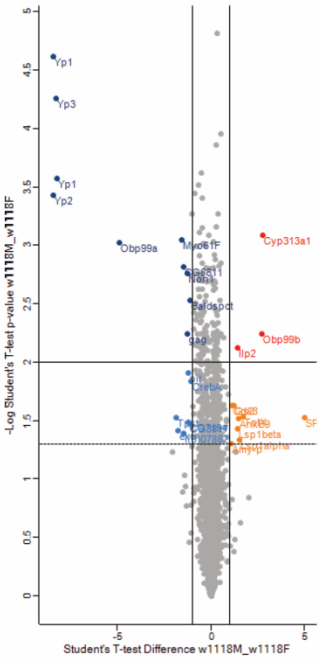
**G**




| -Log Student's T-test p-value | Student's T-test Difference | Genes | -Log Student's T-test p-value | Student's T-test Difference | Genes |
|---|---|---|---|---|---|
| 3.0432 | -7.18577 | Yp1 | 1.61787 | 5.11035 | SP |
| 2.41618 | -7.49375 | Yp1;Yp2 | 1.75782 | 1.14167 | Amy-p |
| 2.8363 | -7.27332 | Yp2 | 1.76187 | 1.08555 | Est-6 |
| 3.04553 | -7.05567 | Yp3 | 1.93796 | 1.71473 | Gld |
| 2.25833 | -1.57718 | MsrA | 3.09239 | 1.17165 | Cyt-b5-r |
| 1.5943 | -1.78962 | gag | 1.85468 | 2.08995 | Gs2 |
| 2.10936 | -1.4643 | Myo61F | 1.68599 | 1.03333 | Cyp12d1-p |
| 1.42773 | -2.05113 | TotC | 2.48513 | 2.2596 | Cyp309a2 |
| 3.02472 | -5.52545 | Obp99a | 1.93983 | 1.28254 | Cyp6a8 |
| 1.3899 | -2.20286 | TotM | 2.31481 | 1.20693 | Reg-2 |
| 1.92634 | -1.07261 | Baldspot | 2.40309 | 3.62739 | Acp36DE |
| 1.93013 | -1.12707 | Lsd-2 | 2.64335 | 1.15341 | UK114 |
| 2.23896 | -1.34869 | Tpst | 2.55168 | 1.64511 | Cyp9b1;Cyp9b2 |
| 1.9764 | -1.56699 | CG1785 | 2.71526 | 1.28456 | Cyp9b2 |
| | | | 2.16528 | 1.5308 | Cyp6a14;Cyp6g1 |
| | | | 2.07562 | 1.16137 | Cyp6g1 |
| | | | 1.47916 | 1.31932 | Cyp6a22 |
| | | | 2.01974 | 1.02588 | CG15093 |
| | | | 1.34508 | 1.12362 | CG1544 |
| | | | 1.98335 | 2.23495 | Obp99b |
| | | | 3.04641 | 2.85249 | Cyp313a1 |
| | | | 1.99324 | 1.07496 | Cyp4ac1 |
| | | | 2.49275 | 1.1818 | CG5262 |
| | | | 2.67675 | 2.83908 | Cyp309a1 |
| | | | 2.28985 | 1.23759 | Cyp305a1 |
| | | | 2.82781 | 1.19369 | SCOT |

**Figure 9.1.1 (G)** t-test result (p<0.05, FDR=0.01) for total proteomic analysis in *trbdC518A* male (*trbdC518A* male vs *trbdC518A* female). Hits that were relatively enriched in control group (*trbdC518A* female), in similar terms downregulated in the test group (*trbdC518A* male), were on the left side and coloured in blue in both volcano plot and table. Hits that were relatively enriched in test group (*trbdC518A* male), in similar terms downregulated in the control group (*trbdC518A* female), were on the left side and coloured in orange in both volcano plot and table.

**H**




| -Log Student's T-test p-value | Student's T-test Difference | Genes | -Log Student's T-test p-value | Student's T-test Difference | Genes |
|---|---|---|---|---|---|
| 4.62141 | -8.46863 | Yp1 | 1.52457 | 5.02181 | SP |
| 3.57994 | -8.25392 | Yp1;Yp2 | 1.30147 | 1.08039 | Amy-p |
| 3.43101 | -8.47223 | Yp2 | 1.33682 | 1.50187 | Lsp1alpha;Lsp1beta |
| 4.26129 | -8.27962 | Yp3 | 1.42986 | 1.4188 | Lsp1beta |
| 2.24419 | -1.28513 | gag | 1.63312 | 1.19873 | Gs2 |
| 1.41824 | -1.77519 | exu | 1.52234 | 1.4796 | AnxB9 |
| 1.84172 | -1.07836 | CrebA | 1.53966 | 1.71993 | TotX |
| 3.04691 | -1.57519 | Myo61F | 2.24636 | 2.73168 | Obp99b |
| 2.82241 | -1.47738 | CG8611 | 3.0923 | 2.76702 | Cyp313a1 |
| 2.76734 | -1.27614 | Non1 | 2.12577 | 1.39152 | Ilp2 |
| 1.4571 | -1.00978 | CG1542 | 1.63203 | 1.12711 | Cdk8 |
| 3.02702 | -4.91292 | Obp99a | | | |
| 1.91176 | -1.22305 | pit | | | |
| 3.2732 | -1.01785 | Non3 | | | |
| 1.39145 | -1.45565 | l(3)07882 | | | |
| 1.47992 | -1.16954 | CG3817 | | | |
| 1.49067 | -1.24952 | CG7194 | | | |
| 2.53319 | -1.14614 | Baldspot | | | |
| 1.52489 | -1.85751 | Tpst | | | |

**Figure 9.1.1 (H)** t-test result (p<0.05, FDR=0.01) for total proteomic analysis in *w*$^{1118}$ male (*w*$^{1118}$ male vs *w*$^{1118}$ female). Hits that were relatively enriched in control group (*w*$^{1118}$ female), in similar terms downregulated in the test group (*w*$^{1118}$ male), were on the left side and coloured in blue in both volcano plot and table. Hits that were relatively enriched in test group (*w*$^{1118}$ male), in similar terms downregulated in the control group (*w*$^{1118}$ female), were on the left side and coloured in orange in both volcano plot and table.

## 9.1.2 Tables for Venn diagram analysis and STRING database search

This section shows the result of Venn diagram analysis Figure 6.2.1 A-D in tables and the search results from of STRING database from each set from Venn diagram.

| 1 common element in "C518AM down" and "C518AF up": | 11 common elements in "C518AM up" and "C2AF up": | 9 common elements in "C518AM down" and "C518AF down": | 18 elements included exclusively in "C518AM down": | 20 elements included exclusively in "C518AM up": | 30 elements included exclusively in "C518AF down": | 58 elements included exclusively in "C518AF up": |
|---|---|---|---|---|---|---|
| Hsc70-4 | cn | up | ps | Nep2 | Aladin | chb |
| | rho-7 | bnb | Rab6 | Tret1-1 | baf | v |
| | Rh2 | Obp19d | Hsp68 | CG5065 | betaTub56D | RpS27A |
| | ninaE | Pp2B-14D | RpL32 | HIP | betaTub60D | Myo31DF |
| | Ubi-p63E | CanA-14F | LanB1 | HIP-R | Nipsnap | lolal |
| | RhoL | UK114 | Gpdh1 | CG1307 | Atpalpha | Hsc70-1 |
| | Cyp4p1 | PPO2 | mt:Cyt-b | Gprk1 | Act57B | Pde6 |
| | GstD3 | Nfs1 | Arl1 | Klc | Act79B | Exd2 |
| | spartin | retinin | Fdh | cpb | Act88F | Zdhhc8 |
| | path | | Hrb87F | Nmdmc | CG42540 | Fas3 |
| | drpr | | Cam | Cyp6a8 | Mfe2 | mthl10 |
| | | | Ppn | Tre1 | CG12262 | sls |
| | | | TotC | spt4 | GstS1 | Sod3 |
| | | | ppl | hll | RpL3 | Arpc2 |
| | | | PPO3 | stac | ND-42 | Hrb98DE |
| | | | CG16935 | Cyp6d4 | Est-6 | wat |
| | | | Obp56a | CG3792 | Tctp | Lis-1 |
| | | | rogdi | wdp | EbpIII | mts |
| | | | | NAAT1 | Glut1 | OtopLc |
| | | | | CG4928 | Tm1 | mask |
| | | | | | Yp1 | rdgBbeta |
| | | | | | Klp68D | olf413 |
| | | | | | ninaC | gag |
| | | | | | Yp3 | CG4603 |
| | | | | | Yp2 | Ythdf |
| | | | | | jdp | CG17486 |
| | | | | | dj-1beta | mon2 |
| | | | | | Nlp | Sdc |
| | | | | | Galphas | CG1598 |
| | | | | | SdhB | Ddc |
| | | | | | | Rpn8 |
| | | | | | | SK |
| | | | | | | Csp |
| | | | | | | Picot |
| | | | | | | MsrA |
| | | | | | | Snmp2 |
| | | | | | | mRpL28 |
| | | | | | | bsk |
| | | | | | | Ctl2 |
| | | | | | | Cyp6w1 |
| | | | | | | ras |
| | | | | | | CG4968 |
| | | | | | | AhcyL1 |
| | | | | | | Arp3 |
| | | | | | | eff |
| | | | | | | Ns3 |
| | | | | | | Ide |
| | | | | | | Cadps |
| | | | | | | Prosbeta3 |
| | | | | | | Pss |
| | | | | | | Vps13 |
| | | | | | | eca |
| | | | | | | anon-35F/36A |
| | | | | | | GstE14 |
| | | | | | | stmA |
| | | | | | | Spase22-23 |
| | | | | | | CG3638 |
| | | | | | | Cyp4d21 |

**Table 9.1.2.1 Result table for Venn diagram analysis (6.2.1A)** Gene names in each set after Venn diagram analysis of ubiquitin GlyGly enrichment by comparing

*trbdC518A* females and males with $w^{1118}$ females and males.

| 3 common elements in "C518AM up" and "w1118 up": | 3 common elements in "C518AM down" and "w1118 down": | 5 elements included exclusively in "C518AM down": | 12 elements included exclusively in "C518AM up": | 5 elements included exclusively in "w1118M down": | 5 elements included exclusively in "w1118M up": |
|---|---|---|---|---|---|
| Obp99b | Yp1 | rost | Rh6 | Glut1 | ninaA |
| Cyp313a1 | Yp2 | MsrA | Est-6 | CG32795 | Cdk5 |
| Cyp4d21 | Yp3 | Sod3 | Gprk1 | hoip | DENR |
| | | Nplp2 | Klp68D | hll | CG4666 |
| | | rogdi | Cyp6a8 | pit | CG3638 |
| | | | CG5009 | | |
| | | | RNASEK | | |
| | | | Ork1 | | |
| | | | Cyp9b2 | | |
| | | | Cyp6g1 | | |
| | | | RhoGAP68F | | |
| | | | CG34401 | | |

**Table 9.1.2.1 (6.2.1B)** Gene names in each set after Venn diagram analysis of ubiquitin GlyGly enrichment by comparing *trbdC518A* and $w^{1118}$ males with *trbdC518A* and $w^{1118}$ females.

| 6 common elements in "C518AM up" and "C518AF up": | 8 common elements in "C518AM down" and "C518AF down": | 8 elements included exclusively in "C518AM down": | 12 elements included exclusively in "C518AM up": | 22 elements included exclusively in "C518AF down": | 7 elements included exclusively in "C518AF up": |
|---|---|---|---|---|---|
| gag | Sting | Sgs5 | AttA | Ass | Cyt-c-d |
| Cyp6a8 | GIP | Lsp1alpha | AttB | Yp1 | Mlc1 |
| Cyp6a9 | Fdh | Hydr2 | Cyp6a21 | Yp2 | MsrA |
| Arc2 | TotX | TotC | Cyp6a23 | Yp3 | Hsp67Bc |
| Arc1 | Cyp6a14 | TotA | Obp56h | Pcp | fln |
| Cyp4p1 | Cyp6a13 | Cyp4g1 | GstD4 | Cys | Obp28a |
| | CG1544 | Lsd-1 | GstD3 | Cyp12d1-p | Hen1 |
| | Rtf1 | Cyp4d20 | GstD2 | Cyp309a2 | |
| | | | FucTB | GstE14 | |
| | | | Akap200 | C1GalTA | |
| | | | Cyp4ac2 | Idgf3 | |
| | | | spartin | UK114 | |
| | | | | l(2)34Fc | |
| | | | | Cyp9b1 | |
| | | | | Cyp9b2 | |
| | | | | Cyp6a22 | |
| | | | | Cyp4ac1 | |
| | | | | Cyp4ac3 | |
| | | | | Cyp309a1 | |
| | | | | CG7194 | |
| | | | | Blos4 | |
| | | | | Cyp305a1 | |

**Table 9.1.2.1 (6.2.1C)** Gene names in each set after Venn diagram analysis of total proteome by comparing *trbdC518A* females and males with $w^{1118}$ females and males.

| 5 common elements in "C518AM up" and "w1118M up": | 8 common elements in "C518AM down" and "w1118M down": | 5 elements included exclusively in "C518AM down": | 21 elements included exclusively in "C518AM up": | 10 elements included exclusively in "w1118M down": | 6 elements included exclusively in "w1118M up": |
|---|---|---|---|---|---|
| SP | Yp1 | MsrA | Est-6 | exu | Lsp1alpha |
| Amy-p | Yp2 | TotC | Gld | CrebA | Lsp1beta |
| Gs2 | Yp3 | TotM | Cyt-b5-r | CG8611 | AnxB9 |
| Obp99b | gag | Lsd-2 | Cyp12d1-p | Non1 | TotX |
| Cyp313a1 | Myo61F | CG1785 | Cyp309a2 | CG1542 | Ilp2 |
| | Obp99a | | Cyp6a8 | pit | Cdk8 |
| | Baldspot | | Reg-2 | Non3 | |
| | Tpst | | Acp36DE | l(3)07882 | |
| | | | UK114 | CG3817 | |
| | | | Cyp9b1 | CG7194 | |
| | | | Cyp9b2 | | |
| | | | Cyp6a14 | | |
| | | | Cyp6g1 | | |
| | | | Cyp6a22 | | |
| | | | CG15093 | | |
| | | | CG1544 | | |
| | | | Cyp4ac1 | | |
| | | | CG5262 | | |
| | | | Cyp309a1 | | |
| | | | Cyp305a1 | | |
| | | | SCOT | | |

**Table 9.1.2.1 (6.2.1D)** Gene names in each set after Venn diagram analysis of total proteome by comparing *trbdC518A* and $w^{1118}$ males with *trbdC518A* and $w^{1118}$ females.

| #category | term ID | term description |
|---|---|---|
| GO Process | GO:0019722 | Calcium-mediated signaling |
| GO Process | GO:0050896 | Response to stimulus |
| GO Function | GO:0016679 | Oxidoreductase activity, acting on diphenols and related substances as donors |
| GO Function | GO:0033192 | Calmodulin-dependent protein phosphatase activity |
| GO Function | GO:0036263 | L-DOPA monooxygenase activity |
| GO Function | GO:0036264 | Dopamine monooxygenase activity |
| GO Component | GO:0005829 | Cytosol |
| GO Component | GO:0110165 | Cellular anatomical entity |
| Reactome | DME-2025928 | Calcineurin activates NFAT |
| Reactome | DME-5607763 | CLEC7A (Dectin-1) induces NFAT activation |
| Reactome | DME-2871809 | FCERI mediated Ca+2 mobilization |
| Reactome | DME-4086398 | Ca2+ pathway |
| GO Component | GO:0071944 | Cell periphery |

**Table 9.1.2.1 STRING database search pathway results (6.2.1A *trbdC518A* male up and down)** Hits from STRING searching for proteins that was differentially expressed between *trbdC518A* male and $w^{1118}$ male from ubiquitin GlyGly enrichment analysis (control $w^{1118}$ male). Blue represented relatively downregulated in *trbdC518A* male and orange represented relatively upregulated in *trbdC518A* male (control $w^{1118}$ male).

| #category | term ID | term description |
|---|---|---|
| GO Component | GO:0099080 | Supramolecular complex |
| GO Component | GO:0099512 | Supramolecular fiber |
| GO Component | GO:0005856 | Cytoskeleton |
| GO Component | GO:0110165 | Cellular anatomical entity |
| GO Component | GO:0099513 | Polymeric cytoskeletal fiber |
| GO Component | GO:0005737 | Cytoplasm |
| GO Component | GO:0005874 | Microtubule |
| GO Component | GO:0015629 | Actin cytoskeleton |
| GO Component | GO:0005865 | Striated muscle thin filament |
| GO Component | GO:0005955 | Calcineurin complex |
| STRING clusters | CL:11519 | Assembly of active LPL and LIPC lipase complexes, and retinol binding |
| STRING clusters | CL:8945 | Mixed, incl. regulation of actin filament length, and muscle protein |
| STRING clusters | CL:9035 | Mixed, incl. muscle protein, and sperm individualization complex |
| STRING clusters | CL:9038 | Mixed, incl. muscle protein, and zasp-like motif |
| Reactome | DME-8963889 | Assembly of active LPL and LIPC lipase complexes |
| Reactome | DME-174824 | Plasma lipoprotein assembly, remodeling, and clearance |
| Reactome | DME-8964058 | HDL remodeling |
| Reactome | DME-1430728 | Metabolism |
| Reactome | DME-1483166 | Synthesis of PA |
| Reactome | DME-556833 | Metabolism of lipids |
| Reactome | DME-983189 | Kinesins |
| Reactome | DME-1483206 | Glycerophospholipid biosynthesis |
| Reactome | DME-5620924 | Intraflagellar transport |

| | | |
|---|---|---|
| GO Process | GO:0009987 | Cellular process |
| GO Process | GO:0007275 | Multicellular organism development |
| GO Process | GO:0051234 | Establishment of localization |
| GO Process | GO:0006810 | Transport |
| GO Process | GO:0009653 | Anatomical structure morphogenesis |
| GO Process | GO:0006568 | Tryptophan metabolic process |
| GO Process | GO:0006576 | Cellular biogenic amine metabolic process |
| GO Process | GO:0009605 | Response to external stimulus |
| GO Process | GO:0030182 | Neuron differentiation |
| GO Process | GO:0044248 | Cellular catabolic process |
| GO Process | GO:0048468 | Cell development |
| GO Process | GO:0048666 | Neuron development |
| GO Process | GO:0048731 | System development |
| GO Process | GO:0048856 | Anatomical structure development |
| GO Process | GO:0051179 | Localization |
| GO Process | GO:1901565 | Organonitrogen compound catabolic process |
| GO Process | GO:0000902 | Cell morphogenesis |
| GO Process | GO:0040011 | Locomotion |
| GO Process | GO:0042330 | Taxis |
| GO Process | GO:0065007 | Biological regulation |
| GO Process | GO:0019748 | Secondary metabolic process |
| GO Process | GO:0050793 | Regulation of developmental process |
| GO Process | GO:0065008 | Regulation of biological quality |
| GO Process | GO:0006520 | Cellular amino acid metabolic process |
| GO Process | GO:0006569 | Tryptophan catabolic process |
| GO Process | GO:0023061 | Signal release |
| GO Process | GO:0048513 | Animal organ development |
| GO Process | GO:0048667 | Cell morphogenesis involved in neuron differentiation |
| GO Process | GO:0051649 | Establishment of localization in cell |
| GO Process | GO:0061564 | Axon development |
| GO Process | GO:1901564 | Organonitrogen compound metabolic process |
| GO Process | GO:1901605 | Alpha-amino acid metabolic process |
| GO Process | GO:0043603 | Cellular amide metabolic process |
| GO Process | GO:0006790 | Sulfur compound metabolic process |
| GO Process | GO:0007413 | Axonal fasciculation |
| GO Process | GO:0031175 | Neuron projection development |
| GO Process | GO:0018958 | Phenol-containing compound metabolic process |
| GO Process | GO:0001505 | Regulation of neurotransmitter levels |
| GO Process | GO:0007411 | Axon guidance |
| GO Process | GO:0032989 | Cellular component morphogenesis |
| GO Process | GO:0021700 | Developmental maturation |
| GO Process | GO:0050896 | Response to stimulus |
| GO Process | GO:0050789 | Regulation of biological process |
| GO Process | GO:0051239 | Regulation of multicellular organismal process |
| GO Process | GO:0070189 | Kynurenine metabolic process |
| GO Process | GO:0048477 | Oogenesis |
| GO Process | GO:0032501 | Multicellular organismal process |
| GO Component | GO:0005737 | Cytoplasm |
| GO Component | GO:0110165 | Cellular anatomical entity |
| GO Component | GO:0005622 | Intracellular |
| GO Component | GO:0031982 | Vesicle |
| GO Component | GO:0030424 | Axon |
| GO Component | GO:0031410 | Cytoplasmic vesicle |
| GO Component | GO:0071944 | Cell periphery |
| GO Component | GO:0120025 | Plasma membrane bounded cell projection |

| | | |
|---|---|---|
| GO Component | GO:0016020 | Membrane |
| GO Component | GO:0043005 | Neuron projection |
| GO Component | GO:0005886 | Plasma membrane |
| GO Component | GO:0012505 | Endomembrane system |
| KEGG | dme04141 | Protein processing in endoplasmic reticulum |
| KEGG | dme00380 | Tryptophan metabolism |
| KEGG | dme04013 | MAPK signaling pathway - fly |
| Reactome | DME-209360 | Ubiquitination and proteolysis of phosphorylated CI |
| Reactome | DME-209461 | Ubiquitination and degradation of phosphorylated ARM |
| Reactome | DME-1280215 | Cytokine Signaling in Immune system |
| Reactome | DME-168249 | Innate Immune System |
| Reactome | DME-2454202 | Fc epsilon receptor (FCERI) signaling |
| Reactome | DME-2871837 | FCERI mediated NF-kB activation |
| Reactome | DME-202424 | Downstream TCR signaling |
| Reactome | DME-209452 | N-HH ligand bound to PTC receptor complex |
| Reactome | DME-168256 | Immune System |
| Reactome | DME-432626 | Circadian Clock pathway |
| Reactome | DME-5252538 | Drosophila signaling pathways |
| Reactome | DME-5607764 | CLEC7A (Dectin-1) signaling |
| Reactome | DME-538864 | Degradation of CRY |
| Reactome | DME-69275 | G2/M Transition |
| Reactome | DME-216167 | Nuclear CI is degraded |
| Reactome | DME-432524 | Degradation of PER |
| Reactome | DME-432395 | Degradation of TIM |
| Reactome | DME-71240 | Tryptophan catabolism |
| Reactome | DME-5689896 | Ovarian tumor domain proteases |
| Reactome | DME-5688426 | Deubiquitination |
| Reactome | DME-449147 | Signaling by Interleukins |
| Reactome | DME-5607761 | Dectin-1 mediated noncanonical NF-kB signaling |
| Reactome | DME-5676590 | NIK-->noncanonical NF-kB signaling |
| Reactome | DME-1169091 | Activation of NF-kappaB in B cells |
| Reactome | DME-1234176 | Oxygen-dependent proline hydroxylation of Hypoxia-inducible Factor Alpha |
| Reactome | DME-450408 | AUF1 (hnRNP D0) binds and destabilizes mRNA |
| Reactome | DME-209459 | Imd pathway |
| Reactome | DME-2262752 | Cellular responses to stress |
| Reactome | DME-446652 | Interleukin-1 family signaling |
| Reactome | DME-450294 | MAP kinase activation |
| Reactome | DME-5654736 | Signaling by FGFR1 |
| Reactome | DME-1280218 | Adaptive Immune System |
| Reactome | DME-195253 | Degradation of beta-catenin by the destruction complex |
| Reactome | DME-5689880 | Ub-specific processing proteases |
| Reactome | DME-71291 | Metabolism of amino acids and derivatives |
| Reactome | DME-983169 | Class I MHC mediated antigen processing & presentation |
| Reactome | DME-8951664 | Neddylation |
| Reactome | DME-450321 | JNK (c-Jun kinases) phosphorylation and  activation mediated by activated human TAK1 |
| Reactome | DME-382551 | Transport of small molecules |
| Reactome | DME-193704 | p75 NTR receptor-mediated signalling |
| Reactome | DME-9033241 | Peroxisomal protein import |
| Reactome | DME-1295596 | Spry regulation of FGF signaling |
| Reactome | DME-68882 | Mitotic Anaphase |
| Reactome | DME-209447 | Activation of the IkappaB kinase complex, KEY:IRD5 dimer:KEY |
| Reactome | DME-69206 | G1/S Transition |
| Reactome | DME-75815 | Ubiquitin-dependent degradation of Cyclin D |
| Reactome | DME-4641258 | Degradation of DVL |
| Reactome | DME-4641257 | Degradation of AXIN |
| Reactome | DME-69601 | Ubiquitin Mediated Degradation of Phosphorylated Cdc25A |
| Reactome | DME-8854050 | FBXL7 down-regulates AURKA during mitotic entry and in early mitosis |
| Reactome | DME-5610780 | Degradation of GLI1 by the proteasome |
| Reactome | DME-983168 | Antigen processing: Ubiquitination & Proteasome degradation |
| Reactome | DME-597592 | Post-translational protein modification |
| Reactome | DME-8939902 | Regulation of RUNX2 expression and activity |
| Reactome | DME-8941858 | Regulation of RUNX3 expression and activity |
| Reactome | DME-4608870 | Asymmetric localization of PCP proteins |
| Reactome | DME-2565942 | Regulation of PLK1 Activity at G2/M Transition |
| Reactome | DME-5358346 | Hedgehog ligand biogenesis |
| Reactome | DME-68827 | CDT1 association with the CDC6:ORC:origin complex |
| Reactome | DME-1236975 | Antigen processing-Cross presentation |
| Reactome | DME-9020702 | Interleukin-1 signaling |
| Reactome | DME-187577 | SCF(Skp2)-mediated degradation of p27/p21 |
| Reactome | DME-2173795 | Downregulation of SMAD2/3:SMAD4 transcriptional activity |
| Reactome | DME-3371568 | Attenuation phase |
| Reactome | DME-450282 | MAPK targets/ Nuclear events mediated by MAP kinases |
| Reactome | DME-5610785 | GLI3 is processed to GLI3R by the proteasome |
| Reactome | DME-174084 | Autodegradation of Cdh1 by Cdh1:APC/C |
| Reactome | DME-174154 | APC/C:Cdc20 mediated degradation of Securin |
| Reactome | DME-2467813 | Separation of Sister Chromatids |
| Reactome | DME-8948751 | Regulation of PTEN stability and activity |
| Reactome | DME-69017 | CDK-mediated phosphorylation and removal of Cdc6 |
| Reactome | DME-8939236 | RUNX1 regulates transcription of genes involved in differentiation of HSCs |

**Table 9.1.2.1 (6.2.1A *trbdC518A* female up and down)** Hits from STRING searching for proteins that was differentially expressed between *trbdC518A* female and $w^{1118}$ female from ubiquitin GlyGly enrichment analysis (control $w^{1118}$ female). Blue represented relatively downregulated in *trbdC518A* female and orange represented relatively upregulated in *trbdC518A* female (control $w^{1118}$ female).

| #category | term ID | term description |
|---|---|---|
| GO Function | GO:0016298 | Lipase activity |
| GO Function | GO:0052689 | Carboxylic ester hydrolase activity |
| STRING clusters | CL:11519 | Assembly of active LPL and LIPC lipase complexes, and retinol binding |
| Reactome | DME-8963889 | Assembly of active LPL and LIPC lipase complexes |
| Reactome | DME-8964058 | HDL remodeling |
| Reactome | DME-1483166 | Synthesis of PA |
| GO Function | GO:0005506 | Iron ion binding |
| GO Function | GO:0016705 | Oxidoreductase activity, acting on paired donors, with incorporation or reduction of molecular oxygen |
| GO Function | GO:0020037 | Heme binding |
| GO Function | GO:0004497 | Monooxygenase activity |
| GO Function | GO:0016491 | Oxidoreductase activity |
| GO Function | GO:0046914 | Transition metal ion binding |
| GO Function | GO:0043167 | Ion binding |

**Table 9.1.2.1 (6.2.1B *trbdC518A* male up and down)** Hits from STRING searching for proteins that was differentially expressed between *trbdC518A* male and *trbdC518A* female from ubiquitin GlyGly enrichment analysis (control *trbdC518A* female). Blue represented relatively downregulated in *trbdC518A* male and orange represented relatively upregulated in *trbdC518A* male (control *trbdC518A* female).

| #category | term ID | term description |
|---|---|---|
| GO Function | GO:0016298 | Lipase activity |
| GO Function | GO:0052689 | Carboxylic ester hydrolase activity |
| STRING clusters | CL:11519 | Assembly of active LPL and LIPC lipase complexes, and retinol binding |
| Reactome | DME-8963889 | Assembly of active LPL and LIPC lipase complexes |
| Reactome | DME-8964058 | HDL remodeling |
| Reactome | DME-1483166 | Synthesis of PA |
| Reactome | DME-556833 | Metabolism of lipids |
| Reactome | DME-382551 | Transport of small molecules |
| Reactome | DME-1430728 | Metabolism |
| COMPARTMENTS | GOCC:0042718 | Yolk granule |
| COMPARTMENTS | GOCC:0060417 | Yolk |
| UniProt Keywords | KW-0765 | Sulfation |
| Pfam | PF00151 | Lipase |
| InterPro | IPR000734 | Triacylglycerol lipase family |
| InterPro | IPR013818 | Lipase/vitellogenin |
| GO Process | GO:0070059 | Intrinsic apoptotic signaling pathway in response to endoplasmic reticulum stress |

**Table 9.1.2.1 (6.2.1 $w^{1118}$ male up and down)** Hits from STRING searching for proteins that was differentially expressed between $w^{1118}$ male and $w^{1118}$ female from ubiquitin GlyGly enrichment analysis (control $w^{1118}$ female). Blue represented relatively downregulated in $w^{1118}$ male and orange represented relatively upregulated in $w^{1118}$ male (control $w^{1118}$ female).

| #category | term ID | term description |
|---|---|---|
| GO Process | GO:0009617 | Response to bacterium |
| GO Process | GO:0034605 | Cellular response to heat |
| GO Function | GO:0005506 | Iron ion binding |
| GO Function | GO:0016491 | Oxidoreductase activity |
| GO Function | GO:0016705 | Oxidoreductase activity, acting on paired donors, with incorporation or reduction of molecular oxygen |
| GO Function | GO:0020037 | Heme binding |
| STRING clusters | CL:20772 | Stress-inducible humoral factor Turandot, and Diedel |
| Reactome | DME-211945 | Phase I - Functionalization of compounds |
| Pfam | PF07240 | Stress-inducible humoral factor Turandot |
| Pfam | PF00067 | Cytochrome P450 |
| InterPro | IPR010825 | Stress-inducible humoral factor Turandot |
| InterPro | IPR001128 | Cytochrome P450 |
| InterPro | IPR002401 | Cytochrome P450, E-class, group I |
| InterPro | IPR017972 | Cytochrome P450, conserved site |
| InterPro | IPR036396 | Cytochrome P450 superfamily |
| GO Function | GO:0005506 | Iron ion binding |
| GO Function | GO:0016705 | Oxidoreductase activity, acting on paired donors, with incorporation or reduction of molecular oxygen |
| GO Function | GO:0020037 | Heme binding |
| GO Function | GO:0016491 | Oxidoreductase activity |
| GO Function | GO:0004364 | Glutathione transferase activity |
| GO Function | GO:0004497 | Monooxygenase activity |
| STRING clusters | CL:22142 | Mixed, incl. cytochrome p450, and udp-glucuronosyl/udp-glucosyltransferase |
| STRING clusters | CL:7753 | Glutathione S-transferase, N-terminal domain |
| STRING clusters | CL:20694 | Attacin, C-terminal |
| STRING clusters | CL:7757 | Detoxification, and Glutathione S-transferase, C-terminal domain |
| STRING clusters | CL:23886 | Mixed, incl. zona pellucida-like domain, and tonb box, conserved site |
| STRING clusters | CL:22145 | Mixed, incl. cytochrome p450, and glycosyl transferase family 1 |
| KEGG | dme00480 | Glutathione metabolism |
| KEGG | dme00980 | Metabolism of xenobiotics by cytochrome P450 |
| KEGG | dme00982 | Drug metabolism - cytochrome P450 |
| KEGG | dme00983 | Drug metabolism - other enzymes |
| Pfam | PF00067 | Cytochrome P450 |
| Pfam | PF13410 | Glutathione S-transferase, C-terminal domain |
| Pfam | PF13409 | Glutathione S-transferase, N-terminal domain |
| Pfam | PF00043 | Glutathione S-transferase, C-terminal domain |
| Pfam | PF02798 | Glutathione S-transferase, N-terminal domain |
| Pfam | PF03768 | Attacin, N-terminal region |
| Pfam | PF03769 | Attacin, C-terminal region |
| Pfam | PF13417 | Glutathione S-transferase, N-terminal domain |
| Pfam | PF14497 | Glutathione S-transferase, C-terminal domain |
| InterPro | IPR001128 | Cytochrome P450 |
| InterPro | IPR002401 | Cytochrome P450, E-class, group I |
| InterPro | IPR017972 | Cytochrome P450, conserved site |
| InterPro | IPR036396 | Cytochrome P450 superfamily |
| InterPro | IPR004045 | Glutathione S-transferase, N-terminal |
| InterPro | IPR004046 | Glutathione S-transferase, C-terminal |
| InterPro | IPR005520 | Attacin, N-terminal |
| InterPro | IPR005521 | Attacin, C-terminal |
| InterPro | IPR010987 | Glutathione S-transferase, C-terminal-like |
| InterPro | IPR036282 | Glutathione S-transferase, C-terminal domain superfamily |

**Table 9.1.2.1 (6.2.1C *trbdC518A* up and down)** Hits from STRING searching for proteins that was differentially expressed between trbdC518A male and $w^{1118}$ male in total proteome analysis (control $w^{1118}$ male). Blue represented relatively downregulated in *trbdC518A* male and orange represented relatively upregulated in *trbdC518A* male (control $w^{1118}$ male).

| #category | term ID | term description |
|---|---|---|
| GO Process | GO:0008152 | Metabolic process |
| GO Function | GO:0005506 | Iron ion binding |
| GO Function | GO:0016705 | Oxidoreductase activity, acting on paired donors, with incorporation or reduction of molecular oxygen |
| GO Function | GO:0020037 | Heme binding |
| GO Function | GO:0016491 | Oxidoreductase activity |
| GO Function | GO:0046914 | Transition metal ion binding |
| GO Function | GO:0043169 | Cation binding |
| GO Function | GO:0003824 | Catalytic activity |
| GO Function | GO:0043167 | Ion binding |
| GO Function | GO:0004497 | Monooxygenase activity |
| GO Function | GO:1901363 | Heterocyclic compound binding |
| GO Function | GO:0097159 | Organic cyclic compound binding |
| STRING clusters | CL:22141 | Mixed, incl. cytochrome p450, and udp-glucuronosyl/udp-glucosyltransferase |
| STRING clusters | CL:22142 | Mixed, incl. cytochrome p450, and udp-glucuronosyl/udp-glucosyltransferase |
| STRING clusters | CL:22145 | Mixed, incl. cytochrome p450, and glycosyl transferase family 1 |
| STRING clusters | CL:11519 | Assembly of active LPL and LIPC lipase complexes, and retinol binding |
| STRING clusters | CL:22147 | Cytochrome P450, and Glycosyl transferase family 1 |
| STRING clusters | CL:22152 | Cytochrome P450, E-class, group I, and Cytochrome P450, E-class, group IV |
| STRING clusters | CL:15534 | Mixed, incl. cyclic-di-gmp binding, and protein trans-autophosphorylation |
| STRING clusters | CL:22273 | Mixed, incl. biotin metabolism, and polyamine oxidase activity |
| Reactome | DME-8963889 | Assembly of active LPL and LIPC lipase complexes |
| Reactome | DME-8964058 | HDL remodeling |
| Reactome | DME-1483166 | Synthesis of PA |
| GO Process | GO:0003012 | Muscle system process |
| GO Function | GO:0020037 | Heme binding |
| GO Component | GO:0043292 | Contractile fiber |

**Table 9.1.2.1 (6.2.1C *trbdC518A* female up and down)** Hits from STRING searching for proteins that was differentially expressed between *trbdC518A* female and $w^{1118}$ female from total proteome analysis (control $w^{1118}$ female). Blue represented relatively downregulated in *trbdC518A* female and orange represented relatively upregulated in *trbdC518A* female (control $w^{1118}$ female).

| #category | term ID | term description |
|---|---|---|
| GO Process | GO:0007548 | Sex differentiation |
| STRING clusters | CL:11519 | Assembly of active LPL and LIPC lipase complexes, and retinol binding |
| STRING clusters | CL:20772 | Stress-inducible humoral factor Turandot, and Diedel |
| Reactome | DME-8963889 | Assembly of active LPL and LIPC lipase complexes |
| Reactome | DME-8964058 | HDL remodeling |
| Reactome | DME-1483166 | Synthesis of PA |
| GO Process | GO:0008152 | Metabolic process |
| GO Process | GO:0046693 | Sperm storage |
| GO Process | GO:0017085 | Response to insecticide |
| GO Process | GO:0046008 | Regulation of female receptivity, post-mating |
| GO Function | GO:0020037 | Heme binding |
| GO Function | GO:0016705 | Oxidoreductase activity, acting on paired donors, with incorporation or reduction of molecular oxygen |
| GO Function | GO:0005506 | Iron ion binding |
| GO Function | GO:0016491 | Oxidoreductase activity |
| GO Function | GO:0043169 | Cation binding |
| GO Function | GO:0003824 | Catalytic activity |
| GO Function | GO:0046872 | Metal ion binding |
| GO Function | GO:0043167 | Ion binding |
| GO Function | GO:0004497 | Monooxygenase activity |
| GO Function | GO:0097159 | Organic cyclic compound binding |
| GO Function | GO:1901363 | Heterocyclic compound binding |
| GO Function | GO:0005488 | Binding |
| STRING clusters | CL:22141 | Mixed, incl. cytochrome p450, and udp-glucuronosyl/udp-glucosyltransferase |
| STRING clusters | CL:22142 | Mixed, incl. cytochrome p450, and udp-glucuronosyl/udp-glucosyltransferase |
| STRING clusters | CL:22143 | Mixed, incl. cytochrome p450, and udp-glucuronosyl/udp-glucosyltransferase |
| STRING clusters | CL:22145 | Mixed, incl. cytochrome p450, and glycosyl transferase family 1 |
| STRING clusters | CL:22147 | Cytochrome P450, and Glycosyl transferase family 1 |
| STRING clusters | CL:22152 | Cytochrome P450, E-class, group I, and Cytochrome P450, E-class, group IV |
| STRING clusters | CL:6740 | Valine, leucine and isoleucine degradation, and Electron transfer flavoprotein domain |
| STRING clusters | CL:22273 | Mixed, incl. biotin metabolism, and polyamine oxidase activity |
| STRING clusters | CL:6656 | Fatty acid metabolic process, and microbody |
| STRING clusters | CL:22295 | Mixed, incl. lauric acid metabolic process, and leucine-rich melanocyte differentiation-associated protein |
| Reactome | DME-71291 | Metabolism of amino acids and derivatives |

**Table 9.1.2.1 (6.2.1D *trbdC518A* male up and down)** Hits from STRING searching for proteins that was differentially expressed between *trbdC518A* male and *trbdC518A* female from total proteome analysis, (control *trbdC518A* female). Blue represented relatively downregulated in *trbdC518A* male and orange represented relatively upregulated in *trbdC518A* male (control *trbdC518A* female).

| #category | term ID | term description |
|---|---|---|
| GO Process | GO:0042254 | Ribosome biogenesis |
| GO Process | GO:0006364 | rRNA processing |
| GO Process | GO:0042273 | Ribosomal large subunit biogenesis |
| GO Process | GO:0000470 | Maturation of lsu-rrna |
| GO Process | GO:0007548 | Sex differentiation |
| GO Process | GO:0006396 | RNA processing |
| GO Component | GO:0005730 | Nucleolus |
| GO Component | GO:0030684 | Preribosome |
| GO Component | GO:0043232 | Intracellular non-membrane-bounded organelle |
| STRING clusters | CL:1130 | Preribosome, and dead/deah box helicase domain |
| STRING clusters | CL:1137 | Preribosome, and rna helicase, dead-box type, q motif |
| STRING clusters | CL:1138 | Ribosomal large subunit biogenesis, and rna helicase, dead-box type, q motif |
| STRING clusters | CL:11519 | Assembly of active LPL and LIPC lipase complexes, and retinol binding |
| STRING clusters | CL:1139 | Mixed, incl. preribosome, large subunit precursor, and rna helicase, dead-box type, q motif |
| STRING clusters | CL:1142 | Preribosome, large subunit precursor, and brix domain |
| STRING clusters | CL:1146 | Preribosome, large subunit precursor, and brix domain |
| Reactome | DME-8963889 | Assembly of active LPL and LIPC lipase complexes |
| Reactome | DME-8964058 | HDL remodeling |
| Reactome | DME-1483166 | Synthesis of PA |
| GO Component | GO:0005576 | Extracellular region |
| GO Component | GO:0005616 | Larval serum protein complex |
| GO Component | GO:0005615 | Extracellular space |
| STRING clusters | CL:21451 | Storage protein, and response to pheromone |
| COMPARTMENTS | GOCC:0005576 | Extracellular region |
| COMPARTMENTS | GOCC:0005615 | Extracellular space |
| COMPARTMENTS | GOCC:0005616 | Larval serum protein complex |

**Table 9.1.2.1 (6.2.1 *w*$^{1118}$ male up and down)** Hits from STRING searching for proteins that was differentially expressed between *w*$^{1118}$ male and *w*$^{1118}$ female from ubiquitin total proteome analysis (control *w*$^{1118}$ female). Blue represented relatively downregulated in *w*$^{1118}$ male and orange represented relatively upregulated in *w*$^{1118}$ male (control *w*$^{1118}$ female).

### 9.1.3 Reagent and material table

| REAGENT or RESOURCE | SOURCE | IDENTIFIER |
|---|---|---|
| **Bacterial and *Drosophila* Strains** | | |
| 5-alpha Competent E. coli | NEB | C2988J |
| Rosetta II DE3 | Novagen | Cat# 71400 |
| *trbdC518A Drosophila* | This study | N/A |
| *UAS-tra$^{RNAi}$* | VDRC | VDRC#2560 |
| *UAS-tra$^{RNAi}$/CyO;TM6B/pri* | This study | N/A |
| *alrm-Gal4/CyO;TM6B/pri* | This study | N/A |
| *J6-Gal4/CyO;TM6B/pri* | This study | N/A |
| **Chemicals, peptides, and recombinant proteins** | | |
| Phusion® High-Fidelity DNA Polymerase | NEB | Cat# M0530S |
| IPTG | VWR | Cat# 437144N |
| cOmplete Protease Inhibitor tablets | Sigma-Aldrich | Cat# 11873580001 |
| Vectashield mounting media | 2BScientific | SKU: H-1000-10 |
| DNaseI | Sigma-Aldrich | Cat# DN25-100mg |
| Lysozyme | Sigma-Aldrich | Cat# L6876-5G |
| Ubiquitin | Elliott et al., 2016 PMID: 27591049 | N/A |
| Triethylammonium bicarbonate (TEAB) | Sigma-Aldrich | T7408-100ML |
| Pierce™ 660nm Protein Assay Reagent | ThermoFisher | Cat# 22660 |
| Ionic Detergent Compatibility Reagent for Pierce™ 660nm Protein Assay Reagent | ThermoFisher | Cat# 22663 |
| Sequencing Grade Modified Trypsin | Promega | Cat# V5117 |
| **Recombinant DNA** | | |
| pMX-dTRABID with codon optimization | This study | N/A |
| poPINS-dTRABID-ANKOTU | This study | N/A |
| poPINS-dTRABID-ANKOTU$^{C518A}$ | This study | N/A |
| **Antibody** | | |
| Rat-Elav-7E8A10 anti-elav | Developmental Studies Hybridoma Bank | AB_528218 |
| 8D12 anti-Repo | Developmental Studies Hybridoma Bank | AB_528448 |
| goat anti-mouse Alexa Fluor 488 | ThermoFisher | Cat# A-11001, AB_2534069 |
| goat anti-rat Alexa Fluor 568 | ThermoFisher | Cat# A-11077, AB_2534121 |
| **Critical commercial assays** | | |
| QIAprep Spin Miniprep Kit | QIAGEN | Cat# 27106 |
| TRIzol™ Plus RNA Purification Kit | ThermoFisher | Cat# 12183555 |
| PureLink® DNase for on-column treatment | ThermoFisher | Cat# 12185010 |

| | | |
|---|---|---|
| SuperScript™ III Reverse Transcriptase | ThermoFisher | Cat# 18080093 |
| SensiFAST™ SYBR® No-ROX Kit | Meridian Bioscience | Cat# Bio-98020 |
| PTMScan® HS Ubiquitin/SUMO Remnant Motif (K-ε-GG) Kit | Cell Signal | Cat# 59322 |
| DAM2 *Drosophila* activity monitor | TRIKINETICS | N/A |
| **Software** | | |
| Pymol | Schrödinger, Inc | https://www.pymol.org/2/ |
| Fiji (ImageJ) | https://www.nature.com/articles/nmeth.2019 | https://imagej.net/software/fiji/ |
| GraphPad Prism | GraphPad | https://www.graphpad.com |
| Jalview | University of Dundee | https://www.jalview.org/ |
| Affinity Designer | Serif | https://affinity.serif.com/en-gb/designer/ |
| Biorender | Biorender | https://biorender.com/ |
| Perseus | MaxQuant | https://maxquant.net/perseus/ |
| R "pcr" package | Ahmed and Kim., 2018 PMID 29576953 | https://cran.r-project.org/web/packages/pcr/pcr.pdf |
| **Other** | | |
| Ni-NTA | QIAGEN | Cat# 30210 |
| Resource Q | Cytiva Life Sciences | Cat# 17117901 |
| HiLoad Superdex75 | Cytiva Life Sciences | Cat# 28989333 |

## 9.2 COVID-19 statement

The study was significantly impacted by the pandemic. Especially from March to August 2020, I were restricted to carry out wet lab experiment. From 2020 to current, I were impacted by the backlogs from logistics to technical support. For example, due to social distancing from August 2020 to April 2021, the maxim capacity in our lab block was limited to 12 people, which limited my progress of performing wet lab experiments. The lab suffered from backlogs of reagent delivery, which including delay of PTMScan kit, 15 ml falcon tubes and fly food ingredients. The initial plan was to conduct RNAseq in *trbdC518A* fly brains, which combined with proteome and ubiquitinome data can provide more insightful knowledge about the regulation of *trbdCC518A.* Additionally, these omics studies were initially planned to carry out at three time points, at day 3, 6 and 18, which represent early adulthood. More timepoints can capture neurodegeneration related molecular changes at earl adulthood. The experiment design was compromised due to the impact of COVID lockdowns.

## 9.3 Bibliography

Aalto, A.L., Mohan, A.K., Schwintzer, L., Kupka, S., Kietz, C., Walczak, H., Broemer, M., Meinander, A., 2019. M1-linked ubiquitination by LUBEL is required for inflammatory responses to oral infection in Drosophila. Cell Death Differ. 26, 860. https://doi.org/10.1038/s41418-018-0164-x

Abbasi, A., Forsberg, K., Bischof, F., 2015. The role of the ubiquitin-editing enzyme A20 in diseases of the central nervous system and other pathological processes. Front. Mol. Neurosci. 8, 21. https://doi.org/10.3389/fnmol.2015.00021

Abdul Rehman, S.A., Kristariyanto, Y.A., Choi, S.-Y., Nkosi, P.J., Weidlich, S., Labib, K., Hofmann, K., Kulathu, Y., 2016. MINDY-1 Is a Member of an Evolutionarily Conserved and Structurally Distinct New Family of Deubiquitinating Enzymes. Mol. Cell 63, 146–155. https://doi.org/10.1016/j.molcel.2016.05.009

Alexopoulou, Z., Lang, J., Perrett, R.M., Elschami, M., Hurry, M.E.D., Kim, H.T., Mazaraki, D., Szabo, A., Kessler, B.M., Goldberg, A.L., Ansorge, O., Fulga, T.A., Tofaris, G.K., 2016. Deubiquitinase Usp8 regulates α-synuclein clearance and modifies its toxicity in Lewy body disease. Proc. Natl. Acad. Sci. 113, E4688–E4697. https://doi.org/10.1073/pnas.1523597113

Al-Lamki, R.S., Mayadas, T.N., 2015. TNF receptors: signaling pathways and contribution to renal dysfunction. Kidney Int. 87, 281–296. https://doi.org/10.1038/ki.2014.285

Amer-Sarsour, F., Kordonsky, A., Berdichevsky, Y., Prag, G., Ashkenazi, A., 2021. Deubiquitylating enzymes in neuronal health and disease. Cell Death Dis. 12, 1–11. https://doi.org/10.1038/s41419-020-03361-5

Atkin, G., Paulson, H., 2014. Ubiquitin pathways in neurodegenerative disease. Front. Mol. Neurosci. 7. https://doi.org/10.3389/fnmol.2014.00063

Auluck, P.K., Chan, H.Y.E., Trojanowski, J.Q., Lee, V.M.-Y., Bonini, N.M., 2002. Chaperone Suppression of α-Synuclein Toxicity in a Drosophila Model for Parkinson's Disease. Science 295, 865–868. https://doi.org/10.1126/science.1067389

Baumann, K., 2014. Lys33-linked ubiquitin in post-Golgi transport. Nat. Rev. Mol. Cell Biol. 15, 365–365. https://doi.org/10.1038/nrm3812

Behl, C., Davis, J.B., Lesley, R., Schubert, D., 1994. Hydrogen peroxide mediates amyloid β protein toxicity. Cell 77, 817–827. https://doi.org/10.1016/0092-8674(94)90131-7

Belote, J.M., Handler, A.M., Wolfner, M.F., Livak, K.J., Baker, B.S., 1985. Sex-specific regulation of yolk protein gene expression in Drosophila. Cell 40, 339–348. https://doi.org/10.1016/0092-8674(85)90148-5

Bienz, M., Clevers, H., 2000. Linking Colorectal Cancer to Wnt Signaling. Cell 103, 311–320. https://doi.org/10.1016/S0092-8674(00)00122-7

Birsa, N., Norkett, R., Wauer, T., Mevissen, T.E.T., Wu, H.-C., Foltynie, T., Bhatia, K., Hirst, W.D., Komander, D., Plun-Favreau, H., Kittler, J.T., 2014. Lysine 27 ubiquitination of the mitochondrial transport protein Miro is dependent on serine 65 of the Parkin ubiquitin ligase. J. Biol. Chem. 289, 14569–14582. https://doi.org/10.1074/jbc.M114.563031

Bombois, S., Derambure, P., Pasquier, F., Monaca, C., 2010. Sleep disorders in aging and dementia. J. Nutr. Health Aging 14, 212–217. https://doi.org/10.1007/s12603-010-0052-7

Booth, H.D.E., Wessely, F., Connor-Robson, N., Rinaldi, F., Vowles, J., Browne, C., Evetts, S.G., Hu, M.T., Cowley, S.A., Webber, C., Wade-Martins, R., 2019. RNA sequencing reveals MMP2 and TGFB1 downregulation in LRRK2 G2019S Parkinson's iPSC-derived astrocytes. Neurobiol. Dis. 129, 56–66. https://doi.org/10.1016/j.nbd.2019.05.006

Burtis, K.C., Coschigano, K.T., Baker, B.S., Wensink, P.C., 1991. The doublesex proteins of Drosophila melanogaster bind directly to a sex-specific yolk protein gene enhancer. EMBO J. 10, 2577–2582.

Butler, B., Pirrotta, V., Irminger-Finger, I., Nöthiger, R., 1986. The sex-determining

gene tra of Drosophila: molecular cloning and transformation studies. EMBO J. 5, 3607–3613. https://doi.org/10.1002/j.1460-2075.1986.tb04689.x

Callis, J., 2014. The Ubiquitination Machinery of the Ubiquitin System. Arab. Book Am. Soc. Plant Biol. 12. https://doi.org/10.1199/tab.0174

Chen, G., Goeddel, D.V., 2002. TNF-R1 Signaling: A Beautiful Pathway. Science 296, 1634–1635. https://doi.org/10.1126/science.1071924

Ciechanover, A., Heller, H., Elias, S., Haas, A.L., Hershko, A., 1980. ATP-dependent conjugation of reticulocyte proteins with the polypeptide required for protein degradation. Proc. Natl. Acad. Sci. 77, 1365–1368. https://doi.org/10.1073/pnas.77.3.1365

Cirelli, C., Bushey, D., 2008. Sleep and wakefulness in Drosophila melanogaster. Ann. N. Y. Acad. Sci. 1129, 323–329. https://doi.org/10.1196/annals.1417.017

Coales, I., Tsartsalis, S., Nurun, F., Weinert, M., Clode, D., Owen, D., Matthews, P., 2022. Alzheimer's disease related transcriptional sex differences in myeloid cells. https://doi.org/10.1186/s12974-022-02604-w

Crowther, D.C., Kinghorn, K.J., Miranda, E., Page, R., Curry, J.A., Duthie, F.A.I., Gubb, D.C., Lomas, D.A., 2005. Intraneuronal Aβ, non-amyloid aggregates and neurodegeneration in a Drosophila model of Alzheimer's disease. Neuroscience 132, 123–135. https://doi.org/10.1016/j.neuroscience.2004.12.025

Dawson, T.M., Golde, T.E., Lagier-Tourenne, C., 2018. Animal models of neurodegenerative diseases. Nat. Neurosci. 21, 1370–1379. https://doi.org/10.1038/s41593-018-0236-8

De Gregorio, E., Spellman, P.T., Tzou, P., Rubin, G.M., Lemaitre, B., 2002. The Toll and Imd pathways are the major regulators of the immune response in Drosophila. EMBO J. 21, 2568–2579. https://doi.org/10.1093/emboj/21.11.2568

Elliott, P.R., Leske, D., Hrdinka, M., Bagola, K., Fiil, B.K., McLaughlin, S.H., Wagstaff, J., Volkmar, N., Christianson, J.C., Kessler, B.M., Freund, S.M.V., Komander, D., Gyrd-Hansen, M., 2016. SPATA2 Links CYLD to LUBAC, Activates CYLD, and Controls LUBAC Signaling. Mol. Cell 63, 990–1005. https://doi.org/10.1016/j.molcel.2016.08.001

Enesa, K., Evans, P., 2014. The Biology of A20-Like Molecules, in: Ferran, C. (Ed.), The Multiple Therapeutic Targets of A20, Advances in Experimental Medicine and Biology. Springer New York, New York, NY, pp. 33–48. https://doi.org/10.1007/978-1-4939-0398-6_3

Evans, P.C., Smith, T.S., Lai, M.-J., Williams, M.G., Burke, D.F., Heyninck, K., Kreike, M.M., Beyaert, R., Blundell, T.L., Kilshaw, P.J., 2003. A Novel Type of Deubiquitinating Enzyme *. J. Biol. Chem. 278, 23180–23186. https://doi.org/10.1074/jbc.M301863200

Evans, P.C., Taylor, E.R., Coadwell, J., Heyninck, K., Beyaert, R., Kilshaw, P.J., 2001. Isolation and characterization of two novel A20-like proteins 7.

Fernando, M.D.A., Kounatidis, I., Ligoxygakis, P., 2014. Loss of Trabid, a New Negative Regulator of the Drosophila Immune-Deficiency Pathway at the

Level of TAK1, Reduces Life Span. PLOS Genet. 10, e1004117. https://doi.org/10.1371/journal.pgen.1004117

Ferreiro, M.J., Pérez, C., Marchesano, M., Ruiz, S., Caputi, A., Aguilera, P., Barrio, R., Cantera, R., 2018. Drosophila melanogaster White Mutant w1118 Undergo Retinal Degeneration. Front. Neurosci. 11. https://doi.org/10.3389/fnins.2017.00732

Feuillette, S., Charbonnier, C., Frebourg, T., Campion, D., Lecourtois, M., 2020. A Connected Network of Interacting Proteins Is Involved in Human-Tau Toxicity in Drosophila. Front. Neurosci. 14.

Fisher, D.W., Bennett, D.A., Dong, H., 2018. Sexual dimorphism in predisposition to Alzheimer's disease. Neurobiol. Aging 70, 308–324. https://doi.org/10.1016/j.neurobiolaging.2018.04.004

Gersch, M., Gladkova, C., Schubert, A.F., Michel, M.A., Maslen, S., Komander, D., 2017. Mechanism and regulation of the Lys6-selective deubiquitinase USP30. Nat. Struct. Mol. Biol. 24, 920–930. https://doi.org/10.1038/nsmb.3475

Guo, L., Zhong, M.B., Zhang, L., Zhang, B., Cai, D., 2022. Sex Differences in Alzheimer's Disease: Insights From the Multiomics Landscape. Biol. Psychiatry 91, 61–71. https://doi.org/10.1016/j.biopsych.2021.02.968

Hampel, H., Vassar, R., De Strooper, B., Hardy, J., Willem, M., Singh, N., Zhou, J., Yan, R., Vanmechelen, E., De Vos, A., Nisticò, R., Corbo, M., Imbimbo, B.P., Streffer, J., Voytyuk, I., Timmers, M., Tahami Monfared, A.A., Irizarry, M., Albala, B., Koyama, A., Watanabe, N., Kimura, T., Yarenis, L., Lista, S., Kramer, L., Vergallo, A., 2021. The β-Secretase BACE1 in Alzheimer's Disease. Biol. Psychiatry 89, 745–756. https://doi.org/10.1016/j.biopsych.2020.02.001

Harris, L.D., Pen, J.L., Scholz, N., Mieszczanek, J., Vaughan, N., Davis, S., Berridge, G., Kessler, B., Bienz, M., Licchesi, J.D.F., 2020. The deubiquitinase TRABID stabilises the K29/K48-specific E3 ubiquitin ligase HECTD1. J. Biol. Chem. jbc.RA120.015162. https://doi.org/10.1074/jbc.RA120.015162

Henn, I.H., Bouman, L., Schlehe, J.S., Schlierf, A., Schramm, J.E., Wegener, E., Nakaso, K., Culmsee, C., Berninger, B., Krappmann, D., Tatzelt, J., Winklhofer, K.F., 2007. Parkin Mediates Neuroprotection through Activation of IκB Kinase/Nuclear Factor-κB Signaling. J. Neurosci. 27, 1868–1878. https://doi.org/10.1523/JNEUROSCI.5537-06.2007

Hicke, L., Schubert, H.L., Hill, C.P., 2005. Ubiquitin-binding domains. Nat. Rev. Mol. Cell Biol. 6, 610–621. https://doi.org/10.1038/nrm1701

Hiltunen, M., Lu, A., Thomas, A.V., Romano, D.M., Kim, M., Jones, P.B., Xie, Z., Kounnas, M.Z., Wagner, S.L., Berezovska, O., Hyman, B.T., Tesco, G., Bertram, L., Tanzi, R.E., 2006. Ubiquilin 1 Modulates Amyloid Precursor Protein Trafficking and Aβ Secretion *. J. Biol. Chem. 281, 32240–32253. https://doi.org/10.1074/jbc.M603106200

Holleufer, A., Winther, K.G., Gad, H.H., Ai, X., Chen, Y., Li, L., Wei, Z., Deng, H., Liu, J., Frederiksen, N.A., Simonsen, B., Andersen, L.L., Kleigrewe, K., Dalskov, L., Pichlmair, A., Cai, H., Imler, J.-L., Hartmann, R., 2021. Two cGAS-like

receptors induce antiviral immunity in Drosophila. Nature 597, 114–118. https://doi.org/10.1038/s41586-021-03800-z

Hornbeck, P.V., Zhang, B., Murray, B., Kornhauser, J.M., Latham, V., Skrzypek, E., 2015. PhosphoSitePlus, 2014: mutations, PTMs and recalibrations. Nucleic Acids Res. 43, D512-520. https://doi.org/10.1093/nar/gku1267

Hoshijima, K., Inoue, K., Higuchi, I., Sakamoto, H., Shimura, Y., 1991. Control of doublesex Alternative Splicing by transformer and transformer-2 in Drosophila. Science 252, 833–836. https://doi.org/10.1126/science.1902987

Hsu, H., Xiong, J., Goeddel, D.V., 1995. The TNF receptor 1-associated protein TRADD signals cell death and NF-κB activation. Cell 81, 495–504. https://doi.org/10.1016/0092-8674(95)90070-5

Hu, H., Brittain, G.C., Chang, J.-H., Puebla-Osorio, N., Jin, J., Zal, A., Xiao, Y., Cheng, X., Chang, M., Fu, Y.-X., Zal, T., Zhu, C., Sun, S.-C., 2013. OTUD7B controls non-canonical NF-κB activation through deubiquitination of TRAF3. Nature 494, 371–374. https://doi.org/10.1038/nature11831

Hua, Y., Zhu, Y., Hu, Y., Kong, F., Duan, R., Zhang, Chao, Zhang, Chuchu, Zhang, S., Jin, Y., Ye, Y., Cai, Q., Ji, S., 2022. A Feedback Regulatory Loop Involving dTrbd/dTak1 in Controlling IMD Signaling in Drosophila Melanogaster. Front. Immunol. 13.

Huang, O.W., Ma, X., Yin, J., Flinders, J., Maurer, T., Kayagaki, N., Phung, Q., Bosanac, I., Arnott, D., Dixit, V.M., Hymowitz, S.G., Starovasnik, M.A., Cochran, A.G., 2012. Phosphorylation-dependent activity of the deubiquitinase DUBA. Nat. Struct. Mol. Biol. 19, 171–175. https://doi.org/10.1038/nsmb.2206

Iijima-Ando, K., Wu, P., Drier, E.A., Iijima, K., Yin, J.C.P., 2005. cAMP-response element-binding protein and heat-shock protein 70 additively suppress polyglutamine-mediated toxicity in Drosophila. Proc. Natl. Acad. Sci. 102, 10261–10266. https://doi.org/10.1073/pnas.0503937102

Inamdar, A.A., Masurekar, P., Hossain, M., Richardson, J.R., Bennett, J.W., 2014. Signaling Pathways Involved in 1-Octen-3-ol-Mediated Neurotoxicity in Drosophila melanogaster: Implication in Parkinson's Disease. Neurotox. Res. 25, 183–191. https://doi.org/10.1007/s12640-013-9418-z

Jack, C.R., Wiste, H.J., Weigand, S.D., Therneau, T.M., Knopman, D.S., Lowe, V., Vemuri, P., Mielke, M.M., Roberts, R.O., Machulda, M.M., Senjem, M.L., Gunter, J.L., Rocca, W.A., Petersen, R.C., 2017. Age-specific and sex-specific prevalence of cerebral β-amyloidosis, tauopathy, and neurodegeneration in cognitively unimpaired individuals aged 50–95 years: a cross-sectional study. Lancet Neurol. 16, 435–444. https://doi.org/10.1016/S1474-4422(17)30077-7

Jenkins, E.C., Shah, N., Gomez, M., Casalena, G., Zhao, D., Kenny, T.C., Guariglia, S.R., Manfredi, G., Germain, D., 2020. Proteasome mapping reveals sexual dimorphism in tissue-specific sensitivity to protein aggregations. EMBO Rep. 21, e48978. https://doi.org/10.15252/embr.201948978

Ji, T., Li, G., Chen, J., Zhao, J., Li, X., Lin, H., Cai, X., Cang, Y., 2016. Distinct role of

interleukin-6 and tumor necrosis factor receptor-1 in oval cell- mediated liver regeneration and inflammation-associated hepatocarcinogenesis. Oncotarget 7, 66635–66646. https://doi.org/10.18632/oncotarget.11365

Jiao, W., Spreemann, G., Ruchti, E., Banerjee, S., Vernon, S., Shi, Y., Stowers, R.S., Hess, K., McCabe, B.D., 2022. Intact Drosophila central nervous system cellular quantitation reveals sexual dimorphism. eLife 11, e74968. https://doi.org/10.7554/eLife.74968

Jin, J., Xie, X., Xiao, Y., Hu, H., Zou, Q., Cheng, X., Sun, S.-C., 2016a. Epigenetic regulation of the expression of *Il12* and *Il23* and autoimmune inflammation by the deubiquitinase Trabid. Nat. Immunol. 17, 259–268. https://doi.org/10.1038/ni.3347

Johnson, I.P., 2015. Age-related neurodegenerative disease research needs aging models. Front. Aging Neurosci. 7. https://doi.org/10.3389/fnagi.2015.00168

Johnson, S.L., Ranxhi, B., Libohova, K., Tsou, W.-L., Todi, S.V., 2020. Ubiquitin-interacting motifs of ataxin-3 regulate its polyglutamine toxicity through Hsc70-4-dependent aggregation. eLife 9, e60742. https://doi.org/10.7554/eLife.60742

Kaneko, M., Koike, H., Saito, R., Kitamura, Y., Okuma, Y., Nomura, Y., 2010. Loss of HRD1-mediated protein degradation causes amyloid precursor protein accumulation and amyloid-beta generation. J. Neurosci. Off. J. Soc. Neurosci. 30, 3924–3932. https://doi.org/10.1523/JNEUROSCI.2422-09.2010

Komander, D., Clague, M.J., Urbé, S., 2009. Breaking the chains: structure and function of the deubiquitinases. Nat. Rev. Mol. Cell Biol. 10, 550–563. https://doi.org/10.1038/nrm2731

Komander, D., Lord, C.J., Scheel, H., Swift, S., Hofmann, K., Ashworth, A., Barford, D., 2008. The Structure of the CYLD USP Domain Explains Its Specificity for Lys63-Linked Polyubiquitin and Reveals a B Box Module. Mol. Cell 29, 451–464. https://doi.org/10.1016/j.molcel.2007.12.018

Kounatidis, I., Chtarbanova, S., Cao, Y., Hayne, M., Jayanth, D., Ganetzky, B., Ligoxygakis, P., 2017. NF-κB Immunity in the Brain Determines Fly Lifespan in Healthy Aging and Age-Related Neurodegeneration. Cell Rep. 19, 836–848. https://doi.org/10.1016/j.celrep.2017.04.007

Kulathu, Y., Komander, D., 2012. Atypical ubiquitylation — the unexplored world of polyubiquitin beyond Lys48 and Lys63 linkages. Nat. Rev. Mol. Cell Biol. 13, 508–523. https://doi.org/10.1038/nrm3394

Kwak, Y.-D., Wang, B., Li, J.J., Wang, R., Deng, Q., Diao, S., Chen, Y., Xu, R., Masliah, E., Xu, H., Sung, J.-J., Liao, F.-F., 2012. Upregulation of the E3 ligase NEDD4-1 by Oxidative Stress Degrades IGF-1 Receptor Protein in Neurodegeneration. J. Neurosci. 32, 10971–10981. https://doi.org/10.1523/JNEUROSCI.1836-12.2012

Kwasna, D., Abdul Rehman, S.A., Natarajan, J., Matthews, S., Madden, R., De Cesare, V., Weidlich, S., Virdee, S., Ahel, I., Gibbs-Seymour, I., Kulathu, Y., 2018. Discovery and Characterization of ZUFSP/ZUP1, a Distinct Deubiquitinase Class Important for Genome Stability. Mol. Cell 70, 150-

164.e6. https://doi.org/10.1016/j.molcel.2018.02.023
Lecona, E., Rodriguez-Acebes, S., Specks, J., Lopez-Contreras, A.J., Ruppen, I., Murga, M., Muñoz, J., Mendez, J., Fernandez-Capetillo, O., 2016. USP7 is a SUMO deubiquitinase essential for DNA replication. Nat. Struct. Mol. Biol. 23, 270–277. https://doi.org/10.1038/nsmb.3185
Lemaitre, B., Kromer-Metzger, E., Michaut, L., Nicolas, E., Meister, M., Georgel, P., Reichhart, J.M., Hoffmann, J.A., 1995. A recessive mutation, immune deficiency (imd), defines two distinct control pathways in the Drosophila host defense. Proc. Natl. Acad. Sci. U. S. A. 92, 9465–9469.
Li, S.-B., Damonte, V.M., Chen, C., Wang, G.X., Kebschull, J.M., Yamaguchi, H., Bian, W.-J., Purmann, C., Pattni, R., Urban, A.E., Mourrain, P., Kauer, J.A., Scherrer, G., de Lecea, L., 2022. Hyperexcitable arousal circuits drive sleep instability during aging. Science 375, eabh3021. https://doi.org/10.1126/science.abh3021
Li, Y.X., Sibon, O.C.M., Dijkers, P.F., 2018. Inhibition of NF-κB in astrocytes is sufficient to delay neurodegeneration induced by proteotoxicity in neurons. J. Neuroinflammation 15, 261. https://doi.org/10.1186/s12974-018-1278-2
Licchesi, J.D.F., Mieszczanek, J., Mevissen, T.E.T., Rutherford, T.J., Akutsu, M., Virdee, S., Oualid, F.E., Chin, J.W., Ovaa, H., Bienz, M., Komander, D., 2012a. An ankyrin-repeat ubiquitin-binding domain determines TRABID's specificity for atypical ubiquitin chains. Nat. Struct. Mol. Biol. 19, 62. https://doi.org/10.1038/nsmb.2169
Limmer, S., Weiler, A., Volkenhoff, A., Babatz, F., Klämbt, C., 2014. The Drosophila blood-brain barrier: development and function of a glial endothelium. Front. Neurosci. 8. https://doi.org/10.3389/fnins.2014.00365
Lin, W.-Y., Williams, C., Yan, C., Koledachkina, T., Luedke, K., Dalton, J., Bloomsburg, S., Morrison, N., Duncan, K.E., Kim, C.C., Parrish, J.Z., 2015. The SLC36 transporter Pathetic is required for extreme dendrite growth in Drosophila sensory neurons. Genes Dev. 29, 1120–1135. https://doi.org/10.1101/gad.259119.115
Lork, M., Verhelst, K., Beyaert, R., 2017. CYLD, A20 and OTULIN deubiquitinases in NF-κB signaling and cell death: so similar, yet so different. Cell Death Differ. 24, 1172–1183. https://doi.org/10.1038/cdd.2017.46
Lukiw, W.J., 2016. Bacteroides fragilis Lipopolysaccharide and Inflammatory Signaling in Alzheimer's Disease. Front. Microbiol. 7.
Madabattula, S.T., Strautman, J.C., Bysice, A.M., O'Sullivan, J.A., Androschuk, A., Rosenfelt, C., Doucet, K., Rouleau, G., Bolduc, F., 2015. Quantitative Analysis of Climbing Defects in a Drosophila Model of Neurodegenerative Disorders. J. Vis. Exp. 52741. https://doi.org/10.3791/52741
Mader, J., Huber, J., Bonn, F., Dötsch, V., Rogov, V.V., Bremm, A., 2020. Oxygen-dependent asparagine hydroxylation of the ubiquitin-associated (UBA) domain in Cezanne regulates ubiquitin binding. J. Biol. Chem. 295, 2160–2174. https://doi.org/10.1074/jbc.RA119.010315
Mao, Y., Senic-Matuglia, F., Di Fiore, P.P., Polo, S., Hodsdon, M.E., De Camilli, P.,

2005. Deubiquitinating function of ataxin-3: Insights from the solution structure of the Josephin domain. Proc. Natl. Acad. Sci. 102, 12700–12705. https://doi.org/10.1073/pnas.0506344102

Martin, M., Hiroyasu, A., Guzman, R.M., Roberts, S.A., Goodman, A.G., 2018. Analysis of Drosophila STING Reveals an Evolutionarily Conserved Antimicrobial Function. Cell Rep. 23, 3537-3550.e6. https://doi.org/10.1016/j.celrep.2018.05.029

Mayne, K., White, J.A., McMurran, C.E., Rivera, F.J., de la Fuente, A.G., 2020. Aging and Neurodegenerative Disease: Is the Adaptive Immune System a Friend or Foe? Front. Aging Neurosci. 12.

Messick, T.E., Russell, N.S., Iwata, A.J., Sarachan, K.L., Shiekhattar, R., Shanks, J.R., Reyes-Turcu, F.E., Wilkinson, K.D., Marmorstein, R., 2008. Structural basis for ubiquitin recognition by the Otu1 ovarian tumor domain protein. J. Biol. Chem. 283, 11038–11049. https://doi.org/10.1074/jbc.M704398200

Mevissen, T.E.T., Hospenthal, M.K., Geurink, P.P., Elliott, P.R., Akutsu, M., Arnaudo, N., Ekkebus, R., Kulathu, Y., Wauer, T., El Oualid, F., Freund, S.M.V., Ovaa, H., Komander, D., 2013. OTU Deubiquitinases Reveal Mechanisms of Linkage Specificity and Enable Ubiquitin Chain Restriction Analysis. Cell 154, 169–184. https://doi.org/10.1016/j.cell.2013.05.046

Mevissen, T.E.T., Komander, D., 2017. Mechanisms of Deubiquitinase Specificity and Regulation. Annu. Rev. Biochem. 86, 159–192. https://doi.org/10.1146/annurev-biochem-061516-044916

Mevissen, T.E.T., Kulathu, Y., Mulder, M.P.C., Geurink, P.P., Maslen, S.L., Gersch, M., Elliott, P.R., Burke, J.E., van Tol, B.D.M., Akutsu, M., El Oualid, F., Kawasaki, M., Freund, S.M.V., Ovaa, H., Komander, D., 2016. Molecular basis of Lys11-polyubiquitin specificity in the deubiquitinase Cezanne. Nature 538, 402–405. https://doi.org/10.1038/nature19836

Misaghi, S., Galardy, P.J., Meester, W.J.N., Ovaa, H., Ploegh, H.L., Gaudet, R., 2005. Structure of the Ubiquitin Hydrolase UCH-L3 Complexed with a Suicide Substrate *. J. Biol. Chem. 280, 1512–1520. https://doi.org/10.1074/jbc.M410770200

Myllymäki, H., Valanne, S., Rämet, M., 2014. The Drosophila Imd Signaling Pathway. J. Immunol. 192, 3455–3462. https://doi.org/10.4049/jimmunol.1303309

Ohtake, F., Saeki, Y., Sakamoto, K., Ohtake, K., Nishikawa, H., Tsuchiya, H., Ohta, T., Tanaka, K., Kanno, J., 2015. Ubiquitin acetylation inhibits polyubiquitin chain elongation. EMBO Rep. 16, 192–201. https://doi.org/10.15252/embr.201439152

Ou, W., Yang, J., Simanauskaite, J., Choi, M., Castellanos, D.M., Chang, R., Sun, J., Jagadeesan, N., Parfitt, K.D., Cribbs, D.H., Sumbria, R.K., 2021. Biologic TNF-α inhibitors reduce microgliosis, neuronal loss, and tau phosphorylation in a transgenic mouse model of tauopathy. J. Neuroinflammation 18, 312. https://doi.org/10.1186/s12974-021-02332-7

Park, J., Al-Ramahi, I., Tan, Q., Mollema, N., Diaz-Garcia, J.R., Gallego-Flores, T., Lu, H.-C., Lagalwar, S., Duvick, L., Kang, H., Lee, Y., Jafar-Nejad, P., Sayegh,

L.S., Richman, R., Liu, X., Gao, Y., Shaw, C.A., Arthur, J.S.C., Orr, H.T., Westbrook, T.F., Botas, J., Zoghbi, H.Y., 2013. RAS–MAPK–MSK1 pathway modulates ataxin 1 protein levels and toxicity in SCA1. Nature 498, 325–331. https://doi.org/10.1038/nature12204

Passmore, L.A., Barford, D., 2004. Getting into position: the catalytic mechanisms of protein ubiquitylation. Biochem. J. 379, 513–525. https://doi.org/10.1042/bj20040198

Pawelec, G., Goldeck, D., Derhovanessian, E., 2014. Inflammation, ageing and chronic disease. Curr. Opin. Immunol., Host pathogens * Immune senescence 29, 23–28. https://doi.org/10.1016/j.coi.2014.03.007

Pickart, C.M., 2001. Mechanisms Underlying Ubiquitination. Annu. Rev. Biochem. 70, 503–533. https://doi.org/10.1146/annurev.biochem.70.1.503

Pickrell, A.M., Youle, R.J., 2015. The roles of PINK1, parkin, and mitochondrial fidelity in Parkinson's disease. Neuron 85, 257–273. https://doi.org/10.1016/j.neuron.2014.12.007

Pieruccini-Faria, F., Black, S.E., Masellis, M., Smith, E.E., Almeida, Q.J., Li, K.Z.H., Bherer, L., Camicioli, R., Montero-Odasso, M., 2021. Gait variability across neurodegenerative and cognitive disorders: Results from the Canadian Consortium of Neurodegeneration in Aging (CCNA) and the Gait and Brain Study. Alzheimers Dement. 17, 1317–1328. https://doi.org/10.1002/alz.12298

Priem, D., Devos, M., Druwé, S., Martens, A., Slowicka, K., Ting, A.T., Pasparakis, M., Declercq, W., Vandenabeele, P., van Loo, G., Bertrand, M.J.M., 2019. A20 protects cells from TNF-induced apoptosis through linear ubiquitin-dependent and -independent mechanisms. Cell Death Dis. 10, 1–16. https://doi.org/10.1038/s41419-019-1937-y

Ramirez-Rios, S., Serre, L., Stoppin-Mellet, V., Prezel, E., Vinit, A., Courriol, E., Fourest-Lieuvin, A., Delaroche, J., Denarier, E., Arnal, I., 2017. Chapter 9 - A TIRF microscopy assay to decode how tau regulates EB's tracking at microtubule ends, in: Feinstein, S.C., LaPointe, N.E. (Eds.), Methods in Cell Biology, Methods in Tau Cell Biology. Academic Press, pp. 179–197. https://doi.org/10.1016/bs.mcb.2017.06.013

Randles, L., Walters, K.J., 2012. Ubiquitin and its binding domains. Front. Biosci. Landmark Ed. 17, 2140–2157.

Rangel-Barajas, C., Coronel, I., Florán, B., 2015. Dopamine Receptors and Neurodegeneration. Aging Dis. 6, 349–368. https://doi.org/10.14336/AD.2015.0330

Ray, A., Speese, S.D., Logan, M.A., 2017. Glial Draper Rescues Aβ Toxicity in a Drosophila Model of Alzheimer's Disease. J. Neurosci. 37, 11881–11893. https://doi.org/10.1523/JNEUROSCI.0862-17.2017

Rebecchi, M.J., Scarlata, S., 1998. Pleckstrin homology domains: a common fold with diverse functions. Annu. Rev. Biophys. Biomol. Struct. 27, 503–528. https://doi.org/10.1146/annurev.biophys.27.1.503

Rehman, S.A.A., Armstrong, L.A., Lange, S.M., Kristariyanto, Y.A., Gräwert, T.W., Knebel, A., Svergun, D.I., Kulathu, Y., 2021. Mechanism of activation and

regulation of deubiquitinase activity in MINDY1 and MINDY2. Mol. Cell 81, 4176-4190.e6. https://doi.org/10.1016/j.molcel.2021.08.024

Rideout, E.J., Narsaiya, M.S., Grewal, S.S., 2015. The Sex Determination Gene transformer Regulates Male-Female Differences in Drosophila Body Size. PLoS Genet. 11, e1005683. https://doi.org/10.1371/journal.pgen.1005683

Rott, R., Szargel, R., Haskin, J., Bandopadhyay, R., Lees, A.J., Shani, V., Engelender, S., 2011. α-Synuclein fate is determined by USP9X-regulated monoubiquitination. Proc. Natl. Acad. Sci. 108, 18666–18671. https://doi.org/10.1073/pnas.1105725108

Roy, M., Rawat, A., Kaushik, S., Jyoti, A., Srivastava, V.K., 2022. Endogenous cysteine protease inhibitors in upmost pathogenic parasitic protozoa. Microbiol. Res. 261, 127061. https://doi.org/10.1016/j.micres.2022.127061

Sahara, N., Murayama, M., Mizoroki, T., Urushitani, M., Imai, Y., Takahashi, R., Murata, S., Tanaka, K., Takashima, A., 2005. In vivo evidence of CHIP up-regulation attenuating tau aggregation. J. Neurochem. 94, 1254–1263. https://doi.org/10.1111/j.1471-4159.2005.03272.x

Sarkar, S., Olsen, A.L., Sygnecka, K., Lohr, K.M., Feany, M.B., 2021. α-synuclein impairs autophagosome maturation through abnormal actin stabilization. PLOS Genet. 17, e1009359. https://doi.org/10.1371/journal.pgen.1009359

Schmidt, M.F., Gan, Z.Y., Komander, D., Dewson, G., 2021. Ubiquitin signalling in neurodegeneration: mechanisms and therapeutic opportunities. Cell Death Differ. 28, 570–590. https://doi.org/10.1038/s41418-020-00706-7

Shimura, H., Schwartz, D., Gygi, S.P., Kosik, K.S., 2004. CHIP-Hsc70 Complex Ubiquitinates Phosphorylated Tau and Enhances Cell Survival*. J. Biol. Chem. 279, 4869–4876. https://doi.org/10.1074/jbc.M305838200

Shrestha, R.K., Ronau, J.A., Davies, C.W., Guenette, R.G., Strieter, E.R., Paul, L.N., Das, C., 2014. Insights into the mechanism of deubiquitination by JAMM deubiquitinases from cocrystal structures of the enzyme with the substrate and product. Biochemistry 53, 3199–3217. https://doi.org/10.1021/bi5003162

Sliter, D.A., Martinez, J., Hao, L., Chen, X., Sun, N., Fischer, T.D., Burman, J.L., Li, Y., Zhang, Z., Narendra, D.P., Cai, H., Borsche, M., Klein, C., Youle, R.J., 2018. Parkin and PINK1 mitigate STING-induced inflammation. Nature 561, 258–262. https://doi.org/10.1038/s41586-018-0448-9

Snow, W.M., Albensi, B.C., 2016. Neuronal Gene Targets of NF-κB and Their Dysregulation in Alzheimer's Disease. Front. Mol. Neurosci. 9.

Stewart, M.D., Ritterhoff, T., Klevit, R.E., Brzovic, P.S., 2016. E2 enzymes: more than just middle men. Cell Res. 26, 423–440. https://doi.org/10.1038/cr.2016.35

Sun, E., Motolani, A., Campos, L., Lu, T., 2022. The Pivotal Role of NF-kB in the Pathogenesis and Therapeutics of Alzheimer's Disease. Int. J. Mol. Sci. 23, 8972. https://doi.org/10.3390/ijms23168972

Sun, F., Zeng, J., Jing, M., Zhou, J., Feng, J., Owen, S.F., Luo, Y., Li, F., Wang, H., Yamaguchi, T., Yong, Z., Gao, Y., Peng, W., Wang, L., Zhang, S., Du, J., Lin, D., Xu, M., Kreitzer, A.C., Cui, G., Li, Y., 2018. A Genetically Encoded

Fluorescent Sensor Enables Rapid and Specific Detection of Dopamine in Flies, Fish, and Mice. Cell 174, 481-496.e19. https://doi.org/10.1016/j.cell.2018.06.042

Sunderhaus, E.R., Kretzschmar, D., 2016. Mass Histology to Quantify Neurodegeneration in Drosophila. J. Vis. Exp. JoVE. https://doi.org/10.3791/54809

Suresh, H.G., Pascoe, N., Andrews, B., 2010. The structure and function of deubiquitinases: lessons from budding yeast. Open Biol. 10, 200279. https://doi.org/10.1098/rsob.200279

Tran, H., Hamada, F., Schwarz-Romond, T., Bienz, M., 2008. Trabid, a new positive regulator of Wnt-induced transcription with preference for binding and cleaving K63-linked ubiquitin chains. Genes Dev. 22, 528–542. https://doi.org/10.1101/gad.463208

Vincent, C.M., Dionne, M.S., 2021. Disparate regulation of IMD signaling drives sex differences in infection pathology in Drosophila melanogaster. Proc. Natl. Acad. Sci. 118, e2026554118. https://doi.org/10.1073/pnas.2026554118

Voet, S., Mc Guire, C., Hagemeyer, N., Martens, A., Schroeder, A., Wieghofer, P., Daems, C., Staszewski, O., Vande Walle, L., Jordao, M.J.C., Sze, M., Vikkula, H.-K., Demeestere, D., Van Imschoot, G., Scott, C.L., Hoste, E., Gonçalves, A., Guilliams, M., Lippens, S., Libert, C., Vandenbroucke, R.E., Kim, K.-W., Jung, S., Callaerts-Vegh, Z., Callaerts, P., de Wit, J., Lamkanfi, M., Prinz, M., van Loo, G., 2018. A20 critically controls microglia activation and inhibits inflammasome-dependent neuroinflammation. Nat. Commun. 9, 2036. https://doi.org/10.1038/s41467-018-04376-5

Wang, B., Alam, S.L., Meyer, H.H., Payne, M., Stemmler, T.L., Davis, D.R., Sundquist, W.I., 2003. Structure and Ubiquitin Interactions of the Conserved Zinc Finger Domain of Npl4 *. J. Biol. Chem. 278, 20225–20234. https://doi.org/10.1074/jbc.M300459200

Wang, X., Deckert, M., Xuan, N.T., Nishanth, G., Just, S., Waisman, A., Naumann, M., Schlüter, D., 2013. Astrocytic A20 ameliorates experimental autoimmune encephalomyelitis by inhibiting NF-κB- and STAT1-dependent chemokine production in astrocytes. Acta Neuropathol. (Berl.) 126, 711–724. https://doi.org/10.1007/s00401-013-1183-9

Wauer, T., Swatek, K.N., Wagstaff, J.L., Gladkova, C., Pruneda, J.N., Michel, M.A., Gersch, M., Johnson, C.M., Freund, S.M.V., Komander, D., 2015. Ubiquitin Ser65 phosphorylation affects ubiquitin structure, chain assembly and hydrolysis. EMBO J. 34, 307–325. https://doi.org/10.15252/embj.201489847

Wertz, I.E., Newton, K., Seshasayee, D., Kusam, S., Lam, C., Zhang, J., Popovych, N., Helgason, E., Schoeffler, A., Jeet, S., Ramamoorthi, N., Kategaya, L., Newman, R.J., Horikawa, K., Dugger, D., Sandoval, W., Mukund, S., Zindal, A., Martin, F., Quan, C., Tom, J., Fairbrother, W.J., Townsend, M., Warming, S., DeVoss, J., Liu, J., Dueber, E., Caplazi, P., Lee, W.P., Goodnow, C.C., Balazs, M., Yu, K., Kolumam, G., Dixit, V.M., 2015. Phosphorylation and linear ubiquitin direct A20 inhibition of inflammation. Nature 528, 370–375.

https://doi.org/10.1038/nature16165
Wilkinson, K.D., Urban, M.K., Haas, A.L., 1980. Ubiquitin is the ATP-dependent proteolysis factor I of rabbit reticulocytes. J. Biol. Chem. 255, 7529–7532.
Wittmann, C.W., Wszolek, M.F., Shulman, J.M., Salvaterra, P.M., Lewis, J., Hutton, M., Feany, M.B., 2001. Tauopathy in Drosophila: Neurodegeneration Without Neurofibrillary Tangles. Science 293, 711–714. https://doi.org/10.1126/science.1062382
Wooten, G.F., Currie, L.J., Bovbjerg, V.E., Lee, J.K., Patrie, J., 2004. Are men at greater risk for Parkinson's disease than women? J. Neurol. Neurosurg. Psychiatry 75, 637–639. https://doi.org/10.1136/jnnp.2003.020982
Xu, S., Zhang, X., Liu, C., Liu, Q., Chai, H., Luo, Y., Li, S., 2021. Role of Mitochondria in Neurodegenerative Diseases: From an Epigenetic Perspective. Front. Cell Dev. Biol. 9.
Yamaguchi, M., Yoshida, H., 2018. Drosophila as a Model Organism, in: Yamaguchi, M. (Ed.), Drosophila Models for Human Diseases, Advances in Experimental Medicine and Biology. Springer, Singapore, pp. 1–10. https://doi.org/10.1007/978-981-13-0529-0_1
Yang, Q., Zhao, J., Chen, D., Wang, Y., 2021. E3 ubiquitin ligases: styles, structures and functions. Mol. Biomed. 2, 23. https://doi.org/10.1186/s43556-021-00043-2
Yau, R., Rape, M., 2016. The increasing complexity of the ubiquitin code. Nat. Cell Biol. 18, 579–586. https://doi.org/10.1038/ncb3358
Yu, Z., Chen, T., Li, X., Yang, M., Tang, S., Zhu, X., Gu, Y., Su, X., Xia, M., Li, W., Zhang, X., Wang, Q., Cao, X., Wang, J., 2016. Lys29-linkage of ASK1 by Skp1−Cullin 1−Fbxo21 ubiquitin ligase complex is required for antiviral innate response. eLife 5, e14087. https://doi.org/10.7554/eLife.14087
Zeng, C., Zhao, C., Ge, F., Li, Y., Cao, J., Ying, M., Lu, J., He, Q., Yang, B., Dai, X., Zhu, H., 2020. Machado-Joseph Deubiquitinases: From Cellular Functions to Potential Therapy Targets. Front. Pharmacol. 11, 1311. https://doi.org/10.3389/fphar.2020.01311
Zhang, F., Zhong, R., Li, S., Fu, Z., Wang, R., Wang, T., Huang, Z., Le, W., 2019. Alteration in sleep architecture and electroencephalogram as an early sign of Alzheimer's disease preceding the disease pathology and cognitive decline. Alzheimers Dement. 15, 590–597. https://doi.org/10.1016/j.jalz.2018.12.004
Zhu, Y., Qu, C., Hong, X., Jia, Y., Lin, M., Luo, Y., Lin, F., Xie, Xiaolong, Xie, Xiaoqi, Huang, J., Wu, Q., Qiu, X., Piao, D., Xing, Y., Yu, T., Lu, Y., Huang, Q., Yu, C., Jin, J., Zhang, Z., 2019. Trabid inhibits hepatocellular carcinoma growth and metastasis by cleaving RNF8-induced K63 ubiquitination of Twist1. Cell Death Differ. 26, 306–320. https://doi.org/10.1038/s41418-018-0119-2